

OBSERVATIONAL CONSTRAINTS ON EQUATION OF STATE PARAMETERS FOR COSMOLOGICAL MODELS OF THE UNIVERSE

A THESIS SUBMITTED TO UNIVERSITY OF NORTH BENGAL

FOR THE AWARD OF

DOCTOR OF PHILOSOPHY
IN
PHYSICS



BY

MR. PRASENJIT THAKUR

GUIDE

DR. BIKASH CHANDRA PAUL

DEPARTMENT OF PHYSICS
UNIVERSITY OF NORTH BENGAL
RAJA RAMMOHUNPUR, DIST. DARJEELING
WEST BENGAL, INDIA 734013
MAY 2014

Th
530.11

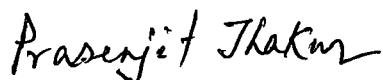
T3570

279008

27 MAY 2016

DECLARATION

I declare that the thesis entitled “**OBSERVATIONAL CONSTRAINTS ON EQUATION OF STATE PARAMETERS FOR COSMOLOGICAL MODELS OF THE UNIVERSE**” has been prepared by me under the guidance of **Dr. Bikash Chandra Paul**, Associate Professor, Department of Physics, University of North Bengal. No part of the thesis has formed the basis for the award of any degree or fellowship previously.



Mr. Prasenjit Thakur

Department of Physics

Alipurduar College, Alipurduar

Dist. Jalpaiguri, Pin-736122

India

Date : 21/05/14

DEPARTMENT OF PHYSICS

UNIVERSITY OF NORTH BENGAL

P.O. North Bengal University, Siliguri, Dist. Darjeeling, West Bengal, Pin - 734013, India

Website: www.nbu.ac.in



Phone: +91-(0) 353 -2776338, Fax: +91-(0) 353-2699001

CERTIFICATE

I certify that Mr. Prasenjit Thakur has prepared the thesis entitled “OBSERVATIONAL CONSTRAINTS ON EQUATION OF STATE PARAMETERS FOR COSMOLOGICAL MODELS OF THE UNIVERSE” for the award of Ph.D. degree of the University of North Bengal, under my guidance. He has carried out the work at the Department of Physics, University of North Bengal.

Dr. Bikash Chandra Paul

Associate Professor

Department of Physics

University of North Bengal

Raja Rammohunpur

Associate Professor
Department of Physics
University of North Bengal



Date : 21/5/14

Abstract

It is now generally accepted that there was an epoch when the universe underwent a phase of rapid expansion known as inflation. In the last 30 years to realize the early inflation a number of gravitational theories with cosmological models published in the literature. But in spite of the attractive features of cosmological inflation, its mechanism of realization still remains *ad hoc*. Consequently, in the literature a number of cosmological models came up to implement the early inflation. In recent years precision experiments in cosmology predicted another interesting phase of expansion of the late universe. It has been predicted that the present universe is expanding at a rate much faster than the rate estimated in the standard model. Such an accelerating phase however cannot be realized in general theory of relativity (GTR) with the fields of the standard model of particle physics. This is a challenge in theoretical physics, to overcome this a modification of the gravitational sector or the matter sector of the Einstein-Hilbert action or a new physics is required. In this thesis cosmological models are investigated which accommodate late accelerating phase making use of exotic matter as a modification of matter sector in Einstein gravity. Cosmological models are also explored in the framework of a modified theory of gravity namely, Horava-Lifshitz gravity in the presence of exotic kind of fluid. Observational constraints on the equation of state (EoS) parameters of the fluid taken to construct cosmological models are also determined.

- In Chapter 1, a brief review of the cosmological models and the methodology adopted here to determine the observational constraints on EoS parameters are presented.
- In Chapter 2, Emergent Universe (EU) model obtained by Mukherjee *et al.* with a non-linear EoS, $p = B\rho - A\rho^{\frac{1}{2}}$ is considered to estimate the constraints on A, B

parameters from cosmological observations. The following observational data namely, $(H(z) - z)$ data (OHD), a model independent BAO peak parameter and CMB shift parameter (WMAP 3 data) are considered to determine the unknown parameters in the theory. We observe that a viable cosmological model is permitted even with $B \rightarrow 0$. The magnitude of B is very small compared to A . The supernovae magnitudes μ vs. redshift (z) curve in the model is plotted which is then compared with the union compilation data. The cosmological model is found in good agreement with the above observations.

- *In Chapter 3*, EU models obtained by Mukherjee *et al.* for different values of B are studied. The parameter B is important as it determines the composition of fluids in the universe. Here we consider cosmologies with the following values of B namely, $B = -\frac{1}{3}, 0, \frac{1}{3}, 1$ respectively to analyze EU model employing the recent observational data. The observed Stern data for Hubble parameter and redshift ($H(z)$ vs. z) (OHD) in addition to a model-independent measurement of BAO peak parameter and CMB shift parameter (WMAP 7 data) are employed here for the analysis. The recent cosmological observations is that the universe is filled with dark matter (DM) and dark energy (DE). It is observed that EU models permit a universe with a composition of DM and DE. Evolution of other relevant cosmological parameters, namely, density parameter (Ω), effective equation of state (EoS) parameter (ω_{eff}) are also investigated. It has also been noted that the model with $B = -\frac{1}{3}$ is ruled out in the light of the above observations.

- *In Chapter 4*, cosmological models have been obtained in GTR considering modified Chaplygin gas (MCG) as a candidate for dark energy and estimated the range of

values for a physically viable cosmological model. The EoS of MCG ($p = B\rho - \frac{A}{\rho^\alpha}$) involves three parameters namely, A , B and α . The constraints imposed on the EoS parameters by the following observations namely, dimensionless age parameter ($H_0 t_0$) and $(H(z) - z)$ data are determined. Specifically the observational constraints on B parameter in terms of α and A is determined in addition to the constraints originated from Cold Dark Matter (CDM) and Unified Dark Matter Energy (UDME) models respectively. The suitable range of B that is permitted by all the observations considered here, has also been determined.

- *In Chapter 5*, cosmological models obtained in GTR with MCG are studied using the linear growth function for the large scale structures of the universe. MCG is considered as one of the prospective candidates for the dark energy. A numerical analysis considering observational growth data for a given range of redshift from the Wiggle-Z measurements and *r.m.s* mass fluctuations from Ly- α measurements is carried out to determine the observational constraints on the parameters of the MCG. The Wang-Steinhardt ansatz for growth index γ and growth function f (defined as $f = \Omega_m^\gamma(a)$) are also considered here for a numerical analysis in addition to the observational data relating Hubble parameter with redshift z (OHD) to constrain the EoS parameters. The best-fit values of the EoS parameters obtained here is employed to study the growth function f , growth index γ and equation of state parameter ω with redshift z . The observational constraints on MCG parameters obtained here are then compared with that of the GCG model for obtaining a viable cosmology. It is also noted that an accelerating phase of the universe followed by a matter domination with MCG is permitted.

- In Chapter 6, Holographic dark energy (in short, HDE) model of the universe is proposed considering MCG. Corresponding holographic dark energy field and the corresponding potential are determined. The stability of the HDE in this case is also discussed.
- In Chapter 7, a modified theory of gravity namely, Horava-Lifshitz theory of gravity is considered to obtain cosmological models with modified Chaplygin gas (MCG). The cosmological models are obtained here employing detailed balance condition. There are three unknown EoS parameters namely, A , α , B required to describe MCG fluid. The range of values of the parameters are determined making use of the observational data namely, $(H(z) - z)(OHD)$, BAO peak parameter and CMB shift data considering the detailed balance condition in HL gravity for a viable cosmological model. Further, the effective neutrino parameter (ΔN_ν) is employed here to determine the effective values of B and A_s by numerical technique.
- In Chapter 8, cosmological models are obtained in the framework of HL gravity considering beyond detailed balance condition with MCG. Using observational data from $(H(z) - z)(OHD)$, BAO peak parameter and CMB shift parameter, we probe cosmological models. The effect of dark radiation on the whole range of the effective neutrino parameter (ΔN_ν) is studied to constrain the matter contributing parameter B in this scenario. It has been observed that greater the dark radiation less is the value of the parameter B in MCG. To check the validity of beyond detailed balance scenario we plot supernovae magnitudes (μ) with redshift of Union2 data and then the variation of state parameter with redshift. It is observed that beyond detailed balance scenario is suitable for cosmological model in HL gravity with MCG.

In the framework of different theories of gravity and fields, a large variants of cosmological models are probed with various observational inputs to trace the observational constraints on EoS parameters.

Preface

The thesis contains a study of cosmological models obtained in different theories of gravity and determination of the observational parameters in terms of recent cosmological and astronomical observations. This thesis is the outcome of my research work carried out at the Department of Physics, University of North Bengal, West Bengal, India. There are total nine Chapters. The first Chapter contains an introduction, aim of the work and brief summary of the work. The other Chapters are based on the following papers:

Chapter 2 is based on:

"Constraints on exotic matter needed for an Emergent Universe", B. C. Paul, P. Thakur and S. Ghose, *Mon. Not. Roy. Astron. Soc. (MNRAS)* **407**, 415 (2010).

Chapter 3 is based on:

(i) *"Emergent Universe from a composition of matter, exotic matter and dark energy"*, B. C. Paul, S. Ghose and P. Thakur, *MNRAS* **413**, 686 (2011);

(ii) *"Observational constraints on the model parameters of a class of Emergent Universe"*. S. Ghose, B. C. Paul and P. Thakur, *MNRAS* **421**, 20 (2012).

Chapter 4 is based on:

"Modified Chaplygin gas and constraints on its B parameter from CDM and UDME cosmological models", P. Thakur, S. Ghose and B. C. Paul, *MNRAS* **397**, 1935 (2009).

Chapter 5 is based on:

"Observational constraints on modified Chaplygin gas from cosmic growth", B. C. Paul and P. Thakur, *JCAP* **11**, 052 (2013).

Chapter 6 is based on:

"Holographic dark energy model with generalized Chaplygin gas", B. C. Paul, P. Thakur and A. Saha, *ICTP IC/IR/2007/006*.

Chapter 7 is based on:

"Modified Chaplygin gas in Horava-Lifshitz gravity and constraints on its B parameter", B. C. Paul, P. Thakur and A. Saha, *Phys. Rev. D* **85**, 024039 (2012).

Chapter 8 is based on:

"Observational constraints on modified Chaplygin gas in Horava-Lifshitz gravity with dark radiation", B. C. Paul, P. Thakur and M. M. Verma, *Pramana, A Journal of physics*, **81**, 691 (2013).

Concluding remark of the research work and future plan are discussed in Chapter 9.

Acknowledgements

I would like to thank my supervisor Dr. B. C. Paul, Associate Professor, Physics Department, University of North Bengal (NBU), without his guidance, support and infinite patience it would have never been completed. In spite of his busy hours as Registrar (Officiating), NBU, he has patiently supervised my thesis work. So, I acknowledge my sincere gratitude to him. This work is carried out in the Department of Physics, University of North Bengal. I express my thank to all the faculties of the Physics Department for their support and help. I am thankful to Mr. Souvik Ghose, Mr. Arindam Saha of Cosmology Group at IUCAA Resource Centre (IRC), Physics Department, NBU for active collaboration. I am thankful to my colleagues specially Mr. P. K. Chattopadhyay and Rajib Bhaumik for their constant boost up. I am also thankful to the Principal of Alipurduar College for his constructive support to complete the work. Finally, I express my gratitude to my parents, elder brothers and my family for their constant encouragement and support throughout my career.

Dedicated to my family.

Contents

Title Page	i
Abstract	iv
Preface	ix
Acknowledgements	x
Dedication	xi
Table of Contents	xii
List of Figures	xv
List of Tables	xviii
1 Introduction and brief review	1
1.1 Methodology	9
1.1.1 Emergent Universe model	12
1.1.2 Horava-Lifshitz gravity	14
1.2 Numerical analysis	15
1.2.1 Likelihood function	16
1.2.2 <i>Chi-square</i> minimization and confidence limits	16
1.3 Testing viability of models	21
2 Observational Constraints on Exotic Matter in Emergent Universe	23
2.1 Introduction	23
2.2 Field equations	25
2.3 ($H(z) - z$) data (OHD) as a constraining tool	26
2.4 Joint analysis with <i>OHD</i> and BAO peak parameter	28
2.5 Joint analysis with <i>OHD</i> , BAO peak parameter and CMB shift parameter (\mathcal{R})	29
2.6 Discussions	32
3 Observational Constraints on EoS parameters for a class of Emergent Universe	34
3.1 Introduction	34
3.2 Field equations	35

3.3	Analysis with observational data	38
3.3.1	Observed Hubble data (OHD)	38
3.3.2	Joint analysis with BAO peak parameter	39
3.3.3	Joint analysis with OHD, BAO peak parameter and CMB shift parameter (\mathcal{R})	41
3.3.4	Goodness of fit	42
3.4	Density parameters in different EU model	45
3.5	Discussion	46
4	Observational Constraints on the B parameter of Modified Chaply- gin gas as DE	47
4.1	Introduction	47
4.2	Analysis of cosmological models	49
4.3	Age of the universe as a constraining tool	51
4.4	$(H(z) - z)$ data as a constraining tool	53
4.5	Test of viability of the model	56
4.6	Discussion	57
5	Observational Constraints on EoS parameters of Modified Chaplygin Gas in Cosmic Growth	61
5.1	Introduction	61
5.2	Field equations	63
5.3	Parametrization of the growth index	64
5.4	Observational constraints	67
5.5	Results	69
5.6	Discussion	76
6	Cosmological models with Holographic Dark Energy	80
6.1	Introduction:	80
6.2	Modified Chaplygin gas in FRW universe:	83
6.3	Holographic dark energy as MCG:	84
6.4	Squared speed of sound:	87
6.5	Discussions:	88
7	Modified Chaplygin Gas in Horava-Lifshitz Gravity and Constraints on its B parameter	90
7.1	Introduction	90
7.2	Horava-Lifshitz cosmology	91
7.2.1	Cosmological model:	92
7.3	Observational constraints on EoS parameters of MCG	94
7.3.1	Constraints obtained from detailed balance	94
7.4	Numerical analysis	97

7.4.1	$(H - z)$ data (OHD) as a tool for constraining	97
7.4.2	BAO peak parameter as a tool for constraining	98
7.4.3	CMB shift parameter as a tool for constraining	98
7.4.4	Joint analysis with OHD + BAO + CMB data	98
7.5	Test of MCG in HL gravity	104
7.6	Discussion	105
8	Observational Constraints on MCG in Horava-Lifshitz Gravity with Dark Radiation	109
8.1	Introduction	109
8.2	HL cosmology with beyond detailed balance condition and projectibility	110
8.3	Observational constraints on EoS parameters	111
8.3.1	Constraints obtained from beyond detailed balance	111
8.4	Numerical analysis	113
8.4.1	$(H-z)$ data (OHD) as a tool for constraining	114
8.4.2	BAO peak parameter as a tool for constraining	114
8.4.3	CMB shift parameter as a tool for constraining	115
8.4.4	Joint analysis with OHD + BAO+ CMB data	115
8.5	Viability of MCG in HL gravity	120
8.6	Discussion	122
9	Concluding remark and Future plan of work	124
9.1	Future plan of work:	129
	Bibliography	131

List of Figures

2.1	$A - B$ contours using $H(z)$ vs. z data (OHD) for $K = 0.0100$ at 95.4% (Solid) and 99.7% (Dashed) confidence level. The best-fit point is shown (0.0122, -0.0823).	26
2.2	$A - B$ contours using OHD data and BAO peak parameter with $K = 0.0101$. 95.4% (Solid) and 99.7% (Dashed) confidence levels are shown in the figure along with the best-fit value (0.0094, -0.1573)	28
2.3	$A - B$ contours using OHD data, BAO peak parameter and CMB shift parameter for $K = 0.0102$. 95.4% (Solid) and 99.7% (Dashed) confidence levels are shown in the figure along with the best-fit value (0.0103, -0.0219)	29
2.4	Comparison of $\mu(z)$ vs. z curve with supernovae data	31
2.5	Variation of density parameter (Ω) for effective dark energy and effective matter content of the universe with redshift.	31
2.6	(a) Variation of effective EoS parameter for EU (ω_{eff}) with redshift (z). (b) Variation of deceleration parameter (q) with redshift (z). Solid, Dashed and Dotted line corresponds to the best-fit values, 95.4% confidence level and 99.7% confidence level respectively.	33
3.1	$K - A$ contours using OHD data for EU with $B = 0$, $B = \frac{1}{3}$, $B = 1$: 68.3%, 95.4% and 99.7% confidence regions are shown	36
3.2	$K - A$ contours using OHD and SDSS (BAO) data for EU with $B = 0$, $B = \frac{1}{3}$ and $B = 1$: 68.3%, 95.4% and 99.7% confidence regions are shown	37
3.3	$K - A$ contours using OHD, SDSS (BAO) and WMAP 7 (CMB shift) data for EU with $B = 0$, $B = \frac{1}{3}$ and $B = 1$: 68.3%, 95.4% and 99.7% confidence regions are shown	40
3.4	$\Omega_1 - \Omega_2$ contours for (a) $B = 0$, (b) $B = \frac{1}{3}$ and (c) $B = 1$: 68.3%, 95.4% and 99.7% confidence regions are shown.	43
4.1	Variation of B with A_s for $\alpha = 0.01$ (Dotted line), $\alpha = 0.20$ (Dashed line) and $\alpha = 0.39$ (Thin line) in CDM model	52

4.2	Variation of B with A_s for $\alpha = 0.01$ (Thin line), $\alpha = 0.50$ (Dotted line) and $\alpha = 0.99$ (Dashed line) in UDME model	52
4.3	Constraints on EoS parameters in CDM model for (a) $\alpha = 0.01$, (b) $\alpha = 0.50$ and (c) $\alpha = 0.99$ using $H(z)$ vs. z data: 1σ , 2σ and 3σ levels are shown.	54
4.4	Constraints on EoS parameters in UDME model for (a) $\alpha = 0.01$, (b) $\alpha = 0.50$ and (c) $\alpha = 0.99$ using $H(z)$ vs. z data: 1σ , 2σ and 3σ levels are shown.	55
4.5	$\mu(z)$ vs. z curves for CDM model and union compilation data	57
4.6	$\mu(z)$ vs. z curves for UDME model and union compilation data	58
4.7	q vs. z curves for CDM & UDME model	58
5.1	(a) $B - A_s$, (b) $\alpha - A_s$ and (c) $\alpha - B$ contours using growth data at 68.3% (Solid), 90.0% (Dashed) and 95.4% (Dotted) confidence limits at best-fit values: $A_s = 0.81$, $B = -0.10$, $\alpha = 0.02$	70
5.2	(a) $B - A_s$, (b) $\alpha - A_s$ and (c) $\alpha - B$ contours using (growth+ $r.m.s$ mass fluctuations (σ_8)) data at 68.3% (Solid), 90.0% (Dashed) and 95.4% (Dotted) confidence limits at best-fit values: $A_s = 0.816$, $B = -0.146$, $\alpha = 0.004$	71
5.3	(a) $B - A_s$, (b) $\alpha - A_s$ and (c) $\alpha - B$ contours using (growth+ $r.m.s$ mass fluctuations (σ_8)+ OHD) data at 68.3% (Solid), 90.0% (Dashed) and 95.4% (Dotted) confidence limits at best-fit values: $A_s = 0.769$, $B = 0.008$, $\alpha = 0.002$	73
5.4	Evolution of growth function f with redshift at best-fit values: $A_s = 0.769$, $B = 0.008$, $\alpha = 0.002$	74
5.5	Evolution of growth index γ with redshift at best-fit values: $A_s = 0.769$, $B = 0.008$, $\alpha = 0.002$	74
5.6	Evolution of the state parameter (ω) at best-fit values: $A_s = 0.769$, $B = 0.008$, $\alpha = 0.002$	75
5.7	Square of sound speed variations with redshift at best-fit values: $A_s = 0.769$, $B = 0.008$, $\alpha = 0.002$	75
6.1	Variation of v_Λ^2 with Ω_Λ for different values of y at $c = 1$, $\gamma = \frac{1}{3}$ and $a = 1$, in the first array the figures are for $y = \frac{\pi}{3}$ and $y = \frac{\pi}{2}$, in the second array for $y = \frac{1.5\pi}{2}$, $y = \pi$ and in the third array for $y = \frac{2.5\pi}{2}$, $y = \frac{3\pi}{2}$	88
7.1	$A_s - B$ contours for (a) $\alpha = 0.999$, (b) $\alpha = 0.500$ and (c) $\alpha = 0.001$ for closed universe using ($OHD + SDSS (BAO) + CMB$ shift) data at 68.3% (Solid), 95.4% (Dashed) and 99.7% (Dotted) confidence level.	99
7.2	$A_s - B$ contours for (a) $\alpha = 0.999$, (b) $\alpha = 0.500$ and (c) $\alpha = 0.001$ for open universe using ($OHD + SDSS (BAO) + CMB$ shift) data at 68.3% (Solid), 95.4% (Dashed) and 99.7% (Dotted) confidence level.	102

7.3	Variation of equation of state parameter for closed (Dotted line) and open (Solid line) universe	105
7.4	The comparison of the Union compilation data with the best-fit values in closed universe.	106
8.1	$A_s - B$ contours for (a) $\alpha = 0.999$, (b) $\alpha = 0.500$ and (c) $\alpha = 0.001$ in beyond detailed balance scenario using ($OHD + SDSS (BAO) + CMB$ shift) data at 68.3% (Solid), 95.4% (Dashed) and 99.7% (Dotted) confidence level.	116
8.2	Constraints in beyond detailed balance for $\alpha = 0.999$ using ($OHD + SDSS (BAO) + CMB$ shift) data at 68.3% (Solid), 95.4% (Dashed) and 99.7% (Dotted) confidence level.	118
8.3	Constraints in beyond detailed balance for $\alpha = 0.001$ using ($OHD + SDSS (BAO) + CMB$ shift) data at 68.3% (Solid), 95.4% (Dashed) and 99.7% (Dotted) confidence level.	119
8.4	Equation of state parameter in beyond detailed balance scenario . .	121
8.5	The comparison of the Union2 data with the best-fit values in beyond detailed balance	122

List of Tables

1.1	Composition of matter in EU	13
2.1	$H(z)$ vs. z data (OHD) [99]	25
2.2	Best-fit values of the EoS parameters	30
2.3	Range of values of the EoS parameters using OHD+BAO+CMB data	30
3.1	Best-fit values using OHD data	39
3.2	Range of values of the EoS parameters using OHD data	39
3.3	Best-fit values using OHD + SDSS (BAO) data	41
3.4	Range of values of the EoS parameters using OHD + BAO data	42
3.5	Best-fit values using <i>OHD + SDSS (BAO) + WMAP 7</i> (CMB shift) data	42
3.6	Range of values of the EoS parameters using <i>OHD + BAO + CMB</i> data	44
3.7	Goodness of fit	44
3.8	Best-fit values of density parameters	45
4.1	$(H - z)$ data from Wu P <i>et al.</i> [130]	49
4.2	Range of values of the EoS parameters in CDM and UDME model using age constraint	56
4.3	Range of values of the EoS parameters in CDM and UDME model using $(H - z)$ data	58
4.4	Best-fit values of the EoS parameters in CDM and UDME model	59
5.1	Observed growth functions (f_{obs}) with redshift	67
5.2	Root mean square mass fluctuations (σ_8) at various redshift	68
5.3	Best-fit values of the EoS parameters	76
5.4	Range of values of the EoS parameters for A_s & B	76
5.5	Range of values of the EoS parameters A_s & α	77
5.6	Range of values of the EoS parameters for B & α	78
5.7	Values of the EoS parameters obtained in different models	78

5.8	Comparison of the values of EoS parameters for Λ CDM, GCG and MCG models	78
7.1	Best-fit values of MCG for $K = 1$	98
7.2	Best-fit values of GCG ($B = 0$) for $K = 1$	100
7.3	Range of values of the EoS parameters for $K = 1$ in MCG	100
7.4	Best-fit values of MCG for $K = -1$	101
7.5	Best-fit values of GCG ($B = 0$) for $K = -1$	101
7.6	Range of values of the EoS parameters for $K = -1$ in MCG	103
8.1	Range of values of the EoS parameters in beyond detailed balance scenario	115
8.2	Acceptable range of B parameter in beyond detailed balance scenario for $\alpha = 0.999$	117
8.3	Acceptable range of B parameter in beyond detailed balance scenario for $\alpha = 0.001$	118

Chapter 1

Introduction and brief review

In 1915, Einstein proposed general theory of relativity (in short, GTR) in which it has been considered that geometry and matter are intimately connected. The matter contained in the space-time manifold is related to its curvature. Subsequently Einstein applied his new theory in understanding the observed universe. The limitations of the observational instruments and available data from astronomers during that time led Einstein to obtain a static model of the universe. However, he failed to obtain such model with his field equation. He believed that there might exist a repulsive force in the universe for which the universe is not collapsing due to attractive nature of gravity. Einstein, consequently modified his field equation by adding a suitable repulsive term to obtain a static model of the universe. The constant term (Λ) which was added in the GTR equation by Einstein is known as cosmological constant. Historically in 1922, Friedmann obtained a dynamical solution of the field equation in the absence of Λ . However, the solutions obtained by Friedmann remained of academic interest only and not accepted by the cosmologists during that time because the solutions

confronted with the observations. In 1929, Hubble made a remarkable discovery that the galaxies that constitutes the universe are not at rest, they are moving away from each other which he ensured from redshifts of galaxies. Hubble's discovery thus ruled out Einstein's static model. Knowing Hubble's discovery of an expanding universe Einstein gave away Λ term, in order to accommodate such universe.

In the expanding universe scenario, the universe originated from a Big Bang. In 1948, Gamow, Herman and Alpher using Big Bang scenario predicted that in the early universe there was a phase of expansion when the universe was dominated by radiation with high temperature which in effect gradually decreases as the universe expands. The universe transits into a matter dominated phase subsequently. The temperature of the decoupled photons of the primordial nucleo-synthesis decreases with the evolution of the universe and the 2.7 K radiation hovering around today as cosmic microwave background radiation (CMBR), is a relic of the Big Bang. In 1965, Penzias and Wilson discovered existence of CMBR [1, 2]. Big bang model of the universe based on perfect fluid assumptions successfully describes the universe from present epoch to 10^{-2} s. When the early era is probed in the Big Bang model a number of problems namely, horizon problem, flatness problem, singularity problem etc. cropped up. Thus a number of observed issues came up which have no explanation in Big Bang model with perfect fluid assumption.

In 1981, Guth [3] proposed inflationary universe scenario using temperature dependent phase transition mechanism in order to get rid of the problems of the Big Bang cosmology. In this scenario there was a phase of expansion of the universe when a small causally coherent region grew into a huge size to encompass the present

universe. Thus the cosmological constant which was thrown away by Einstein earlier again reintroduced in cosmology to understand the observed universe. Subsequently, it is found that a graceful exit from inflation is a serious problem in the scenario. A new inflation is then proposed by Linde [4, 5], Albrecht and Steinhardt [6] where the graceful exit is natural. The period of inflation was very short in which the whole universe grew rapidly so that at a later epoch it engulf the different parts we see today, to come in causal contact with each other, thereby explaining the isotropy of the observed universe. Eventually, the quantum vacuum state decays, dumping its energy into the form of thermal radiation and subsequently the Big Bang Friedmann model takes over.

In 1983, Linde [7] proposed a suitable inflationary universe model which does not require temperature dependent phase transition mechanism instead, the universe can be realized from a chaotic distribution of a homogeneous scalar field. In the Linde's chaotic inflationary scenario sufficient inflation, required to solve the problems of the Big Bang model, may be realized if a causally coherent region grow out with an initial scalar field which picks up values $\phi_i > 3M_P$, where M_P represents the Planck mass. Quantum gravity region is not important in this case as $V(\phi) \geq M_P^4$. Linde [7] further shown that a kinetic energy dominated region can pass on to an inflationary era afterwards as the potential energy domination sets in at a late epoch in scalar field cosmology. Paul *et al.* [8] shown that chaotic scenario is more realistic as it can be accommodated even in the presence of an anisotropy. Thus, an inflationary universe model is important as it opens up new avenues not only in cosmology but also in particle physics. It can solve some of the outstanding conceptual issues in cosmology

and particle physics not understood before. In the last three decades a number of inflationary models of the universe came up in the literature in the framework of different theories. These are given below

- (1980-1989): R^2 -inflation [9, 10], Old inflation [3], New inflation [11], Chaotic inflation [7, 12], Power-law inflation [13, 14, 15, 16, 17], Extended inflation [18, 19], SUGRA inflation [20], Double inflation [21].
- (1990-1999): Hybrid inflation [22, 23, 24], SUSY D-term inflation [25, 26], Brane inflation [27, 28, 29, 30, 31, 32], assisted inflation [33, 34].
- (2000-2008): Super-natural inflation [35], K-inflation [36], D3-D7 inflation [37, 38, 39, 40, 41], Tachyon inflation [42], Racetrack inflation [43, 44], Hill top inflation [45, 46], DBI inflation [47, 48].

Due to advancement of technology the present era is witnessing a transition of cosmology from speculative science to experimental science. A number of astronomical and cosmological observations in the recent past made it possible to visualize the universe which is different from what we understood a decade ago. Perlmutter *et al.* [49, 50] and Riess *et al.* [51, 52] found that the present universe is accelerating during large redshift surveys of supernovae. This late acceleration cannot be realized in the framework of standard model of particle physics. It is one of the challenge in theoretical physics to develop a consistent theory to address the issue. It is found that old cosmological constant term of Einstein again can help to obtain such a late accelerating universe. However, origin of a cosmological constant term required at late epoch is not known. When observational results are analyzed in the Big Bang model, existence of a new kind of energy that fills the space is required which is termed as

dark energy. It has a negative pressure and negative gravitational effect causing a gravitational repulsion. As the universe expands, dark energy stays at nearly constant energy density and, as the matter in the universe thins out, the dark energy begins to dominate. The repulsive effect of dark energy seems to guarantee that the universe might continue to expand forever.

Thus it is evident that ordinary matter fields available from standard model of particle physics fails to account for the present observations. Consequently, to address the recent issues a modification of the matter sector of the Einstein-Hilbert action with exotic matter is considered in the contemporary literature. Chaplygin gas (CG) is considered to be one such candidate for dark energy. The equation of state (henceforth, EoS) for CG is

$$p = -\frac{A}{\rho} \quad (1.1)$$

where A is positive constant. It may be important to mention here that the initial idea of CG originated in Aerodynamics [53]. It is also interesting to note that the CG may be considered as an alternative to quintessence [54]. In the context of string theory Chaplygin gas emerges from the dynamics of a generalized d-brane in a $(d+1, 1)$ space time. It can be described by a complex scalar field which is obtained from a generalized Born-Infeld action. But CG is ruled out in cosmology, as cosmological models are not consistent with observational data of supernovae Ia (SNIa), Baryon Acoustic Oscillation (BAO), Cosmic Microwave Background (CMB) and so on [55, 56]. Subsequently, the equation of state for CG is generalized to incorporate different aspects of the observational universe. The equation of state for

generalized Chaplygin gas (in short, GCG) [57, 58] is given by

$$p = -\frac{A}{\rho^\alpha} \quad (1.2)$$

with $0 \leq \alpha \leq 1$. In the above EoS, $\alpha = 1$ reduces to Chaplygin gas [53]. It has two free parameters, A and α . It is known that GCG is capable of explaining background dynamics [59] and other features of a homogeneous isotropic universe satisfactorily. The feature that the GCG corresponds to almost dust ($p = 0$) at high density does not agree completely with our universe. It is also known that the GCG model suffers from serious problems at the perturbation level. The matter power spectrum of GCG exhibits strong oscillations or instabilities, unless GCG model reduces to Λ CDM [60]. The oscillations for the baryon component with GCG leads to undesirable features in CMB spectrum [61]. Thus a modification to the GCG is considered by adding a positive linear term in density to the EoS, known as modified Chaplygin gas (in short, MCG). The equation of state for the MCG is given by:

$$p = B\rho - \frac{A}{\rho^\alpha} \quad (1.3)$$

where A, B, α are positive constants with $0 \leq \alpha \leq 1$. The above EoS reduces to that of GCG model [57, 58] when one sets $B = 0$. A cosmological constant Λ emerges by setting $\alpha = -1$ and $A = 1 + B$. For $A = 0$, eq. (1.3) reduces to an EoS which describes a perfect fluid with $\omega = B$, *e.g.*, a quintessence model [62]. MCG contains one more free parameter namely, B over GCG. It may be pointed out here that MCG is a single fluid model which unify dark matter and dark energy. The MCG model is suitable for obtaining a constant negative pressure at low density accommodating late acceleration and radiation dominated era (with $B = \frac{1}{3}$) at a high density. Thus a

universe with MCG may be described starting from the radiation epoch to the epoch dominated by the dark energy consistently. On the other hand GCG describes evolution of the universe from matter dominated to dark energy dominated regime (as $B = 0$). So, compared to GCG the proposed MCG is suitable to describe the evolution of the universe over a wide range of epoch [63]. Although the distinction between Λ CDM and GCG model are very little, GCG is not attractive to describe EoS for dark energy. Another motivation for considering MCG as a dark energy candidate is that the exact EoS for dark energy not yet known. MCG is an attempt to find something interesting that is not exactly Λ CDM. Wu *et al.* [64] studied the dynamics of the MCG model. Bedran *et al.* [65] studied the evolution of the temperature function in the presence of MCG. Cosmological models with MCG are found consistent with perturbation study [66] and spherical collapse problem [67].

Another interesting cosmological model with a non-linear EoS is obtained by Mukherjee *et al.* [68] in a flat universe known as emergent universe. Ellis and Maartens [69] first proposed an emergent universe in a closed model where the emergent universe scenario replaces the initial singularity by an Einstein static phase in which the scale factor of the Friedmann-Robertson-Walker (FRW) metric does not vanish and, accordingly, the energy density, pressure etc. do not diverge. In the emergent universe scenario the initial size of the universe was large enough so that quantum gravity effect is not important [69, 70]. In this model the horizon and flatness problems do not arise. In the EU scenario, the universe evolves from a static phase in the infinite past into an inflationary phase at a later epoch. In the usual description with a scalar field it is shown that a universe starts expanding from the above phase, later on smoothly

joins with a stage of exponential expansion followed by a standard reheating phase. It then approaches the classical thermal radiation dominated era of the conventional Big Bang cosmology [69]. Later Ellis and Maarten [69] shown that the potential needed to realize EU may be obtained naturally in a higher derivative gravity with conformal transformation. Mukherjee *et al.* however shown that a non-linear EoS is enough to realize in EU scenario. The matter in the universe may be considered as a composition of three types of fluid depending on EoS parameter. EU with non-linear EoS will be considered here to estimate the unknowns using observational data.

There are theories considered in the literature to accommodate late acceleration either by a modification of the gravitational sector or by a modification of the matter sector introducing exotic matter fields in the Einstein-Hilbert action. Alternative theories of gravity namely, Horava-Lifshitz gravity [71, 72], massive gravity $F(T)$ [73, 74, 75], $f(R)$ gravity [76, 77, 78, 79, 80] are also discussed in the literature. In Horava-Lifshitz (in short, HL) gravity one can obtain a cosmological model which is singularity free. Horava proposed the theory in cosmology in 2009, motivated from its success in solid state physics. The Big Bang initial singularity may be avoided in the framework of HL cosmology due to the presence of higher order terms in the spatial curvatures R_{ij} . In the ultraviolet (UV) limit, HL gravity has a Lifshitz-like anisotropic scaling as $t \rightarrow l^z t$ and $x^i \rightarrow l x^i$, between space and time, characterized by the dynamical critical exponent $z = 3$ and thus breaks the Lorentz invariance; while in the infra-red (IR) limit, the scale reduces to $z = 1$. Therefore, a classical general relativistic theory of gravity may emerge out of HL gravity in the low energy limit. The Friedmann equation in HL gravity is modified by an extra $\frac{1}{a^4}$ term [81, 82, 83],

where a represents the scale factor of a non-flat universe. HL gravity will be considered here to realize late accelerating phase and to determine various parameters for a viable cosmology.

1.1 Methodology

The Einstein-Hilbert action in 4-dimension is given by

$$I = \int \left(\frac{1}{16\pi G} R + L_m \right) \sqrt{-g} d^4x \quad (1.4)$$

where R represents Ricci tensor, g represents the determinant of the space-time metric and L_m represents the matter Lagrangian. The variation of the action with respect to the metric yields the Einstein's field equation which is given by

$$R_{\mu\nu} - \frac{1}{2} g_{\mu\nu} R = -8\pi G T_{\mu\nu} \quad (1.5)$$

where $R_{\mu\nu}$ is the Ricci tensor, R is the Ricci scalar, $g_{\mu\nu}$ is the 4-dimensional metric and $T_{\mu\nu}$ is the energy momentum tensor and G is the Newton's gravitational constant. Greek letters μ, ν can take up the values $(0, 1, 2, 3)$ respectively. The left hand side of eq. (1.5) is determined from space-time geometry, whereas the right hand side is determined by the matter content in the universe.

The most general space-time metric, consistent with homogeneity and isotropy of the universe is given by Robertson-Walker (RW) metric which is given by

$$ds^2 = -dt^2 + a^2(t) \left[\frac{dr^2}{1 - kr^2} + r^2 (d\theta^2 + \sin^2 \theta d\phi^2) \right] \quad (1.6)$$

where $(k = +1, 0, -1)$, $k = +1$ for positively curved spatial sections (closed universe), $k = 0$ for flat universe and $k = -1$ for negatively curved spatial sections (open universe), $a(t)$ represents the scale factor of the universe. Using the energy-momentum

tensor for perfect fluid, $T^\mu_\nu = \text{diag}[\rho, -p, -p, -p]$ where ρ and p are energy density and pressure respectively. The time-time and space-space components of the Einstein field equation becomes

$$\left(\frac{\dot{a}}{a}\right)^2 + \frac{k}{a^2} = \frac{8\pi G\rho}{3}, \quad (1.7)$$

$$2\frac{\ddot{a}}{a} + \frac{\dot{a}^2}{a^2} + \frac{k}{a^2} = -8\pi Gp \quad (1.8)$$

where $(\dot{})$ represents derivative w.r.t. time. In the case of a flat universe ($k = 0$) the Friedmann equation is obtained from eq. (1.7) which is given by

$$H^2 = \left(\frac{\dot{a}}{a}\right)^2 = \frac{8\pi G\rho}{3}, \quad (1.9)$$

where H is the Hubble parameter. Using eqs. (1.7) and (1.8) one obtains the Raychaudhuri equation which is given by

$$\frac{\ddot{a}}{a} = -\frac{4\pi G(\rho + 3p)}{3}. \quad (1.10)$$

The equation of state for barotropic fluid is

$$p = \omega\rho \quad (1.11)$$

where ω is the EoS parameter. The conservation equation is given by

$$\frac{d\rho}{dt} + 3H(p + \rho) = 0 \quad (1.12)$$

consequently, the Raychaudhuri equation becomes

$$\frac{\ddot{a}}{a} = -\frac{4\pi G(1 + 3\omega)\rho}{3}. \quad (1.13)$$

It is evident that to accommodate the early inflation matter with $\omega \leq -\frac{1}{3}$ is essential. Perfect fluid model does not permit matter with a negative pressure. Consequently,

a semi-classical approximation where the geometry is classical but the matter is described by quantum fields becomes essential in cosmology for describing early universe. The energy density and pressure in terms of a homogeneous scalar field ($\phi = \phi(t)$) are given by

$$\rho = \frac{1}{2}\dot{\phi}^2 + V(\phi), \quad p = \frac{1}{2}\dot{\phi}^2 - V(\phi). \quad (1.14)$$

Therefore,

$$\rho + 3p = 2(\dot{\phi}^2 - V(\phi)). \quad (1.15)$$

Using the above equation in Raychaudhuri equation (1.10) we obtain the condition for an inflationary universe which is $\dot{\phi}^2 < V(\phi)$ demanding potential energy dominated regime. Thus a suitable scalar field potential which satisfies the above condition permits inflation. While the field rolls down near the minimum of the potential and it oscillates, which subsequently produces particle. In the early universe $\omega = -1$ is favourable. However, in recent times we observe that the present universe can be described by matter with $\omega < -\frac{1}{3}$. The usual scalar field description thus failed to obtain accelerating phase at late time. Therefore, an exotic form of matter ($p < 0$) is essential to address late phase of expansion. In this thesis cosmological models are studied using generalized Chaplygin gas (GCG) and modified Chaplygin (MCG) separately as the candidates for exotic matter. A non-linear equation of state required for emergent universe model is taken into account to determine the observed constraints. Using different observational predictions from Observed Hubble data (OHD), Baryon Acoustic Oscillation (BAO) parameter, Cosmic microwave background (CMB) shift parameter and dimensionless age parameter, growth parameter, *r.m.s* mass fluctuation data, we determine the observational constraints.

1.1.1 Emergent Universe model

Mukherjee *et al.* [68] assumed the following salient features of emergent universe (EU) model.

1. The universe is isotropic and homogeneous at large scales.
2. The predicted value of density parameter from observations points towards a flat universe ($\Omega_o \sim 1$).
3. The universe is sufficiently large so that quantum gravity effects are not important so that classical description of space-time is adequate.
4. No singularity and there exists a time like vector.
5. The universe is accelerating (Type Ia Supernovae data).
6. The matter or in general, the source of gravity has to be described by quantum field theory.
7. The universe may contain exotic matter so that energy condition may be violated.

In the case of flat universe the energy density and pressure can be expressed as

$$\rho = 3 \frac{\dot{a}^2}{a^2} \quad (1.16)$$

$$p = - \left(2 \frac{\ddot{a}}{a} + \frac{\dot{a}^2}{a^2} \right) \quad (1.17)$$

where we consider $8\pi G = 1$. The above eqs. (1.16) and (1.17) leads to a second order differential equation with a non-linear EoS given by

$$p = B\rho - A\rho^{\frac{1}{2}} \quad (1.18)$$

where A and B are the state parameters. The solution permits an emergent universe scenario where the scale factor evolves as

$$a(t) = a_0 (\beta + \exp(\alpha t))^\omega \quad (1.19)$$

B	$\frac{\rho_2}{\Lambda}$ in unit $\frac{K}{A}$	ω_2	$\frac{\rho_3}{\Lambda}$ in unit $(\frac{K}{A})^2$	ω_3	Composition
$-\frac{1}{3}$	$\frac{9}{2a}$	$-\frac{2}{3}$	$\frac{9}{4a^2}$	$-\frac{1}{3}$	DE, domain wall and cosmic string
0	$\frac{2}{8a^{\frac{3}{2}}}$	$-\frac{1}{2}$	$\frac{1}{a^3}$	0	DE, exotic matter and dust
$\frac{1}{3}$	$\frac{9}{8a^2}$	$-\frac{1}{3}$	$\frac{9}{8a^4}$	$\frac{1}{3}$	DE, cosmic string and radiation
1	$\frac{1}{2a^3}$	0	$\frac{1}{4a^6}$	1	DE, dust and stiff matter

Table 1.1: Composition of matter in EU

where $a_0 = (\frac{\sqrt{3}K(B+1)}{A})^{\frac{2}{3(B+1)}}$, $\beta = \frac{\sqrt{3}A}{2}$, $\alpha = \frac{\sqrt{3}A\sigma}{2K}$, $\omega = \frac{2}{3(B+1)}$ are positive constants. The non-vanishing scale factor (a_0) at time ($t = 0$) indicates that universe is ever existing. Under such conditions the scale factor as well as the size of the universe can never attain singularity. The present universe emerged out from a static Einstein phase in the infinite past in this model. The static de Sitter solution is unstable, therefore, at a later epoch the universe which emerged provides the observed universe. The expression for energy density and pressure obtained using eqs. (1.18) and (1.12) are given by

$$\rho = \rho_1 + \rho_2 + \rho_3 \quad (1.20)$$

$$p = p_1 + p_2 + p_3 \quad (1.21)$$

with $\rho_1 = \frac{A^2}{(B+1)^2}$, $\rho_2 = \frac{2KA}{(B+1)^2} \frac{1}{a^{\frac{3(B+1)}{2}}}$, $\rho_3 = \frac{K^2}{(B+1)^2} \frac{1}{a^{3(B+1)}}$ and $p_1 = -\frac{A^2}{(B+1)^2}$, $p_2 = \frac{KA(B-1)}{(B+1)^2} \frac{1}{a^{\frac{3(B+1)}{2}}}$, $p_3 = \frac{BK^2}{(B+1)^2} \frac{1}{a^{3(B+1)}}$. Thus effectively, it permits a universe composed of three types of fluid determined by B parameter. In Table-(1.1), the different composition of fluids in the universe based on the value of B are presented. The EU model has been explored in a flat universe which is supported by recent observations. Subsequently, the EU model was taken up to examine the suitability of implementing

it in the context of various theories [67, 84, 85, 86]. A similar type of EoS was considered in the literature as a double component dark energy model [87] where the model parameters are constrained from Type Ia supernova data. The EoS considered by Fabris [87] is basically a special form of a more general EoS of the form, $p = B\rho - A\rho^\alpha$; which represents Chaplygin gas with $\alpha < 0$ [57, 58]. However for $\alpha > 0$ it coincides to EU scenario [68].

1.1.2 Horava-Lifshitz gravity

Horava-Lifshitz (in short, HL) theory of gravity [71, 82, 83] is considered as one of the important theory in cosmology motivated by its successes in solid state physics. According to the Arnowitt-Deser-Misner (in short, ADM) decomposition form the metric is given by

$$ds^2 = -N^2 dt^2 + g_{ij}(dx^i + N^i dt)(dx^j + N^j dt) \quad (1.22)$$

where the basic variables are lapse function N , shift vector N_i and the spatial metric corresponds to g_{ij} . The scaling transformation of the co-ordinates are $t \rightarrow l^3 t$ and $x^i \rightarrow l x^i$. Both the shift vector N^i and the 3 dimensional spatial metric g_{ij} depend on the time coordinate t and the spatial coordinate x^i . However, the lapse function N is assumed to depend on time only. This condition imposed on the lapse function is called the projectibility condition. The gravitational action of HL gravity consists of kinetic and potential energy terms which is given by

$$I_g = I_K + I_V = \int dt d^3x \sqrt{g} N (L_K + L_V). \quad (1.23)$$

The action with kinetic term is

$$I_K = \int dt d^3x \sqrt{g} N \left[\frac{2(K_{ij}K^{ij} - \lambda K^2)}{\kappa^2} \right] \quad (1.24)$$

where

$$K_{ij} = \frac{(\dot{g}_{ij} - \nabla_i N_j - \nabla_j N_i)}{2N} \quad (1.25)$$

is the extrinsic curvature in which dot represents derivative w.r.t time (t). There are two cases in HL gravity namely, (i) detailed balance condition and (ii) beyond detailed balance condition that are used in cosmology. In the case of detailed balance condition the potential Lagrangian is derivable from a super potential, whereas in the case of beyond detailed balance condition the potential Lagrangian can not be derived from super potential. Both cases are important in cosmology for describing evolution.

1.2 Numerical analysis

The cosmological models obtained with a MCG or a non-linear EoS contains some unknown parameters which play an important role in understanding the evolution of the universe. The range of permitted values of these parameters may be determined making use of the cosmological and astronomical observational data by numerical analysis. The observational data namely, $(H(z)-z)$, BAO peak parameter, CMB shift parameter, dimensionless age parameter, growth parameter, *r.m.s* mass fluctuation data will be employed for numerical analysis defining a suitable *Chi-square* function and thereafter range of values of the parameters are determined by minimizing the above *Chi-square* function.

1.2.1 Likelihood function

In the case of a likelihood function defined by L for a probability distribution function y we know

$$L(EoS \text{ parameters}) \propto \exp \left(- \sum \frac{[y_{th}(EoS \text{ parameters}, z) - y_{obs}(z)]^2}{2\sigma_z^2} \right), \quad (1.26)$$

where $y_{obs}(z)$ is the observed parameter at redshift z and σ_z is the associated error with that particular observation for a function y_{th} . Likelihood function also can be expressed in terms of *Chi-square* function as

$$L(EoS \text{ parameters}) \propto \exp \left(\frac{-\chi_y^2(EoS \text{ parameters})}{2} \right), \quad (1.27)$$

where

$$\chi_y^2(EoS \text{ parameters}) = \sum \frac{[y_{th}(EoS \text{ parameters}, z) - y_{obs}(z)]^2}{\sigma_z^2} \quad (1.28)$$

The above likelihood function can be maximized for EoS parameters by (i) analytic method, (ii) grid search method and (iii) numerical method. This maximization of the likelihood function corresponds to the minimization of the *Chi-square* function.

1.2.2 *Chi-square* minimization and confidence limits

Chi-square function can be constructed for certain distribution with the observed value and the corresponding errors of the distribution. Confidence limit is a common practice to summarize a distribution rather than presenting all details of a distribution. A confidence region (confidence interval) is just a region that contains a certain percentage of the total probability distribution. A certain region may be marked as,

99.7% confidence region, that means there is 99.7 percent chance that the true parameter value falls within the region. Confidence intervals are categorized as 68.3%, 95.4%, 99.7% depending on 1σ , 2σ and 3σ respectively. We use following *Chi-square* function for numerical analysis:

• **Chi-square function for the set of observed $(H(z) - z)$ data:**

We define the **Chi-square** function as

$$\chi_{OHD}^2(EoS \text{ parameters}) = \sum \frac{[H_{th}(EoS \text{ parameters}, z) - H_{obs}(z)]^2}{\sigma_z^2} \quad (1.29)$$

where $H_{obs}(z)$ is the observed Hubble parameter at redshift z and σ_z is the associated error with that particular observation.

• **Chi-square function for the Baryon Acoustic Oscillation (BAO) peak parameter.**

Baryon Acoustic Oscillations (BAO) are frozen relics left over from the pre-decoupling universe. Eisenstein *et al.* [88] detected baryon acoustic oscillations through redshift-space correlation function of the Sloan Digital Sky Survey (SDSS) Luminous Red Galaxies (LRG) sample. This detection confirms that the oscillations occur at $z \approx 1000$ and it survive the intervening time to be detected at low redshift.

Two measured quantities $\Omega_m h^2$ and $D_V(0.35)$ can be combined to a single parameter called BAO peak parameter (\mathcal{A}) which is given as $\mathcal{A} = D_V(z = 0.35) \frac{\sqrt{\Omega_m H_0^2}}{0.35c}$ where $D_V = [D_M^2 \frac{cz}{H(z)}]^{1/3}$ and D_M is the co-moving angular distance.

This model independent BAO peak parameter at low redshift (z_1) can be re-written in flat universe as:

$$\mathcal{A} = \frac{\sqrt{\Omega_m}}{E(z_1)^{1/3}} \left(\frac{\int_0^{z_1} \frac{dz}{E(z)}}{z_1} \right)^{2/3} \quad (1.30)$$

27 MAY 2016

279008



where Ω_m is the matter density parameter for the Universe. The *Chi-square* function may now be defined as follows:

$$\chi_{BAO}^2 = \frac{(\mathcal{A} - 0.469)^2}{(0.017)^2} \quad (1.31)$$

where we have used the measured value for \mathcal{A} (0.469 ± 0.017) as was obtained by [88] from the SDSS data for LRG (Luminous Red Galaxies) survey.

• **CMB shift parameter (\mathcal{R}) is given by:**

To determine constraints on dark energy models a distance scale called CMB shift parameter is useful. The CMB shift parameter determines the shift of the peaks in the CMB power spectrum when cosmological parameters are varied [89, 90, 91]. This parameter can be used as a probe for dark energy if the models have almost identical CMB power spectra and this criteria will be fulfilled if the matter densities (i) $\omega_c = \Omega_c h^2$, (ii) $\omega_b = \Omega_b h^2$ (where $\omega_m = \omega_c + \omega_b$) and (iii) primordial fluctuation spectrum are same [92]. In this case CMB shift parameter is given by

$$\mathcal{R} = \frac{\omega_m^{\frac{1}{2}}}{\omega_k^{\frac{1}{2}}} \sin n_k[\omega_k^{\frac{1}{2}} y] \quad (1.32)$$

where $\sin n_k(x) = \sin(x), x, \sinh(x)$ for $k = +1, 0, 1$ respectively with

$$y = \int_{a_r}^1 \frac{da}{\sqrt{\omega_m a + \omega_k a^2 + \omega_\Lambda a^4 + \omega_Q a^{1-3\omega}}} \quad (1.33)$$

where $\omega_c, \omega_m, \omega_k, \omega_\Lambda, \omega_Q$ represents energy density corresponding to cold dark matter, matter, curvature, cosmological constant and quintessence respectively. ω is the EoS for quintessence and a_r is the scale factor at recombination. In the case of flat universe the CMB shift parameter reduces to

$$\mathcal{R} = \sqrt{\Omega_m} \int_0^{z_{ls}} \frac{dz'}{E(z')} \quad (1.34)$$

where z_{ls} is the z at the surface of the last scattering. The WMAP 7 data gives us $\mathcal{R} = 1.726 \pm 0.018$ at $z = 1091.3$ [93]. The corresponding *Chi-square* function in this case is defined as:

$$\chi_{CMB}^2 = \frac{(\mathcal{R} - 1.726)^2}{(0.018)^2}. \quad (1.35)$$

• The logarithmic growth factor f , according to Wang and Steinhardt is given by

$$f = \Omega_m^\gamma(a) \quad (1.36)$$

where $f = \frac{d \log \delta}{d \log a}$, $\delta = \frac{\delta \rho_m}{\rho_m}$ (δ is the matter density perturbation, $\delta \rho_m$ represents the fluctuations of matter density ρ_m) and γ is the growth index parameter. In the case of flat dark energy model with constant equation of state ω_0 , the growth index γ is given by

$$\gamma = \frac{3(\omega_0 - 1)}{6\omega_0 - 5}. \quad (1.37)$$

For MCG it is approximated to

$$\gamma = \frac{3(1 - \omega_{mcg})}{5 - 6\omega_{mcg}} + (1 - \Omega_m) \frac{3(1 - \omega_{mcg})(1 - \frac{3\omega_{mcg}}{2})}{125(1 - \frac{6\omega_{mcg}}{5})^3}. \quad (1.38)$$

Using the expression of ω_{mcg} in the above, γ can be parametrized with MCG parameters. Therefore the *Chi-square* function corresponding to the growth function f is defined as

$$\chi_f^2(EoS \text{ parameters}) = \Sigma \left[\frac{f_{obs}(z_i) - f_{th}(z_i, \gamma)}{\sigma_{f_{obs}}} \right]^2 \quad (1.39)$$

where f_{obs} and $\sigma_{f_{obs}}$ are observed values of growth functions and associated errors respectively. However, $f_{th}(z_i, \gamma)$ is obtained from cosmological theories.

• The *r.m.s* mass fluctuation $\sigma_8(z)$ is derived from matter density perturbation $\delta(z)$.

The mass fluctuation parameter or over density field for mass (δ) contributes on all cosmological scales. At a very small scales it can have huge value which is insignificant in cosmology. We are interested in determining the properties of the smoothed over density field. Hence a filtering concept is used to filter out the contribution below a certain length scale where the contribution is significant. Mathematically, this is obtained by convolving over density with some window function $W(R)$, i.e. $\delta_R(t, x) = (\delta * W)(t, x) = \int \delta(t, x - x') W(|x'|, R) dx'^3$. The second moment of the smoothed mass density field called variance of mass fluctuations is defined as $\sigma_R^2(t) \equiv \langle \delta_R^2(t, x) \rangle = \langle \delta_R(t, x) \delta_R(t, x) \rangle$. This variance of mass fluctuations can be expressed in terms of linear power spectrum as

$$\sigma^2(R, z) = \int_0^{\text{inf}} W^2(kR) \Delta^2(k, z) \frac{dk}{k} \quad (1.40)$$

where

$$W(kR) = 3 \left(\frac{\sin(kR)}{(kR)^3} - \frac{\cos(kR)}{(kR)^2} \right), \quad (1.41)$$

$$\Delta^2(kz) = 4\pi k^3 P_\delta(k, z), \quad (1.42)$$

with $P_\delta(k, z) \equiv (\delta_k^2)$ is the mass power spectrum at redshift z . The *r.m.s* mass fluctuations ($\sigma_8(z)$) is the variance of mass fluctuations at $R = 8h^{-1}$ Mpc. $\sigma_8(z)$ is the measure of mass that fluctuates within the box $R = 8h^{-1}$ Mpc in the present day universe. The function $\sigma_8(z)$ is connected to $\delta(z)$ as

$$\sigma_8(z) = \frac{\delta(z)}{\delta(0)} \sigma_8|_{(z=0)} \quad (1.43)$$

which implies

$$s_{th}(z_1, z_2) \equiv \frac{\sigma_8(z_1)}{\sigma_8(z_2)} = \frac{\delta(z_1)}{\delta(z_2)} = \frac{\exp \left[\int_1^{\frac{1}{1+z_1}} \Omega_m(a) \gamma \frac{da}{a} \right]}{\exp \left[\int_1^{\frac{1}{1+z_2}} \Omega_m(a) \gamma \frac{da}{a} \right]}. \quad (1.44)$$

Currently available data points $\sigma_8(z_i)$ originate from the observed redshift evolution of the flux power spectrum of Ly- α forest [94, 95, 96]. Finally, we define a new *Chi-square* function which is given by

$$\chi_s^2(EoS \text{ parameters}) = \Sigma \left[\frac{s_{obs}(z_i, z_{i+1}) - s_{th}(z_i, z_{i+1})}{\sigma_{s_{obs},i}} \right]^2, \quad (1.45)$$

where $\sigma_{s_{obs},i}$ is the associated error.

In addition to *Chi-square* analysis we adopted the following functional analysis also :

• **Age Parameter :**

Using the definition of the age parameter [97]

$$t_0 = \int_0^1 \left[\frac{da}{aH(a)} \right] \quad (1.46)$$

where $\frac{a}{a_0} = \frac{1}{1+z}$ and $H(a)$ is the Hubble parameter, the predicted age of the universe becomes

$$t_0 = \frac{1}{H_0} \int_0^1 \left[\frac{da}{aE(a, EoS \text{ parameters})} \right] \quad (1.47)$$

with

$$E(a, EoS \text{ parameters}) = \frac{H(a)}{H_0}. \quad (1.48)$$

We consider $H_0 t_0 = 0.95$ from observational prediction. Although it has some error limits, we take this value as standard.

1.3 Testing viability of models

The viability of cosmological models is tested by a comparison of values of distance modulus (μ) in theoretical models with that of observations. For an object

of luminosity L at a distance D from us, the apparent magnitude (m) and absolute magnitude (M) are defined as

$$m = -2.5 \log \left(\frac{L}{4\pi D^2} \right) + \text{constant}, \quad (1.49)$$

$$M = -2.5 \log(L) + \text{constant}. \quad (1.50)$$

The distance modulus (*i.e.*, supernovae magnitudes) (μ) is defined in terms of the apparent and absolute magnitudes as

$$\mu = m - M. \quad (1.51)$$

The distance modulus can be expressed in terms of luminosity distance d_L as

$$\mu = 5 \log(d_L) + 25 \quad (1.52)$$

where the luminosity distance d_L in the unit of mega parsec is given by

$$d_L = r_1(1+z)a(t_0) \quad (1.53)$$

and

$$\int_0^{r_1} \frac{dr}{\sqrt{1-kr^2}} = \int_{t_1}^{t_0} \frac{dt}{a(t)}. \quad (1.54)$$

The age parameter will also be used to analyze cosmological models.

Chapter 2

Observational Constraints on Exotic Matter in Emergent Universe

2.1 Introduction

EU model proposed by Mukherjee *et al.* [68] in GTR is considered to be an important cosmological model of the universe which is ever existing having no initial singularity and which accommodates a late accelerating phase satisfactorily. In EU model, the universe began to expand from an initial non-singular phase, thereafter smoothly joins with a phase of exponential inflation followed by a standard reheating phase and finally it approaches the classical thermal radiation dominated era analogous to the conventional Big Bang model [69].

The EoS for EU model contains two parameters A and B where $A > 0$. The pecu-

liarity of the model obtained by Mukherjee *et al.* [68] is that it permits a universe with a composition of three types of fluid determined by one parameter B (shown in Table-(1.1)).

It may be mentioned here that in EoS eq. (1.3) for $\alpha = -\frac{1}{2}$, it leads to the EoS required for emergent universe (EU) model. Subsequently existence of EU model in Gauss-Bonnet gravity [86], Brane world gravity [67, 84], Brans-Dicke theory [98] have been examined. Universe in this model is sufficiently big enough to begin with which might stay at the phase for a large enough time to avoid quantum gravitational effects even in the very early universe. Therefore the quantum gravity effect can be avoided. The EoS parameters A, B are arbitrary which can be determined from the observational data. Initially the best-fitted EoS parameters A, B with integration constant K are determined using the observed data set. It is thus worth to investigate the viability of such an EU model with the recent observational data. Nevertheless we intend to explore in this Chapter the allowed range of values of the parameter A ($A > 0$), B for a viable cosmological scenario by observations.

To determine the range of values for A and B permitted by observations we adopt the following techniques as follows: (i) χ^2 minimization technique corresponding to $H(z)$ *vs.* z data (OHD) [99] given in Table-(2.1), (ii) joint analysis of $H(z)$ *vs.* z data and a model independent BAO peak parameter and (iii) joint analysis of $H(z)$ *vs.* z data, BAO peak parameter and CMB shift parameter together. We explore here the suitability of the model with the help of supernovae data (union compilation data) finally.

Table 2.1: $H(z)$ vs. z data (OHD) [99]

z Data	$H(z)$	σ
0.00	73	± 8.0
0.10	69	± 12.0
0.17	83	± 8.0
0.27	77	± 14.0
0.40	95	± 17.4
0.48	90	± 60.0
0.88	97	± 40.4
0.90	117	± 23.0
1.30	168	± 17.4
1.43	177	± 18.2
1.53	140	± 14.0
1.75	202	± 40.4

2.2 Field equations

The Hubble parameter (H) in terms of redshift parameter z is written as

$$H(z) = -\frac{1}{1+z} \frac{dz}{dt} \quad (2.1)$$

using $a = \frac{1}{1+z}$, taking a_0 (a at the present time) = 1. Since components of matter (baryon) and dark energy (exotic matter) are conserved separately, we use energy conservation equation together with EoS given by eq. (1.18) to determine the expression for the energy density. Consequently eq. (1.12) yields:

$$\rho_{emu} = \left[\frac{A}{1+B} + \frac{1}{B+1} \frac{K}{a^{\frac{3(B+1)}{2}}} \right]^2, \quad (2.2)$$

where K is an integration constant which is positive quantity. From eq. (2.2) it is evident that the energy density is composed of three different terms, where a constant term $(\frac{A}{1+B})^2$ may be identified with a cosmological constant and the other two terms are identified with two different types of fluid determined by the parameter B . Using the Friedmann equation (1.9) we express H in terms of redshift parameter z for the

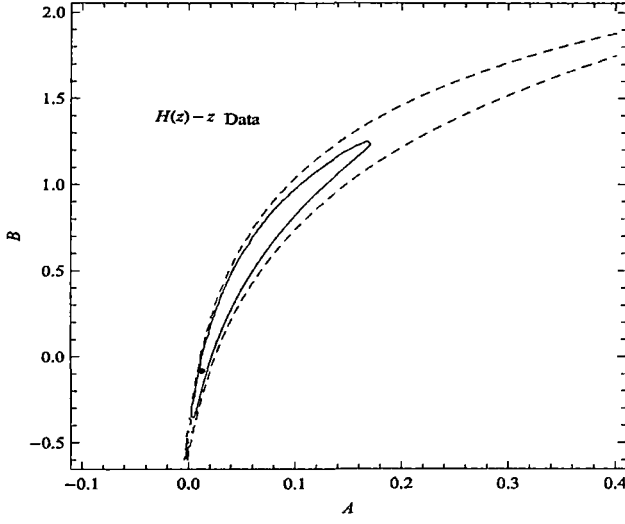


Figure 2.1: $A - B$ contours using $H(z)$ vs. z data (OHD) for $K = 0.0100$ at 95.4% (Solid) and 99.7% (Dashed) confidence level. The best-fit point is shown (0.0122, -0.0823).

model, which is given by

$$H(z) = H_0 \left[\Omega_{b_0}(1+z)^3 + (1 - \Omega_{b_0}) \left(\frac{A + K(1+z)^{\frac{3(B+1)}{2}}}{A + K} \right)^2 \right]^{\frac{1}{2}}, \quad (2.3)$$

with $\Omega = \Omega_{b_0} + \Omega_{em_0} = 1$, where Ω is composed of baryon and exotic fluids. Ω_{b_0} represents baryon energy density and Ω_{em_0} represents the exotic fluid density.

2.3 $(H(z) - z)$ data (OHD) as a constraining tool

The EU model obtained by Mukherjee *et al.* [68] is implemented in a flat universe. Consequently we consider a composition of baryonic matter and the exotic matter in a flat Friedmann universe permitted by EoS given by eq. (1.18) to constrain the EoS parameters. The Hubble parameter given by eq. (2.3) is a function of a number of

variables, which can be re-written as :

$$H^2(H_0, A, B, K, z) = H_0^2 E^2(A, B, K, z), \quad (2.4)$$

where

$$E(A, B, K, z) = \left[\Omega_{b_0}(1+z)^3 + (1 - \Omega_{b_0}) \left(\frac{A + K(1+z)^{\frac{3(B+1)}{2}}}{A + K} \right)^2 \right]^{\frac{1}{2}} \quad (2.5)$$

is the dimensionless Hubble parameter. The best-fit values for the unknown parameters of the model, namely A , B and K are determined by minimizing $\chi^2_{(H-z)}$ function which is given below

$$\chi^2_{(H-z)}(H_0, A, B, K, z) = \sum \frac{[H(H_0, A, B, K, z) - H_{obs}(z)]^2}{\sigma_z^2} \quad (2.6)$$

where $H_{obs}(z)$ is the observed Hubble parameter at redshift z and σ_z is the error associated with that particular observation, the suffix $(H - z)$ corresponds to use of Hubble parameter *vs.* redshift data [99]. Since we are interested in determining the model parameters, H_0 is not important for our analysis. So we marginalize the function over H_0 to get the probability distribution function in terms of A, B, K only, which is given by

$$L(A, B, K) = \int dH_0 P(H_0) \exp \left(\frac{-\chi^2_{(H-z)}(H_0, A, B, K, z)}{2} \right), \quad (2.7)$$

where $P(H_0)$ is the prior distribution function for the present Hubble constant. Here we consider Gaussian priors with $H_0 = 72 \pm 8$ [100]. The function χ^2 is minimized by maximizing the likelihood function $L(A, B, K)$. We fix K at the best-fitted value and contours in A - B plane are drawn at different confidence limit. However, fixing of K is allowed as we are interested to obtain range of A and B which is related to the EoS

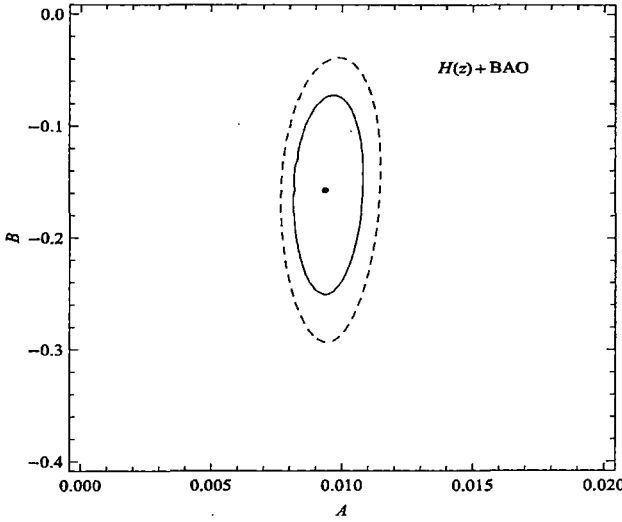


Figure 2.2: $A - B$ contours using OHD data and BAO peak parameter with $K = 0.0101$. 95.4% (Solid) and 99.7% (Dashed) confidence levels are shown in the figure along with the best-fit value (0.0094, -0.1573)

given by eq. (1.18). K enters in the theory as an integration constant which is always positive ($K > 0$). In fig. (2.1) we draw 95.4% and 99.7% contours on A - B plane. We see that within 95.4% confidence limit A and B lies in the range $-0.0011 \leq A \leq 0.1731$ and $-0.5864 \leq B \leq 1.254$. We see that within 99.7% confidence limit A and B lies in the range $-0.0022 \leq A \leq 0.389$ and $-0.5949 \leq B \leq 1.663$. A positive value of A permits a viable cosmological scenario.

2.4 Joint analysis with OHD and BAO peak parameter

In this section we use the technique adopted by [88] to study the BAO peak parameter \mathcal{A} (which is determined by A). For a flat universe \mathcal{A} is given by eq. (1.30) with $\Omega_m = \Omega_b + (1 - \Omega_b)(1 - \frac{A}{K+A})^2$. From observations, we get the values

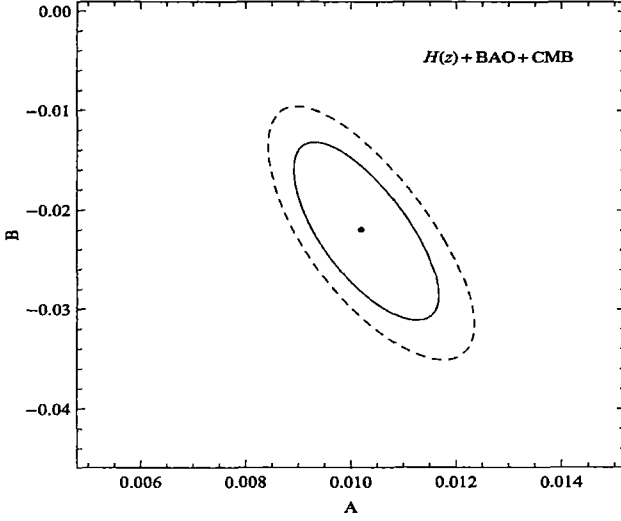


Figure 2.3: $A - B$ contours using OHD data, BAO peak parameter and CMB shift parameter for $K = 0.0102$. 95.4% (Solid) and 99.7% (Dashed) confidence levels are shown in the figure along with the best-fit value (0.0103, -0.0219)

$A = 0.469 \pm 0.017$ at $z_1 = 0.35$. For joint analysis we consider $\chi_{joint}^2 = \chi_{(H-z)}^2 + \chi_{BAO}^2$ where χ_{BAO}^2 is given by eq. (1.31). The joint analysis with BAO here sets a new constraints on A and B , which are $0.0082 \leq A \leq 0.0108$ and $-0.2527 \leq B \leq -0.0715$ up to 95.4% confidence level and $0.0077 \leq A \leq 0.0116$ and $-0.3053 \leq B \leq -0.0306$ up to 99.7% confidence level.

2.5 Joint analysis with OHD , BAO peak parameter and CMB shift parameter (\mathcal{R})

In this section we use CMB shift parameter (\mathcal{R}) given by eq. (1.34). The WMAP 3 data gives us $\mathcal{R} = 1.70 \pm 0.03$ [101]. Thus we define $\chi_{CMB}^2 = \frac{(\mathcal{R}-1.70)^2}{(0.03)^2}$ in $\chi_{Tot}^2 = \chi_{(H-z)}^2 + \chi_{BAO}^2 + \chi_{CMB}^2$ which impose additional constraints on the model parameters. The statistical analysis with χ_{Tot}^2 further tightens up the bounds on A and B . In fig.

<i>Data</i>	<i>A</i>	<i>B</i>	<i>K</i>
<i>OHD</i>	0.0122	-0.0823	0.0100
<i>OHD + BAO</i>	0.0094	-0.1573	0.0101
<i>OHD + BAO + CMB</i>	0.0103	-0.0219	0.0102

Table 2.2: Best-fit values of the EoS parameters

<i>Data</i>	<i>CL</i>	<i>A</i>	<i>B</i>
<i>OHD</i>	95.4%	(-0.0011, 0.1731)	(-0.5864, 1.254)
	99.7%	(-0.0022, 0.389)	(-0.5949, 1.663)
<i>OHD + BAO</i>	95.4%	(0.0082, 0.0108)	(-0.2527, -0.0715)
	99.7%	(0.0077, 0.0116)	(-0.3053, -0.0306)
<i>OHD + BAO + CMB</i>	95.4%	(0.0089, 0.0117)	(-0.0313, -0.0131)
	99.7%	(0.0080, 0.013)	(-0.037, -0.009)

Table 2.3: Range of values of the EoS parameters using OHD+BAO+CMB data

(2.3), 95.4% and 99.7% contours are plotted on A - B plane. We determine constraints from this analysis: within 95.4% confidence limit we get $0.0089 \leq A \leq 0.0117$ and $-0.0313 \leq B \leq -0.0131$. However, within 99.7% confidence level $0.008 \leq A \leq 0.013$ and $-0.037 \leq B \leq -0.009$. The best-fit value obtained here is given by $A = 0.0103$, $B = -0.0219$ and $K = 0.0102$. The best-fit values of the model parameters obtained from different data are shown in Table-(2.2) and the corresponding range are shown in Table-(2.3). Finally we draw a supernovae magnitudes $\mu(z)$ vs. redshift z curve for our model with the best-fit values of A , B and K and also show the same curve drawn from union compilation data for SNIa [102] in fig. (2.4).

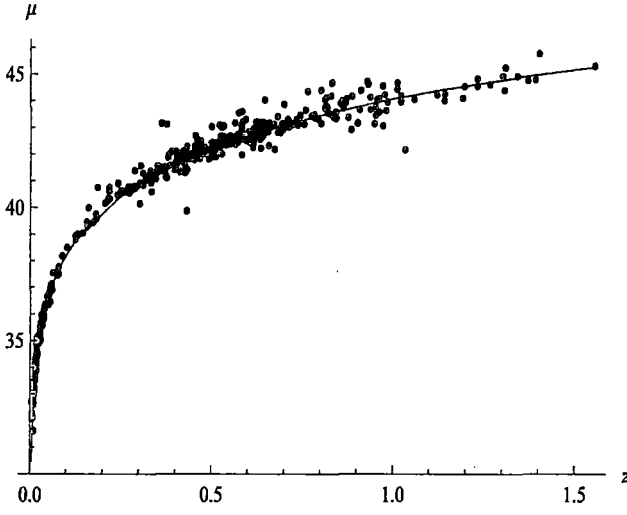


Figure 2.4: Comparison of $\mu(z)$ vs. z curve with supernovae data

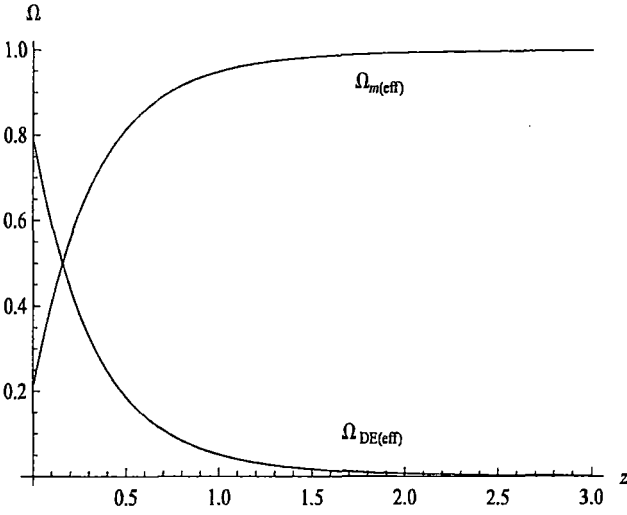


Figure 2.5: Variation of density parameter (Ω) for effective dark energy and effective matter content of the universe with redshift.

2.6 Discussions

The emergent universe model obtained with a non-linear equation of state contains two arbitrary parameters A and B which are determined using observational data. We obtain range of values of the EoS parameters by numerical analysis. The best-fit values of A and B are determined which are given by $A = 0.0103$, $B = -0.0219$ with integration constant $K = 0.0102$. Within 99.7% confidence level the parameter A and B lies in the following range $0.008 \leq A \leq 0.013$ and $-0.037 \leq B \leq -0.009$. The evolution of various cosmological parameters of the model are also studied. The density parameter for effective dark energy and effective matter content of the universe with the redshift are plotted in fig. (2.5). It is noted that almost 80% of the present matter-energy content is dominated by effective dark energy and the remaining constituents are baryonic and non-baryonic matters. The effective equation of state (ω_{eff}) for EU remains negative which is plotted in fig. (2.6 a). The transition of the universe from a deceleration phase to an accelerating phase in recent past is evident from the plot of deceleration parameter against redshift in fig. (2.6 b). Supernovae magnitudes $\mu(z)$ vs. redshift z curve is drawn at the best-fit values of A , B and K and compared with union compilation data for SNeIa [102] in fig. (2.4). The results are in agreement with observations.

1

^{1*} We use EoS for emergent universe $p = B\rho - A\rho^{\frac{1}{2}}$ which is different from that used in the published paper $p = A\rho - B\rho^{\frac{1}{2}}$ for a consistent representation with MCG

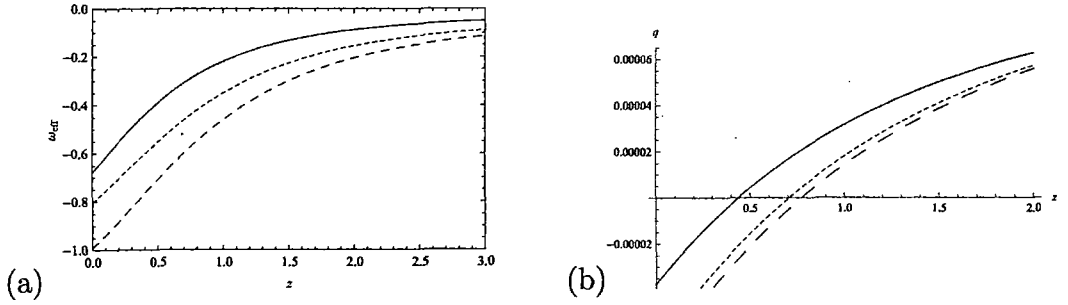


Figure 2.6: (a) Variation of effective EoS parameter for EU (ω_{eff}) with redshift (z). (b) Variation of deceleration parameter (q) with redshift (z). Solid, Dashed and Dotted line corresponds to the best-fit values, 95.4% confidence level and 99.7% confidence level respectively.

Chapter 3

Observational Constraints on EoS parameters for a class of Emergent Universe

3.1 Introduction

Emergent universe scenario in the GTR which can be realized in the presence of a non-linear equation of state (in short, EoS) is discussed in the previous Chapter. There are two unknowns in the EoS namely A and B which are arbitrary constants. It is interesting to note that the non-linear EoS admits a cosmological model effectively with a composition of three different fluids for a given B . Mukherjee *et al.* [68] tabulated the composition of fluids for discrete values of B^* namely, $-\frac{1}{3}, 0, \frac{1}{3}, 1$. Cosmological model with $B = 0$ is very interesting as it can accommodate dust, exotic matter and dark energy.

In this Chapter EU is analyzed using observational data namely, Observed Hubble data (OHD) [99], SDSS data measuring a model independent BAO peak parameter [88] and WMAP 7 measurement of CMB shift parameter. The permissible range of values of A and B are determined from the observations. The evolution of density in each of the model from early to late era is also studied.

3.2 Field equations

The Hubble parameter H corresponding to a flat universe which may be obtained from the Einstein's field equation (1.9). The matter conservation equation is given by eq. (1.12). Using the EoS given by eq. (1.18) in eq. (1.12) one obtains:

$$\rho(z) = \left(\frac{A}{B+1}\right)^2 + \frac{2AK}{(B+1)^2} (1+z)^{\frac{3(B+1)}{2}} + \left(\frac{K}{B+1}\right)^2 (1+z)^{3(B+1)} \quad (3.1)$$

where z represents the cosmological redshift. The first term in the right hand side of eq. (3.1) is a constant which can be interpreted as cosmological constant and useful for describing dark energy. Eq. (3.1) can be re-written as:

$$\rho(z) = \rho_0 + \rho_1 (1+z)^{\frac{3(B+1)}{2}} + \rho_2 (1+z)^{3(B+1)} \quad (3.2)$$

where $\rho_0 = \left(\frac{A}{B+1}\right)^2$, $\rho_1 = \frac{2AK}{(B+1)^2}$ and $\rho_2 = \left(\frac{K}{B+1}\right)^2$ are the densities of the fluid components at the present epoch. The Friedmann equation (1.9) can be re-written in terms of redshift and density parameters as follows:

$$H^2(z) = H_0^2 \left[\Omega_0 + \Omega_1 (1+z)^{\frac{3(B+1)}{2}} + \Omega_2 (1+z)^{3(B+1)} \right] \quad (3.3)$$

where we define density parameter: $\Omega = \frac{8\pi G\rho}{3H_0^2} = \Omega(A, B, K)$. Fixing B one can re-write eq. (3.3) as:

$$H^2(H_0, A, K, z) = H_0^2 E^2(A, K, z) \quad (3.4)$$

08.3%, 95.4% and 99.7% confidence regions are shown with $B = 0$, $B = \frac{2}{3}$, $B = 1$:

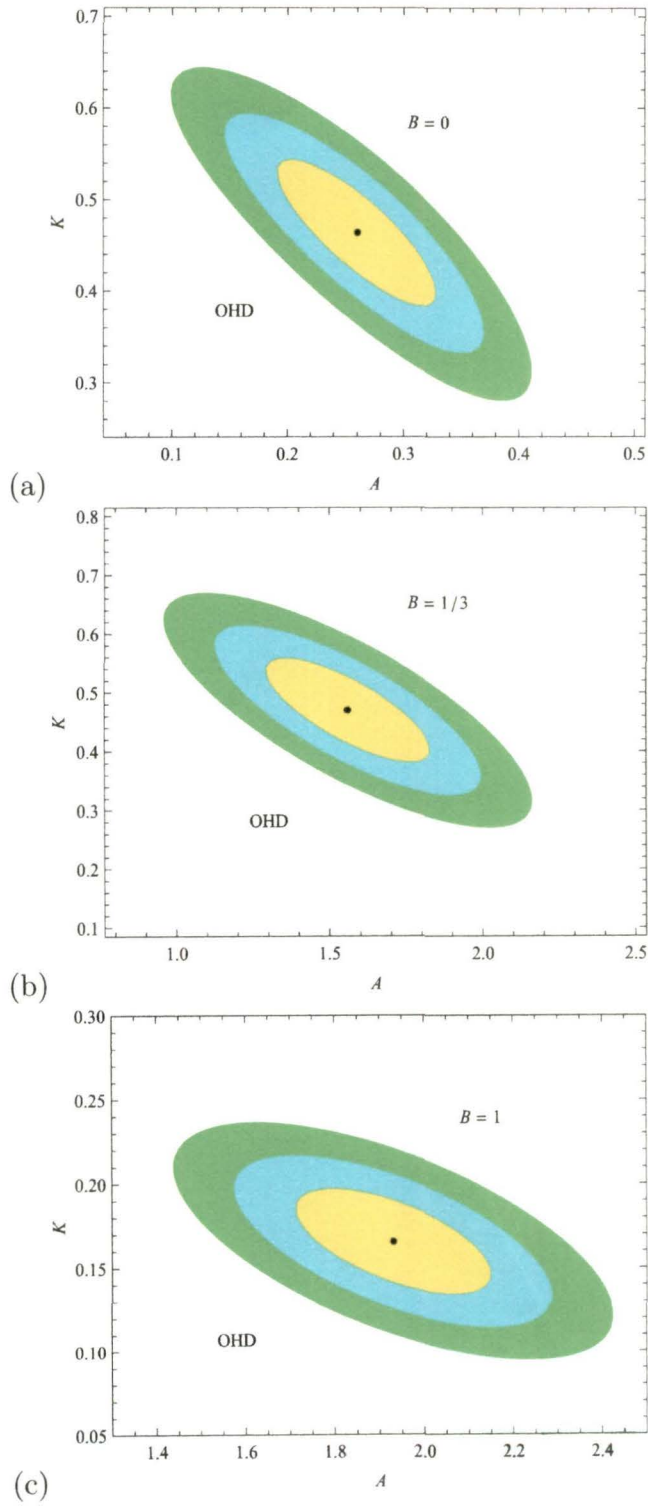


Figure 3.1: $K - A$ contours using OHD data for EU with $B = 0$, $B = \frac{1}{3}$, $B = 1$: 68.3%, 95.4% and 99.7% confidence regions are shown

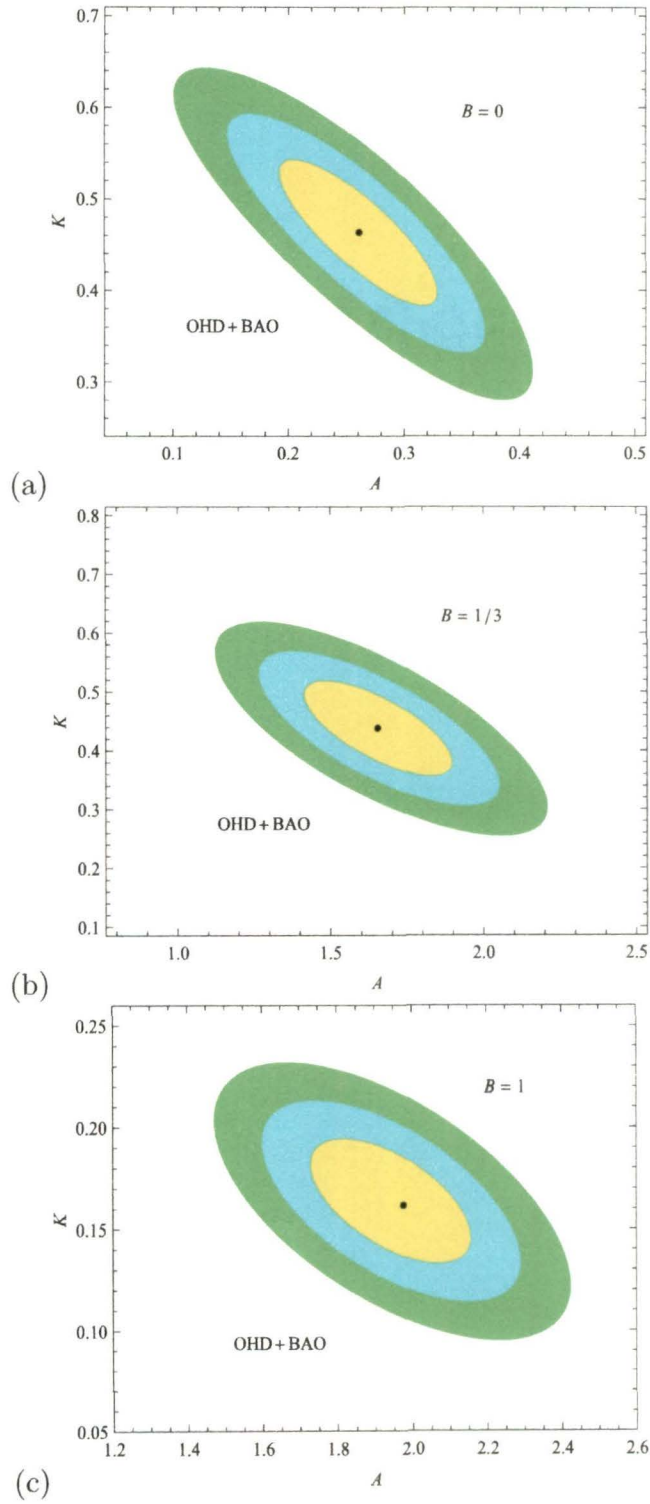


Figure 3.2: $K - A$ contours using *OHD* and SDSS (BAO) data for EU with $B = 0$, $B = \frac{1}{3}$ and $B = 1$: 68.3%, 95.4% and 99.7% confidence regions are shown

where,

$$E^2(A, K, z) = \Omega_\Lambda + \Omega_1 (1+z)^{\frac{3(B+1)}{2}} + \Omega_2 (1+z)^{3(B+1)}. \quad (3.5)$$

The constant part of the density parameter is represented by Ω_Λ , which corresponds to dark energy.

3.3 Analysis with observational data

In the next section we use data from OHD, BAO peak parameter, CMB shift parameter to analyze cosmological models.

3.3.1 Observed Hubble data (OHD)

Using observed value of Hubble parameter at different redshifts (*twelve data points listed in Observed Hubble data [99] shown in Table-(2.1)*) we analyze the Emergent Universe model in this section. Let us define a *Chi-square* function as follows:

$$\chi_{OHD}^2 = \sum \frac{(H_{Th}(H_0, A, K, z) - H_{Ob})^2}{\sigma^2} \quad (3.6)$$

where H_{Th} and H_{Ob} are theoretical and observational values of Hubble parameter at different redshifts respectively and σ is the corresponding error. Here, H_0 is a nuisance parameter and can be safely marginalized. We consider $H_0 = 72 \pm 8$ [100] with a fixed prior distribution. A reduced *Chi-square* function (χ_{red}^2) can be defined as follows:

$$\chi_{red}^2 = -2 \ln \int \left[e^{-\frac{\chi_{OHD}^2}{2}} P(H_0) \right] dH_0 \quad (3.7)$$

where $P(H_0)$ is the prior distribution.

For the numerical analysis we consider cosmologies for three different values of B

Model	A	K	χ^2_{min} (d.o.f)
$B = 0$	0.2604	0.4640	1.026
$B = \frac{1}{3}$	1.559	0.4702	0.737
$B = 1$	1.931	0.1656	0.818

Table 3.1: Best-fit values using OHD data

Model	CL	A	K
$B = 0$	68.3%	(0.1907, 0.3263)	(0.3807, 0.5461)
	95.4%	(0.1445, 0.3696)	(0.3287, 0.5980)
	99.7%	(0.0983, 0.410)	(0.2787, 0.6461)
$B = \frac{1}{3}$	68.3%	(1.299, 1.817)	(0.3781, 0.5606)
	95.4%	(1.124, 1.991)	(0.3212, 0.6175)
	99.7%	(0.9608, 2.160)	(0.2674, 0.6713)
$B = 1$	68.3%	(1.713, 2.144)	(0.1343, 0.1968)
	95.4%	(1.581, 2.290)	(0.1135, 0.2187)
	99.7%	(1.443, 2.425)	(0.0947, 0.2364)

Table 3.2: Range of values of the EoS parameters using OHD data

which are 0, $\frac{1}{3}$, 1. We plot contours of A with K for different B . In drawing the above contours we consider positive values of A and K . The regions of 68.3%, 95.4% and 99.7% confidence level are shown in fig. (3.1 a), fig. (3.1 b) and in fig. (3.1 c) for $B = 0$, $B = \frac{1}{3}$ and $B = 1$ respectively. The best-fit values and the range of values of the parameters in this case corresponds to the OHD data which are tabulated in Table-(3.1) and Table-(3.2) respectively.

3.3.2 Joint analysis with BAO peak parameter

In this section we consider analysis that is independent of the measurement of H_0 and does not consider any particular dark energy model. For this a method proposed by Eisenstein *et al.* [88] is considered here. A model independent BAO

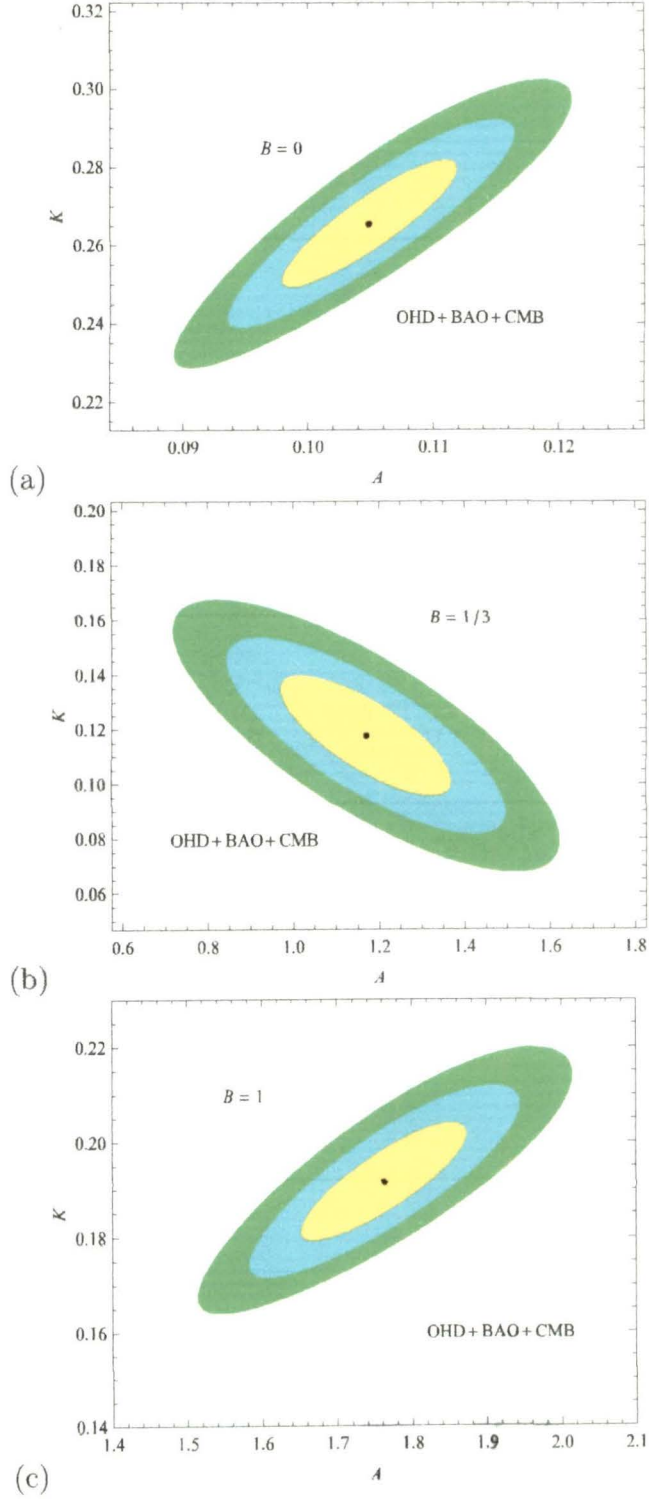


Figure 3.3: $K - A$ contours using OHD, SDSS (BAO) and WMAP 7 (CMB shift) data for EU with $B = 0$, $B = \frac{1}{3}$ and $B = 1$: 68.3%, 95.4% and 99.7% confidence regions are shown

Model	A	K	χ_{min}^2 (d.o.f)
$B = 0$	0.2609	0.4636	1.168
$B = \frac{1}{3}$	1.6525	0.4383	0.707
$B = 1$	1.9768	0.1617	0.875

Table 3.3: Best-fit values using OHD + SDSS (BAO) data

(Baryon Acoustic Oscillation) peak parameter can be defined for low redshift (z_1) measurements in a flat universe as in eq. (1.30), where Ω_m is the matter density parameter for the Universe. The definition of *Chi-square* function is same as given in eq. (1.31). The measured value for \mathcal{A} (0.469 ± 0.017) as was obtained in Ref. [88] from the SDSS data for LRG (*Luminous Red Galaxies*) survey is considered here. The total *Chi-square* function for joint analysis is defined as:

$$\chi_{tot}^2 = \chi_{red}^2 + \chi_{BAO}^2. \quad (3.8)$$

The 68.3%, 95.4% and 99.7% regions obtained from this joint analysis are shown in figs. (3.2 a), (3.2 b), (3.2 c) for $B = 0$, $B = \frac{1}{3}$ and $B = 1$ respectively. The best-fit values and the range of values of the parameters of importance for $B = 0$, $B = \frac{1}{3}$, $B = 1$ from the OHD+BAO data are tabulated in Table-(3.3) and Table-(3.4) respectively.

3.3.3 Joint analysis with OHD, BAO peak parameter and CMB shift parameter (\mathcal{R})

In addition to OHD and BAO peak parameter we analyze cosmological models using CMB shift parameter (\mathcal{R}) which is given by eq. (1.34). The WMAP 7 data gives us $\mathcal{R} = 1.726 \pm 0.018$ at $z = 1091.3$ [93]. Thus the new *Chi-square* function

Model	CL	A	K
$B = 0$	68.3%	(0.1921, 0.3277)	(0.3826, 0.5442)
	95.4%	(0.1459, 0.3710)	(0.3307, 0.5961)
	99.7%	(0.0998, 0.4114)	(0.2806, 0.6442)
$B = \frac{1}{3}$	68.3%	(1.413, 1.893)	(0.3541, 0.5187)
	95.4%	(1.266, 2.051)	(0.3003, 0.5726)
	99.7%	(1.119, 2.203)	(0.2524, 0.6175)
$B = 1$	68.3%	(1.727, 2.156)	(0.1343, 0.1968)
	95.4%	(1.606, 2.285)	(0.1136, 0.2145)
	99.7%	(1.472, 2.419)	(0.0948, 0.2324)

Table 3.4: Range of values of the EoS parameters using OHD + BAO data

Model	A	K	χ^2_{min} (d.o.f)
$B = 0$	0.1048	0.2654	1.341
$B = \frac{1}{3}$	1.169	0.1175	0.925
$B = 1$	1.762	0.192	0.925

Table 3.5: Best-fit values using *OHD+SDSS (BAO)+WMAP 7* (CMB shift) data

is defined as $\chi^2_{tot} = \chi^2_{(H-z)} + \chi^2_{BAO} + \chi^2_{CMB}$ which imposes additional constraints on the model parameters. The statistical analysis with the new *Chi-square* function χ^2_{tot} puts further tight bounds on the range of permissible values of A and K . In figs. (3.3 a), (3.3 b) and (3.3 c) we plot contours with $B = 0$, $B = \frac{1}{3}$ and $B = 1$ respectively at different confidence level. The best-fit values and the range of values of the parameters corresponding to $B = 0$, $B = \frac{1}{3}$, $B = 1$ obtained from the OHD+BAO+CMB data analysis are tabulated in Table-(3.5) and Table-(3.6) respectively .

3.3.4 Goodness of fit

In the above numerical analysis the values of χ^2 per degrees of freedom are determined. Generally, numerical value of χ^2 per degree of freedom should be 1. However, a better qualitative assessment may be obtained determining χ^2 -probability as dis-

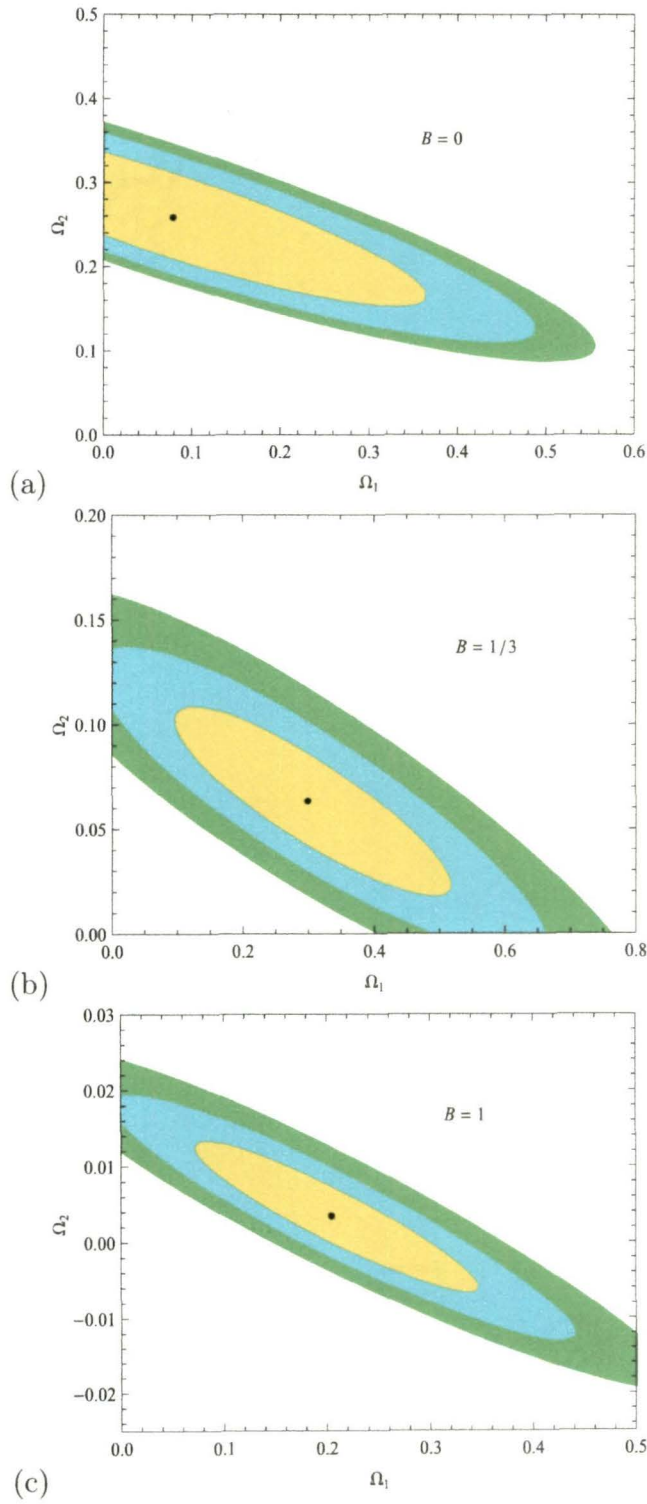


Figure 3.4: $\Omega_1 - \Omega_2$ contours for (a) $B = 0$, (b) $B = \frac{1}{3}$ and (c) $B = 1$: 68.3%, 95.4% and 99.7% confidence regions are shown.

Model	CL	A	K
$B = 0$	68.3%	(0.0979, 0.1118)	(0.2488, 0.2818)
	95.4%	(0.0934, 0.1164)	(0.2384, 0.2922)
	99.7%	(0.0892, 0.1210)	(0.2284, 0.3021)
$B = \frac{1}{3}$	68.3%	(0.9657, 1.368)	(0.0952, 0.1401)
	95.4%	(0.8368, 1.497)	(0.0808, 0.1544)
	99.7%	(0.7157, 1.618)	(0.0672, 0.1688)
$B = 1$	68.3%	(1.655, 1.873)	(0.1791, 0.204)
	95.4%	(1.581, 1.947)	(0.1715, 0.212)
	99.7%	(1.514, 2.016)	(0.1638, 0.2201)

Table 3.6: Range of values of the EoS parameters using *OHD + BAO + CMB* data

Model	$P(OHD)$	$P(BAO)$	$P(CMB)$
$B = -\frac{1}{3}$	0.715	0.004	$0 << .001$
$B = 0$	0.698	0.664	0.194
$B = \frac{1}{3}$	0.689	0.733	0.004
$B = 1$	0.5721	0.562	0.520

Table 3.7: Goodness of fit

cussed in Ref. [103]. In the case of a model where χ^2 is a function of one variable say, x for n degrees of freedom, the probability distribution is given by:

$$P(n, x) = \frac{1}{\Gamma\left(\frac{n}{2}\right)} \int_{x/2}^{\infty} e^{-u} u^{n/2-1} du. \quad (3.9)$$

However, this strictly holds good for normally distributed errors. In the case of non-Gaussian distribution the probability P decreases. Generally, models with $P > 0.001$ is considered acceptable. For different EU models, we tabulated P in Table-(3.7). Note that the EU model with $B = -\frac{1}{3}$ yields very poor fit with WMAP 7 data. So the above model fails the credibility test and cosmological model with $B = -\frac{1}{3}$ is ruled out by observations.

Model	Ω_1	Ω_2	Ω_Λ
$B = 0$	0.079	0.259	0.662
$B = \frac{1}{3}$	0.299	0.063	0.638
$B = 1$	0.205	0.004	0.791

Table 3.8: Best-fit values of density parameters

3.4 Density parameters in different EU model

In the previous section the parameters A and K are determined for $B = 0, \frac{1}{3}, 1$ respectively. In this section we study the evolution of density parameters. In fig. (3.4) contours are drawn on $\Omega_1 - \Omega_2$ plane. The different contours for 68.3%, 95.4% and 99.7% confidence level are also shown. Here Ω_2, Ω_1 represent dust and exotic matter for $B = 0$ which is shown in fig. (3.4 a). It is noted that at best-fit value $\Omega_1 + \Omega_2 = 0.338$ leads to $\Omega_\Lambda = 0.662$. It is also observed that $\Omega_\Lambda \approx 0.72$ and $\Omega_2 \approx 0.04$ are not ruled out within 68.3% confidence level. For $B = \frac{1}{3}$ in fig. (3.4 b), Ω_1 represents density parameter (DP) for cosmic strings and Ω_2 represents DP for radiation. EU model with $B = 1$ leads to a universe with a composition of dark energy (Ω_Λ), dust (Ω_1) and stiff matter (Ω_2) [68] which is plotted in fig. (3.4 c). The best-fit values for Ω_1 and Ω_2 for different models are obtained which in turn determines the best-fit values for Ω_Λ in the corresponding model as:

$$\Omega_\Lambda = 1 - \Omega_1 - \Omega_2. \quad (3.10)$$

The best-fit values for the density parameters of EU are tabulated in Table-(3.8).

3.5 Discussion

A class of EU models are permitted in GTR with a composition of three different types of fluid where one of the constituents is dark energy as shown by [68] for $B = -\frac{1}{3}, 0, \frac{1}{3}, 1$ respectively. The EoS parameters of the EU are constrained using the observed Hubble data (OHD) as well as using a joint analysis with the measurement of a BAO peak parameter. Using the definition of BAO peak parameter as proposed in [88] we analyze cosmological models. Also we obtain observational constraints on EoS parameter from the measurement of CMB shift parameter (\mathcal{R}) as predicted by WMAP 7. It is found from the numerical analysis that the case $B = -\frac{1}{3}$ cannot be fitted well with WMAP 7 data and hence the EU model corresponding to the above B value is ruled out. In the other cases for $B = 0$, $B = \frac{1}{3}$ and $B = 1$ one obtains cosmological models with physically realistic density parameters. Consequently density in $\Omega_1 - \Omega_2$ plane are plotted at 68.3%, 95.4% and 99.7% confidence level which are shown in fig. (3.4). The best-fit values for the model parameters A and K are determined and the corresponding contours are drawn at 68.3%, 95.4% and 99.7% confidence level for $B = 0$, $B = \frac{1}{3}$ and $B = 1$. Using *OHD*, *OHD + BAO*, *OHD + BAO + CMB* data we plot contours between A and K , which are shown in the figs. (3.1), (3.2), (3.3) respectively. It is found that the model admits dark energy density close to that predicted by observations in Λ CDM cosmology.

1

^{1*} Please note that the EoS for emergent universe expressed here as $p = B\rho - A\rho^{\frac{1}{2}}$ which is different from the convention used in the published paper $p = A\rho - B\rho^{\frac{1}{2}}$, this is done to keep similarity with modified Chaplygin gas EoS.

Chapter 4

Observational Constraints on the B parameter of Modified Chaplygin gas as DE

4.1 Introduction

The discovery of late accelerating universe from different cosmological observations namely, high redshift surveys of SNe Ia [49, 50, 51, 52, 104], CMBR ([105]-[109]), WMAP ([110]-[114]) etc. posed a challenge to the theoretical arena of physics. The fields available in the standard model of particle physics fails to accommodate such a phase of acceleration in late universe in the framework of GTR. A modified matter sector of the Einstein gravity with exotic matter are taken up in the literature to understand this issue. The main problem with usual matter and scalar field is that it cannot permit a phase of the matter with pressure $p < 0$ and EoS parameter $\omega < -\frac{1}{3}$.

The new kind of matter/energy required to describe the accelerating expansion of the late universe is called dark energy. When cosmological observations are analyzed in the framework of Big Bang cosmology it is estimated that dark energy constitutes about 73% of the matter/energy of the universe.

In the literature, cosmological constant is considered as one of the candidates for dark energy which is uniformly distributed in the form of vacuum energy density. But cosmological constant is not suitable for describing late universe as it leads to cosmic coincidence problem [115, 116, 117]. A number of unusual fields namely, phantoms [118, 119, 120], tachyons [121, 122, 123], quintessence [124, 125, 126], K-essence [127, 128, 129], exotic matter etc. are considered in the literature. One of the promising candidates for exotic matter namely, Chaplygin gas (CG) which has positive energy density in the early universe with a negative pressure is considered recently to construct model of the universe accommodating late acceleration. But CG is ruled out by observations. Subsequently GCG and MCG are proposed to address the cosmological issues. Here cosmological models are discussed with MCG that are relevant from observational aspects. There are three parameters for MCG which are to be constrained from observations. Considering a dimensionless age parameter $H_0 t_0$ [97] and $(H(z) - z)$ data [130], we analyze cosmological models with MCG and thereafter determine the EoS parameters.

The age parameter $(H_0 t_0)$ is a dimensionless quantity which is constant irrespective of the cosmological models. For simplicity we choose its standard value to be 0.95 (ignoring error). Using the constant age parameter we determine the effective ranges of values of the free parameters in this model. Subsequently using $(H(z) - z)$ data

Table 4.1: $(H - z)$ data from Wu P *et al.* [130]

z Data	$H(z)$	σ
0.09	69	± 12.0
0.17	83	± 8.3
0.27	70	± 14.0
0.40	87	± 17.4
0.88	117	± 23.4
1.30	168	± 13.4
1.43	177	± 14.2
1.53	140	± 14.0
1.75	202	± 40.4

we further determine the constraints on the parameters in terms of age parameter analysis. Using Hubble parameter *vs.* redshift data given in Table-(4.1) we analyze cosmological models. The χ^2 minimization technique is used here. There are nine data points of $H(z)$ at different redshift z which are used to constrain the EoS parameters of the MCG. Both Cold Dark Matter (CDM) and Unified Dark Matter Energy (UDME) models are considered in next sections. UDME model refers to the model in which the modified Chaplygin gas (MCG) may be regarded as dark matter and dark energy as a whole, where the total energy density comprises of radiation, baryon and MCG energy density. In the case of CDM model, the constituents of the universe are considered to be radiation, CDM and MCG.

4.2 Analysis of cosmological models

Using eq. (1.3) in eq. (1.12), the expression for the energy density of MCG can be expressed in terms of the scale factor of the universe $a(t)$, which is given by

$$\rho = \left[\frac{A}{1+B} + \frac{C}{a^{3n}} \right]^{\frac{1}{1+\alpha}} \quad (4.1)$$

where C is an arbitrary constant and we denote $(1+B)(1+\alpha) = n$. Equation (4.1) can be further re-written as

$$\rho = \rho_o \left[A_s + \frac{1 - A_s}{a^{3n}} \right]^{\frac{1}{1+\alpha}}, \quad (4.2)$$

where

$$A_s = \frac{A}{1 + B} \frac{1}{\rho_o^{\alpha+1}}, \quad (4.3)$$

$$\frac{a}{a_0} = \frac{1}{1+z} \quad (4.4)$$

a_0 being the scale factor of the universe at the present epoch, we choose $a_0 = 1$ for convenience. It reduces to GCG model when we set $B = 0$. The Friedmann's equation obtained from eq. (1.9) and eqs. (4.2-4.4), can be expressed as

$$H(z) = H_0 \left[\Omega_{r0}(1+z)^4 + \Omega_{j0}(1+z)^3 + (1 - \Omega_{r0} - \Omega_{j0}) \left[A_s + (1 - A_s)(1+z)^{3n} \right]^{\frac{1}{1+\alpha}} \right]^{\frac{1}{2}} \quad (4.5)$$

where H_0 is the present Hubble parameter. The above equation in terms of a is given by

$$H(a) = H_0 \left[\frac{\Omega_{r0}}{a^4} + \frac{\Omega_{j0}}{a^3} + (1 - \Omega_{r0} - \Omega_{j0}) \left[A_s + \frac{1 - A_s}{a^{3n}} \right]^{\frac{1}{1+\alpha}} \right]^{\frac{1}{2}} \quad (4.6)$$

where $j = m$ for CDM model and $j = b$ for UDME model. The above equations corresponds to GCG model for $B = 0$. The deceleration parameter ($q_0 = -(\frac{a\ddot{a}}{\dot{a}^2})_{t_0}$) at the present time can be written as

$$q_0 = \frac{3}{2} \left[\frac{\Omega_{j0} + \frac{4}{3}\Omega_{r0} + (1+B)(1 - \Omega_{j0} - \Omega_{r0})(1 - A_s)}{\Omega_{j0} + \Omega_{Cg_0} + \Omega_{r0}} \right] - 1 \quad (4.7)$$

where $j = m$ for CDM model and $j = b$ for UDME model. The deceleration parameter can be estimated both in CDM and UDME model. For a flat universe we have

$\Omega_{j0} + \Omega_{Cg0} + \Omega_{r0} = 1$ which will be used to measure the parameters in the next section. In the above Ω_{Cg0} represents the present day modified Chaplygin gas energy density, Ω_{j0} is the present energy density of either Cold Dark Matter (in CDM model) or baryon energy density (in UDME model) and Ω_{r0} represents the present radiation energy density of our universe.

4.3 Age of the universe as a constraining tool

Let us consider the age parameter [97] given by

$$t_0 = \int_0^1 \left[\frac{da}{aH(a)} \right] \quad (4.8)$$

where $H(a)$ is given by eq. (4.6). The age of the universe in MCG model becomes

$$t_0 = \frac{1}{H_0} \int_0^1 \left[\frac{da}{aE(a, \Omega_{j0}, \Omega_{r0}, A_s, B, \alpha)} \right] \quad (4.9)$$

with

$$E(a, \Omega_{j0}, \Omega_{r0}, A_s, B, \alpha) = \frac{H(a)}{H_0} \quad (4.10)$$

and $H_0 t_0 = 0.95$. For a given value of α we plot the variation of A_s with B . We note the following: Fig. (4.1): shows variation of B with A_s for $\alpha = 0.01, 0.20, 0.39$ by dotted, dashed and thin lines respectively in CDM model. It is evident that as the value of A_s approaches 1 (0.97 to 1) for $0 \leq \alpha \leq 0.39$, the B parameter picks up positive values with a maximum 0.20.

Fig. (4.2): shows variation of B with A_s for $\alpha = 0.01, 0.50$ and 0.99 with thin, dotted and dashed lines respectively in UDME model. In this case as the value of A_s is increased from 0.7 to 1 it is evident that the B parameter picks up positive value up

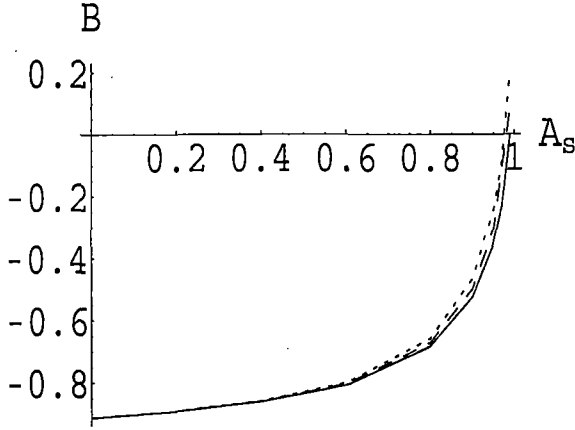


Figure 4.1: Variation of B with A_s for $\alpha = 0.01$ (Dotted line), $\alpha = 0.20$ (Dashed line) and $\alpha = 0.39$ (Thin line) in CDM model

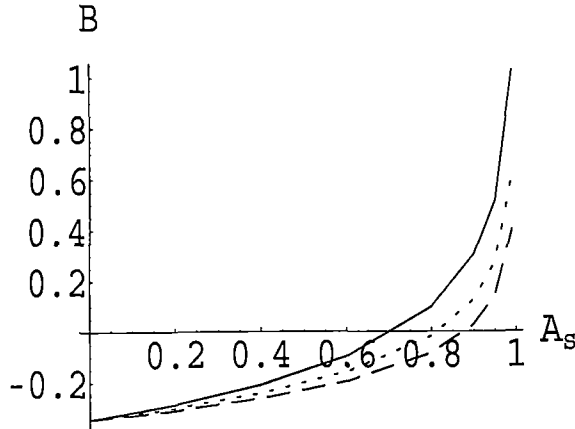


Figure 4.2: Variation of B with A_s for $\alpha = 0.01$ (Thin line), $\alpha = 0.50$ (Dotted line) and $\alpha = 0.99$ (Dashed line) in UDME model

to a maximum 1.02 for $0 \leq \alpha \leq 1$ in UDME model. The set of curves shown in fig. (4.1) and fig. (4.2) are useful to determine the range of values of B for both CDM and UDME models respectively. We note that in CDM model B lies between 0 to 0.20, whereas in UDME model B lies between 0 to 1.02. Moreover, in CDM model B is positive when $0 \leq \alpha \leq 0.39$ and A_s between 0.97 to 1. In UDME model we note that B is positive for $0 \leq \alpha \leq 1$ and A_s between 0.7 to 1.

4.4 $(H(z) - z)$ data as a constraining tool

For a flat universe containing only radiation, cold dark matter (or baryon) and the MCG, the Friedmann equation can be expressed as

$$H^2(H_0, A_s, B, \alpha, z) = H_0^2 E^2(A_s, B, \alpha, z) \quad (4.11)$$

where,

$$E = \left[\Omega_{r0}(1+z)^4 + \Omega_{j0}(1+z)^3 + (1 - \Omega_{r0} - \Omega_{j0})[A_s + (1 - A_s)(1+z)^{3n}]^{\frac{1}{1+\alpha}} \right]^{\frac{1}{2}} \quad (4.12)$$

with $j = m$ for CDM model and $j = b$ for UDME model. The best-fit values for model parameters A_s , B , α and H_0 can be determined by minimizing the following

Chi-square function

$$\chi^2(H_0, A_s, B, \alpha, z) = \sum \frac{[H(H_0, A_s, B, \alpha, z) - H_{obs}(z)]^2}{\sigma_z^2}. \quad (4.13)$$

Since we are interested in determining the model parameters, H_0 is not an important parameter here. So we marginalize over H_0 to evaluate the probability distribution function for A_s , B , α as

$$L(A_s, B, \alpha) = \int \left[dH_0 P(H_0) \exp \left(\frac{-\chi^2(H_0, A_s, B, \alpha, z)}{2} \right) \right] \quad (4.14)$$

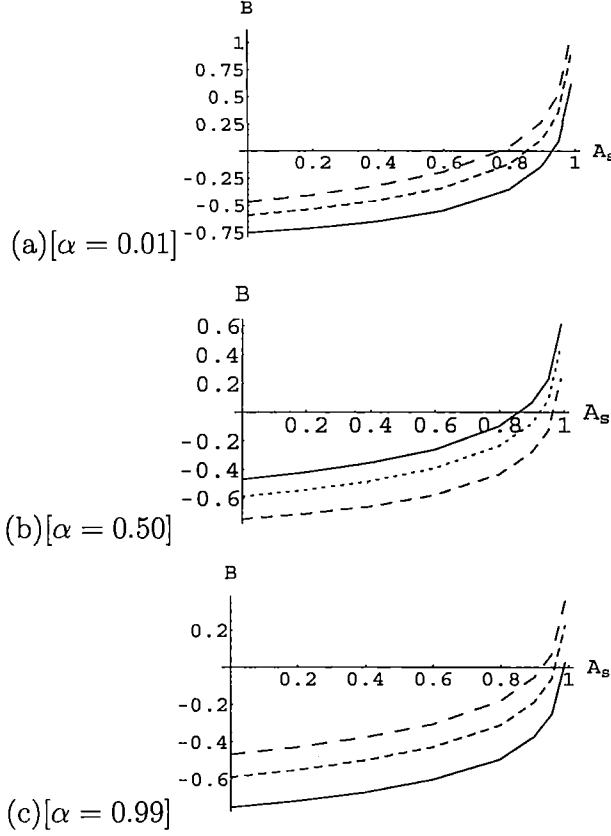


Figure 4.3: Constraints on EoS parameters in CDM model for (a) $\alpha = 0.01$, (b) $\alpha = 0.50$ and (c) $\alpha = 0.99$ using $H(z)$ vs. z data: 1σ , 2σ and 3σ levels are shown.

where $P(H_0)$ is the prior distribution function for the present Hubble constant. We consider Gaussian prior here with $H_0 = 72 \pm 8$ [100]. Minimizing χ^2 determines the maximum $L(A_s, B, \alpha)$ value. We determine the maximum value of the function $L(A_s, B, \alpha)$ at three different values of α to obtain a relation between B and A_s . Thus a relation between B and A_s for various α can be established by minimizing χ^2 .

In CDM model, variation of B with A_s (related to A) for $\alpha = 0.01$, 0.50 , 0.99 at 1σ , 2σ and 3σ levels respectively are shown in figs. (4.3 a - 4.3 c). It is observed that as the value of A_s tends to 1 we see that the B parameter picks up positive values (i) up

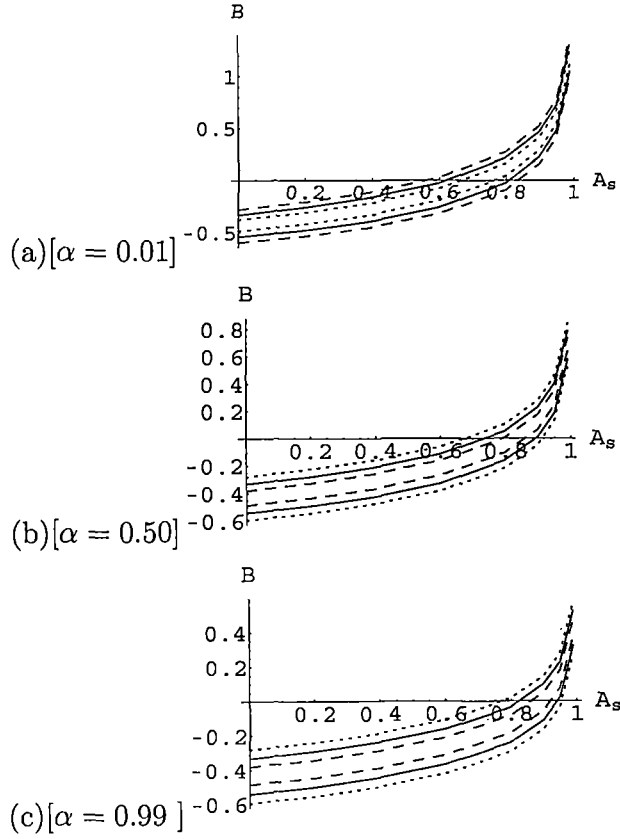


Figure 4.4: Constraints on EoS parameters in UDME model for (a) $\alpha = 0.01$, (b) $\alpha = 0.50$ and (c) $\alpha = 0.99$ using $H(z)$ vs. z data: 1σ , 2σ and 3σ levels are shown.

<i>Model</i>	<i>Data</i>	A_s	B	α
<i>CDM</i>	<i>Age – constraint</i>	(0.97, 1.0)	(0, 0.20)	(0, 0.39)
<i>UDME</i>	<i>Age – constraint</i>	(0.70, 1.0)	(0, 1.02)	(0, 1.0)

Table 4.2: Range of values of the EoS parameters in CDM and UDME model using age constraint

to 1.07 (fig. 4.3 a), (ii) up to 0.62 (fig. 4.3 b), (iii) up to 0.36 (fig. 4.3 c) at 3σ level in accordance with the $(H(z) - z)$ data [130]. Thus it is evident that as α increases, B decreases. In UDME model variation of B with A_s for $\alpha = 0.01, 0.50, 0.99$ at $1\sigma, 2\sigma$ and 3σ levels respectively are shown in figs. (4.4 a - 4.4 c). We note that as the value of A_s tends to 1, it is observed that the B parameter picks up positive values (i) up to 1.35 (fig. 4.4 a), (ii) up to 0.84 (fig. 4.4 b), (iii) up to 0.58 (fig. 4.4 c) at 3σ level in accordance with the $(H(z) - z)$ data [130]. Thus it is evident that as α increases, B decreases but compared to CDM model the variation of B parameter values is more for a given α and A_s in UDME model.

Thus in CDM model the range for B lies between 0 and 1.07 and in UDME model the range lies between 0 and 1.35 up to 3σ (*i.e.* 99.7% confidence) level. In CDM model B is positive only when A_s is within 0.76 to 1 for α between 0 to 1 and in UDME model B is positive (so, permissible) only when A_s is within 0.57 to 1 for α lying between 0 to 1.

4.5 Test of viability of the model

The best-fit values of the parameters for the cosmological models with MCG are determined using $(H(z) - z)$ data. The best-fit values of the parameters in the CDM model are $A_s = 0.99, B = 0.01, \alpha = 0.01$ and in UDME model $A_s = 0.80, B = 0.06,$

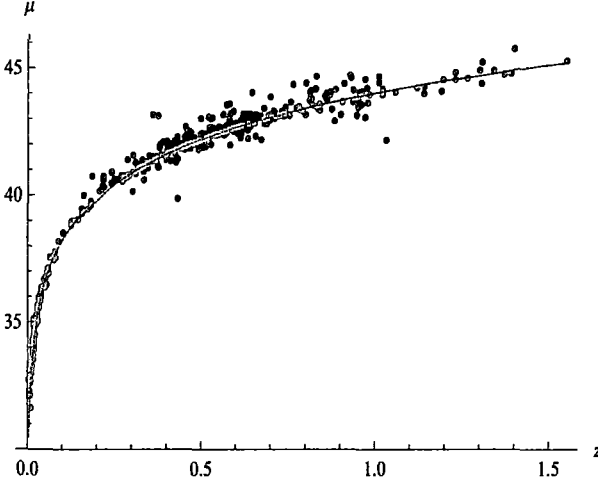


Figure 4.5: $\mu(z)$ *vs.* z curves for CDM model and union compilation data

$\alpha = 0.11$. In order to test the reliability we use the best-fit values to draw supernovae magnitudes (μ) at different redshift (z) in the two cases. We compare μ *vs.* z curves for the models with that of the original curve from union compilation data [102] (between those two parameters). Fig. (4.5) shows a plot of $\mu(z)$ *vs.* z obtained from the CDM model (the continuous line) with that obtained from union compilation data (the dots). Similar curves are drawn for the UDME model in Fig. (4.6) (continuous line for UDME model and dots for union compilation data). It is evident from the plots that both the CDM and UDME models are in excellent agreement with union compilation data.

4.6 Discussion

Cosmological models with modified Chaplygin gas contains three EoS parameters defined as: A_s , B and α are arbitrary. We determine the range of values of B

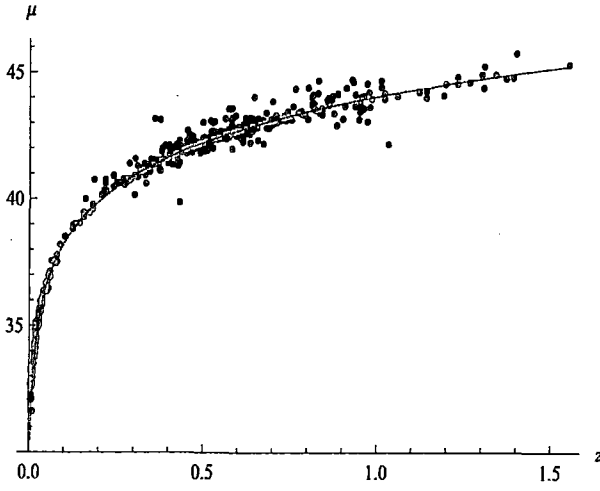


Figure 4.6: $\mu(z)$ vs. z curves for UDME model and union compilation data

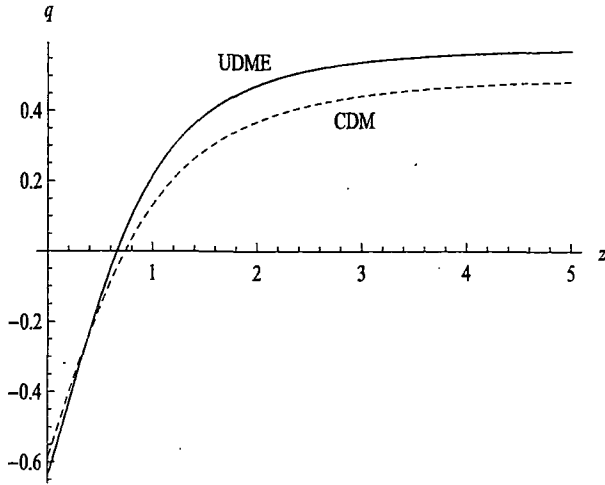


Figure 4.7: q vs. z curves for CDM & UDME model

<i>Model</i>	<i>Data</i>	<i>CL</i>	A_s	B	α
<i>CDM</i>	$(H - z)$	99.7%	(0.76, 1.0)	(0, 1.07)	(0, 1.0)
<i>UDME</i>	$(H - z)$	99.7%	(0.56, 1.0)	(0, 1.35)	(0, 1.0)

Table 4.3: Range of values of the EoS parameters in CDM and UDME model using $(H - z)$ data

<i>Model</i>	A_s	B	α
<i>CDM</i>	0.99	0.01	0.01
<i>UDME</i>	0.80	0.06	0.11

Table 4.4: Best-fit values of the EoS parameters in CDM and UDME model

parameter from the age constancy. In section (4.3) we plot B vs. A_s for different values of α in figs. (4.1) and (4.2). The figures are plotted for both positive and negative values of B . In the case of CDM model we note that B can pick up positive values up to 0.20 for the range of values: $0.97 \leq A_s < 1$, $0 \leq \alpha \leq 0.39$. However, for UDME model we note that B can pick up positive values up to 1.02 for the range of values $0.7 \leq A_s < 1$, $0 \leq \alpha \leq 1$ shown in Table-(4.2).

In section (4.4) we define *Chi-square* function and determine the constraints on B by minimizing the *Chi-square* function for the Hubble parameter vs. redshift data. For positive values of B a viable cosmology with MCG may be obtained. The constraints on B are: (i) $0 \leq B \leq 1.07$ for $0.76 \leq A_s < 1$, $0 \leq \alpha \leq 1$ in CDM model and (ii) $0 \leq B \leq 1.35$ for $0.56 \leq A_s < 1$, $0 \leq \alpha \leq 1$ in UDME model at 99.7% confidence limit as shown in Table-(4.3). For UDME model the range of values of B is found to be more than that of CDM model. If the age constant parameter is decreased then we note that the values of B permitted by CDM and UDME models are in agreement with that obtained from *Chi-square* minimization of the observed $H(z)$ vs. z data [130]. Consequently the limiting value of the age of our universe is pushed to lower values ($t < 13.6$ Billion years). The best-fit values of the parameters obtained here for CDM and UDME models are in agreement with union compilation data. We note that the best-fit values of our models are $A_s = 0.99$, $B = 0.01$, $\alpha = 0.01$ for CDM

model and $A_s = 0.80$, $B = 0.06$, $\alpha = 0.11$ for UDME model as shown in Table-(4.4). Fig. (4.7) shows a plot of deceleration parameter q vs. z for the CDM and UDME model at the best-fit values. Both the model shows a transition from decelerating phase to accelerating phase at recent past. In the UDME model this transition occurs at lower redshift than CDM model ($z_{CDM} = 0.73$, $z_{UDME} = 0.66$). The magnitude of present acceleration is more in UDME model than CDM model ($q_{CDM}(0) = -0.57$, $q_{UDME}(0) = -0.65$).

Chapter 5

Observational Constraints on EoS parameters of Modified Chaplygin Gas in Cosmic Growth

5.1 Introduction

During the last decade a number of precision cosmological and astronomical observations have made it possible to test the suitability of a theoretical model of the universe. In the previous Chapters we have investigated some of the cosmological models obtained by us in this direction and tested the viability of the models. The constraints on the model parameters imposed by observational data are also determined by analytical method. In this Chapter cosmic growth data are employed to determine the cosmological model parameters in addition to the $(H(z) - z)$ data set considered in Chapter 4. The cosmic growth function is related to the evolution of the

inhomogeneous part of the universe for its structure formation and plays an important role in probing matter formation era. The density perturbation due to quantum fluctuations of matter fields is connected with the cosmic growth. The growth of the large scale structures of the universe is derived from linear matter density contrast defined as $\delta(z) \equiv \frac{\delta\rho_m}{\rho_m}$ plays an important role in constraining cosmological model parameters. In this case it is preferable to parametrize the growth function $f = \frac{d\log\delta}{d\log a}$ in terms of growth index γ which is important to describe the evolution of the inhomogeneous energy density. The above parametrization of δ with γ was initiated by Peebles [131]. Later Wang and Steinhardt also used the above parametrized form of δ in Ref. [132]. The above parametrization is useful to construct cosmological models and used in different contexts in the literature ([133]-[142]). It is, therefore, important to analyze cosmological models with observed expansion rate $H(z)$ in addition to growth of matter density contrast $\delta(z)$ as it may provide a significant insight on the dark energy content of the universe. In cosmology Chaplygin gas [53] is considered seriously as a substitute for dark energy. A modified form of CG called MCG, is widely considered in the literature. The observational constraints on EoS parameters for MCG are determined here using the recent cosmological observations. We use both the growth data and the Stern data set [99] related to $H(z)$ vs. z data (OHD) (Table-(2.1)) for the analysis. The first growth data set given by Table-(5.1) is related with growth function f at various redshifts. It may be pointed out here that at a given redshift estimation of the linear growth rate from observations is important for model construction. An estimation on different EoS parameters for GCG employing above data is discussed in Ref. ([143]). A cosmological model dominated by viscous

dark fluid is also discussed in Ref. ([144]) where it is found that viscous fluid mimics as Λ CDM model when co-efficient of viscosity varies as $\rho^{-1/2}$ providing excellent agreement with supernova and $(H - z)$ data. In cosmology it has been observed ([144]) that a viscous universe is analogous to a universe with GCG. Cosmological models will be analyzed here using various observational data, namely, the redshift distortion of galaxy power spectra [145], root mean square (*r.m.s*) mass fluctuation ($\sigma_8(z)$) obtained from galaxy and Ly- α surveys at various redshifts [94, 95], weak lensing statistics [146], Baryon Acoustic Oscillations (BAO) [88], X-ray luminous galaxy clusters [147], Integrated Sachs-Wolfs (ISW) Effect ([148]-[152]) which are given in Table-(5.2).

It is known that the redshift distortions are caused by velocity flow induced by gravitational potential gradient which evolves due to the growth of the universe. The dilution of the potentials are however due to the cosmic expansion. The gravitational growth index γ is an important parameter in the context of redshift distortion which is discussed in Ref. [133]. The cluster abundance evolution, however, strongly depends on *r.m.s* mass fluctuations ($\sigma_8(z)$) [132], which will be used here for analysis of cosmological models.

5.2 Field equations

The Hubble parameter in terms of redshift using the field eq. (1.9) can be written as

$$H(z) = H_0 \left[\Omega_{b0}(1+z)^3 + (1 - \Omega_{b0})[A_s + (1 - A_s)(1+z)^{3(1+B)(1+\alpha)}]^{\frac{1}{1+\alpha}} \right]^{\frac{1}{2}} \quad (5.1)$$

where Ω_{b0} , H_0 represents the present baryon density and present Hubble parameter respectively. The square of the sound speed is given by

$$c_s^2 = \frac{\delta p}{\delta \rho} = \frac{\dot{p}}{\dot{\rho}} \quad (5.2)$$

which reduces to

$$c_s^2 = B + \frac{A_s \alpha (1 + B)}{[A_s + (1 - A_s)(1 + z)^{3(1+B)(1+\alpha)}]}. \quad (5.3)$$

In terms of state parameter it becomes

$$c_s^2 = -\alpha\omega + B(1 + \alpha). \quad (5.4)$$

It may be mentioned here that the perturbation is stable when square of the sound speed c_s^2 is a positive definite [62]. A positive sound speed puts a upper bound $c_s^2 \leq 1$ which arises from causality condition.

5.3 Parametrization of the growth index

The growth rate of the large scale structures is derived from matter density perturbation $\delta = \frac{\delta \rho_m}{\rho_m}$ (where $\delta \rho_m$ represents the fluctuation of matter density ρ_m) in the linear regime [153, 154] is given by

$$\ddot{\delta} + 2\frac{\dot{a}}{a}\dot{\delta} - 4\pi G_{eff}\rho_m\delta = 0. \quad (5.5)$$

The field equations for the background cosmology with matter and MCG are

$$\left(\frac{\dot{a}}{a}\right)^2 = \frac{8\pi G}{3}(\rho_b + \rho_{mcg}), \quad (5.6)$$

$$2\frac{\ddot{a}}{a} + \left(\frac{\dot{a}}{a}\right)^2 = -8\pi G\omega_{mcg}\rho_{mcg} \quad (5.7)$$

where ρ_b represents the background energy density and ω_{mcg} represents the state parameter for MCG which is given by

$$\omega_{mcg} = B - \frac{A_s(1+B)}{[A_s + (1-A_s)(1+z)^{3(1+B)(1+\alpha)}]}. \quad (5.8)$$

Replacing the time t variable to $\ln a$ in eq. (5.5) one obtains

$$(\ln \delta)'' + (\ln \delta)'^2 + (\ln \delta)' \left[\frac{1}{2} - \frac{3}{2}\omega_{mcg}(1 - \Omega_m(a)) \right] = \frac{3}{2}\Omega_m(a) \quad (5.9)$$

where $\Omega_m(a) = \frac{\rho_m}{\rho_m + \rho_{mcg}}$. The effective matter density is $\Omega_m = \Omega_b + (1 - \Omega_b)(1 - A_s)^{\frac{1}{1+\alpha}}$ [155]. Using the energy conservation eq. (1.12) and changing the variable from $\ln a$ to $\Omega_m(a)$ once again, the eq. (5.9) can be expressed in terms of the logarithmic growth factor $f = \frac{d \log \delta}{d \log a}$ which is given by

$$3\omega_{mcg}\Omega_m(1 - \Omega_m)\frac{df}{d\Omega_m} + f^2 + f \left[\frac{1}{2} - \frac{3}{2}\omega_{mcg}(1 - \Omega_m(a)) \right] = \frac{3}{2}\Omega_m(a). \quad (5.10)$$

In the case of a flat universe, the dark energy state parameter ω_0 is a constant and the growth index γ is given by eq. (1.37). For a Λ CDM model, it reduces to $\frac{6}{11}$ [133, 156], for a matter dominated model, it reduces to $\gamma = \frac{4}{7}$ [157, 158]. One can also express γ in terms of redshift parameter z . One such parametrization is $\gamma(z) = \gamma(0) + \gamma' z$, with $\gamma' \equiv \frac{d\gamma}{dz}|_{(z=0)}$ [159, 160]. It has been shown recently [161] that the parametrization smoothly interpolates a low and intermediate redshift range to a high redshift range [162]. Here, we parametrize γ in terms of MCG parameters namely, A_s , α and B . Therefore, we begin with the following ansatz which is given by

$$f = \Omega_m^{\gamma(\Omega_m)}(a) \quad (5.11)$$

where the growth index parameter $\gamma(\Omega_m)$ can be expanded in Taylor series around $\Omega_m = 1$ as

$$\gamma(\Omega_m) = \gamma|_{(\Omega_m=1)} + (\Omega_m - 1) \frac{d\gamma}{d\Omega_m}|_{(\Omega_m=1)} + O(\Omega_m - 1)^2. \quad (5.12)$$

Equation (5.12) can be re-written in terms of γ as

$$3\omega_{mcg}\Omega_m(1-\Omega_m) \ln \Omega_m \frac{d\gamma}{d\Omega_m} - 3\omega_{mcg}\Omega_m(\gamma - \frac{1}{2}) + \Omega_m^\gamma - \frac{3}{2}\Omega_m^{1-\gamma} + 3\omega_{mcg}\gamma - \frac{3}{2}\omega_{mcg} + \frac{1}{2} = 0. \quad (5.13)$$

Differentiating once again the above equation around $\Omega_m = 1$, one obtains zeroth order term in the expansion for γ which is given by

$$\gamma = \frac{3(1 - \omega_{mcg})}{5 - 6\omega_{mcg}}, \quad (5.14)$$

this is in consequence with dark energy model with a constant ω_0 (eq. 1.37). In the same way differentiating the expression twice and thereafter by a Taylor expansion around $\Omega_m = 1$, one obtains a first order term in the expansion which is given by

$$\frac{d\gamma}{d\Omega_m}|_{(\Omega_m=1)} = \frac{3(1 - \omega_{mcg})(1 - \frac{3\omega_{mcg}}{2})}{125(1 - \frac{6\omega_{mcg}}{5})^3}. \quad (5.15)$$

Substituting it in eq. (5.12), γ up to the first order term becomes

$$\gamma(B, \alpha, A_s) = \frac{3(1 - \omega_{mcg})}{5 - 6\omega_{mcg}} + (1 - \Omega_m) \frac{3(1 - \omega_{mcg})(1 - \frac{3\omega_{mcg}}{2})}{125(1 - \frac{6\omega_{mcg}}{5})^3}. \quad (5.16)$$

Using the expression of ω_{mcg} in the above, γ may be parametrized in terms of B , α , A_s and z . We define normalized growth function g as

$$g(z) \equiv \frac{\delta(z)}{\delta(0)}. \quad (5.17)$$

z	f_{obs}	σ	<i>Ref.</i>
0.15	0.51	0.11	[145, 163]
0.22	0.60	0.10	[164]
0.32	0.654	0.18	[165]
0.35	0.70	0.18	[166]
0.41	0.70	0.07	[164]
0.55	0.75	0.18	[167]
0.60	0.73	0.07	[164]
0.77	0.91	0.36	[168]
0.78	0.70	0.08	[164]
1.4	0.90	0.24	[169]
3.0	1.46	0.29	[170]

Table 5.1: Observed growth functions (f_{obs}) with redshift

The corresponding approximate normalized growth function obtained from the parametrized form of f which follows from eq. (5.11) is given by

$$g_{th}(z) = \exp \left[\int_1^{\frac{1}{1+z}} \Omega_m(a)^\gamma \frac{da}{a} \right]. \quad (5.18)$$

A *Chi-square* function is constructed with $g_{th}(z)$ in the next section to study numerically.

5.4 Observational constraints

The redshift distortion parameter β , is related to the growth function f as $\beta = \frac{f}{b}$, where b represents the bias factor connecting total matter perturbation (δ) and galaxy perturbations (δ_g) ($b = \frac{\delta_g}{\delta}$) [164, 166, 167, 169]. The values for β and b at various redshifts are obtained from cosmological observations [164, 171] considering Λ CDM model. Here we analyze cosmological models in the presence of MCG using cosmic growth function. Various power spectrum amplitudes of Lyman- α forest data in SDSS

z	σ_8	σ_{σ_8}	<i>Ref</i>
2.125	0.95	0.17	[94]
2.72	0.92	0.17	
2.2	0.92	0.16	[95]
2.4	0.89	0.11	
2.6	0.98	0.13	
2.8	1.02	0.09	
3.0	0.94	0.08	
3.2	0.88	0.09	
3.4	0.87	0.12	
3.6	0.95	0.16	
3.8	0.90	0.17	
0.35	0.55	0.10	[96]
0.6	0.62	0.12	
0.8	0.71	0.11	
1.0	0.69	0.14	
1.2	0.75	0.14	
1.65	0.92	0.20	

Table 5.2: Root mean square mass fluctuations (σ_8) at various redshift

are also useful to determine β .

The *Chi-square* function for growth parameter f is defined as

$$\chi_f^2(A_s, B, \alpha) = \Sigma \left[\frac{f_{obs}(z_i) - f_{th}(z_i, \gamma)}{\sigma_{f_{obs}}} \right]^2 \quad (5.19)$$

where f_{obs} and $\sigma_{f_{obs}}$ are obtained from Table-(5.1). However, $f_{th}(z_i, \gamma)$ is obtained from eqs. (5.11) and (5.16). Another observational probe for the matter density perturbation $\delta(z)$ is derived from the redshift dependence of the *r.m.s* mass fluctuation $\sigma_8(z)$. A new *Chi-square* function using the above probe is given by

$$\chi_s^2(A_s, B, \alpha) = \Sigma \left[\frac{s_{obs}(z_i, z_{i+1}) - s_{th}(z_i, z_{i+1})}{\sigma_{s_{obs},i}} \right]^2 \quad (5.20)$$

where s_{obs} , s_{th} represents observed and theoretical values of the function which is analyzed using data from Table-(5.2). From the Hubble parameter *vs.* redshift data

(OHD) [99] another *Chi-square* $\chi^2_{(H-z)}$ function is defined which is given by

$$\chi^2_{(H-z)}(H_0, A_s, B, \alpha, z) = \sum \frac{[H(H_0, A_s, B, \alpha, z) - H_{obs}(z)]^2}{\sigma_z^2} \quad (5.21)$$

where $H_{obs}(z)$ is the observed Hubble parameter at redshift (z) and σ_z is the error associated with that particular observation as cited in Table-(2.1). The total *Chi-square* function is given by

$$\chi^2_{total}(A_s, B, \alpha) = \chi^2_f(A_s, B, \alpha) + \chi^2_s(A_s, B, \alpha) + \chi^2_{(H-z)}(A_s, B, \alpha). \quad (5.22)$$

The best-fit values are obtained first by minimizing the *Chi-square* function thereafter the contours are drawn at different confidence limit. The limits imposed by the contours corresponds to available range of values of the EoS parameters of the MCG for a viable cosmology.

5.5 Results

The best-fit values of the EoS parameters are obtained minimizing the *Chi-square* function $\chi^2_f(A_s, B, \alpha)$ making use of the growth rate data. The corresponding contours relating A_s and B are drawn in fig. (5.1). The best-fit values of the parameters A_s, B, α are $A_s = 0.81, B = -0.10, \alpha = 0.02$. We note the following from contours:
(i) $0.6638 < A_s < 0.8932$ and $-0.9758 < B < 0.1892$ at 95.4 % confidence limit.

The best-fit values of the parameters A_s, B, α are determined once again using $\chi^2_f(A_s, B, \alpha) + \chi^2_s(A_s, B, \alpha)$ which are $A_s = 0.816, B = -0.146, \alpha = 0.004$. Using the best-fit values contours for A_s with B are drawn in fig. (5.2), which puts the following constraints: (i) $0.6649 < A_s < 0.896$ and $-1.5 < B < 0.1765$ at 95.4 % confidence

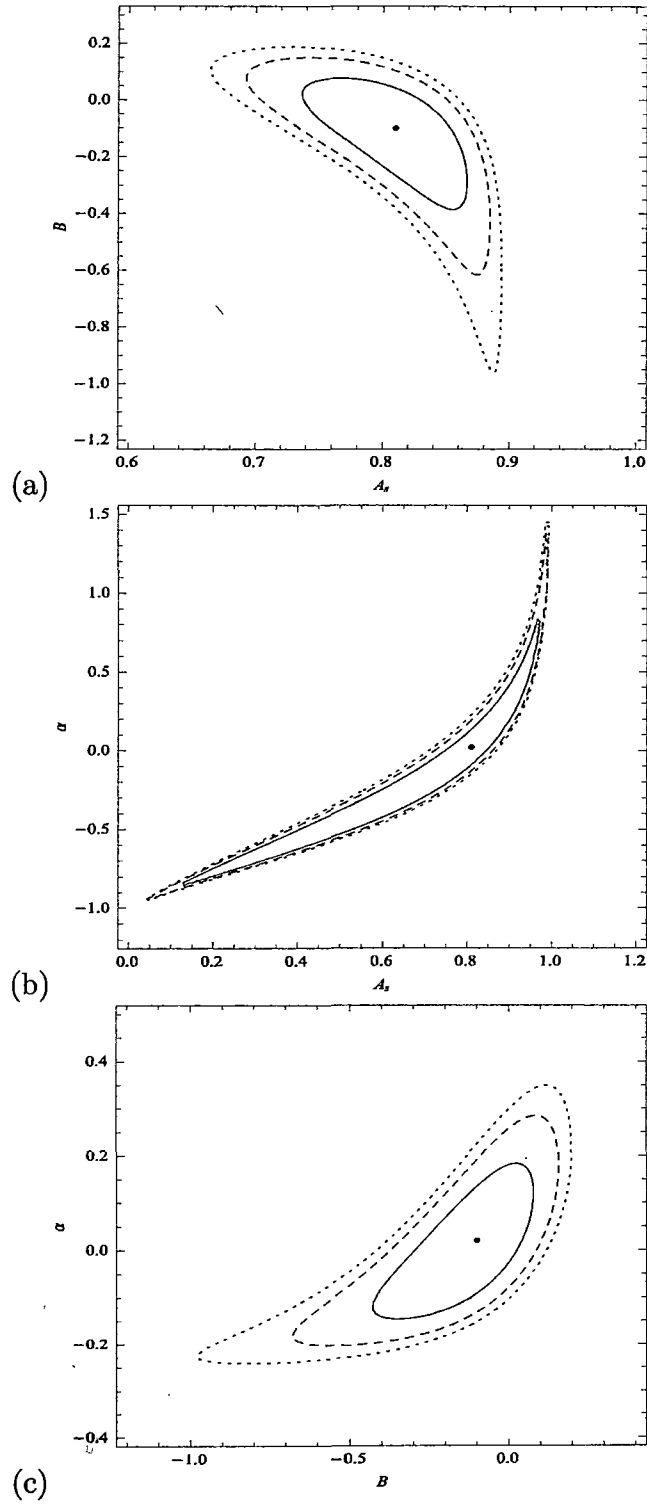


Figure 5.1: (a) $B - A_s$, (b) $\alpha - A_s$ and (c) $\alpha - B$ contours using growth data at 68.3% (Solid), 90.0% (Dashed) and 95.4% (Dotted) confidence limits at best-fit values: $A_s = 0.81$, $B = -0.10$, $\alpha = 0.02$.

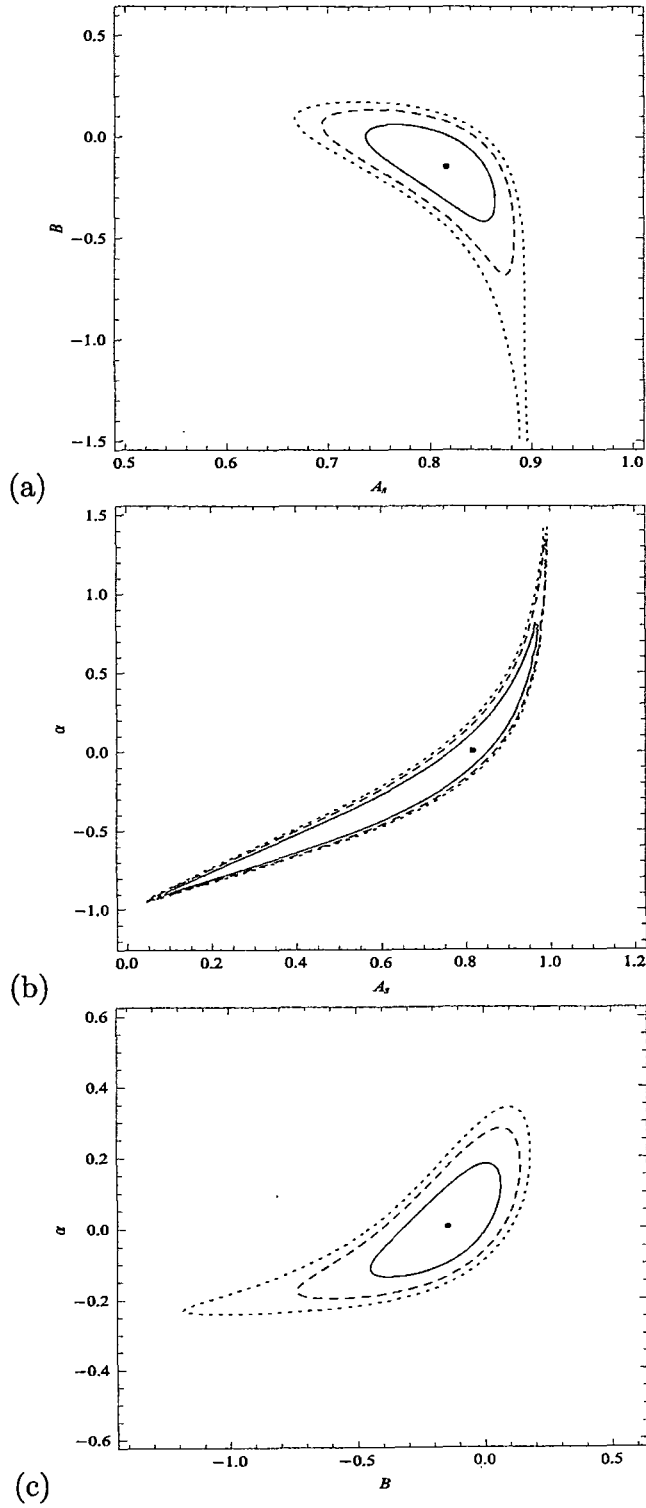


Figure 5.2: (a) $B - A_s$, (b) $\alpha - A_s$ and (c) $\alpha - B$ contours using (growth+*r.m.s* mass fluctuations (σ_8)) data at 68.3% (Solid), 90.0% (Dashed) and 95.4% (Dotted) confidence limits at best-fit values: $A_s = 0.816$, $B = -0.146$, $\alpha = 0.004$

limit.

Finally, a total *Chi-square* function $\chi^2_{tot}(A_s, B, \alpha)$ is used to determine the best-fit values of the parameters A_s , B , α which gives $A_s = 0.769$, $B = 0.008$, $\alpha = 0.002$. The contours are plotted in fig. (5.3) which puts the following limiting values (i) $0.6711 < A_s < 0.8346$ and $-0.1412 < B < 0.1502$ at 95.4 % confidence limit. It is observed that at 2σ level A_s ($0.6711 < A_s < 0.8346$) admits positive values but B can take either a positive or negative value in the range ($-0.1412 < B < 0.1502$). Thus a viable cosmological model is permitted here with all the three parameters which are positive.

In fig. (5.4) the growth function f vs. *redshift* (z) with best-fit values of model parameters is plotted, f is found to vary from 0.472 to 1.0 for redshift variation $z = 0$ to $z = 5$. Initially f is constant but it falls sharply at low redshifts, indicating the fact that the major growth of our universe completed at the early stage of the universe with moderate redshift. The variation of the growth index (γ) with redshift (z) is plotted in fig. (5.5). The growth index (γ) varies between 0.562 to 0.60 for the redshift $z = 0$ to $z = 5$. A smooth fall for the values of γ at low redshift is noticed.

The variation of the state parameter (ω) with z is plotted in fig. (5.6). It is evident that the state parameter (ω) varies from -0.767 at the present epoch ($z = 0$) to $\omega \rightarrow 0$ at intermediate redshift ($z = 5$). This result is in support of the observation that present universe is now passing through an accelerating phase which is dominated by dark energy whereas in the early universe ($z > 5$) it was dominated by matter where it admits a decelerating phase.

In fig. (5.7) the variation of square of sound speed c_s^2 is plotted with z . It is evident

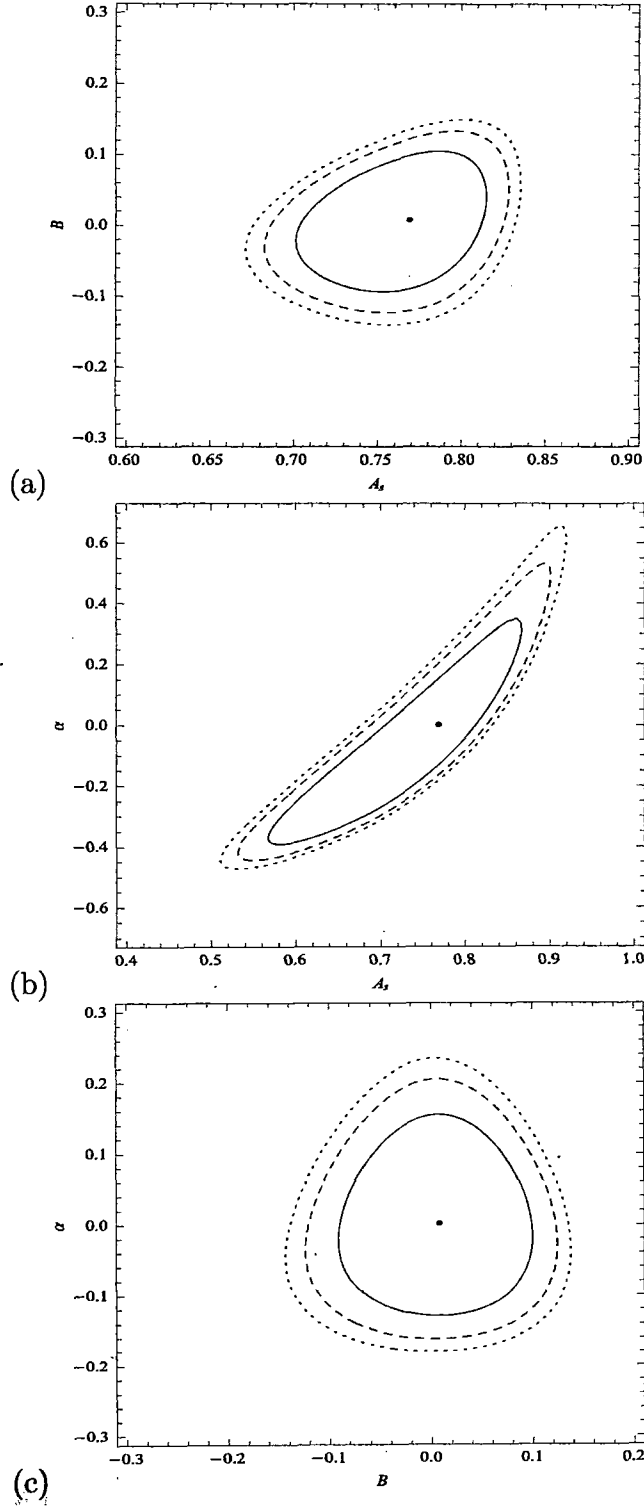


Figure 5.3: (a) $B - A_s$, (b) $\alpha - A_s$ and (c) $\alpha - B$ contours using (growth+r.m.s mass fluctuations (σ_8) + OHD) data at 68.3% (Solid), 90.0% (Dashed) and 95.4% (Dotted) confidence limits at best-fit values: $A_s = 0.769$, $B = 0.008$, $\alpha = 0.002$

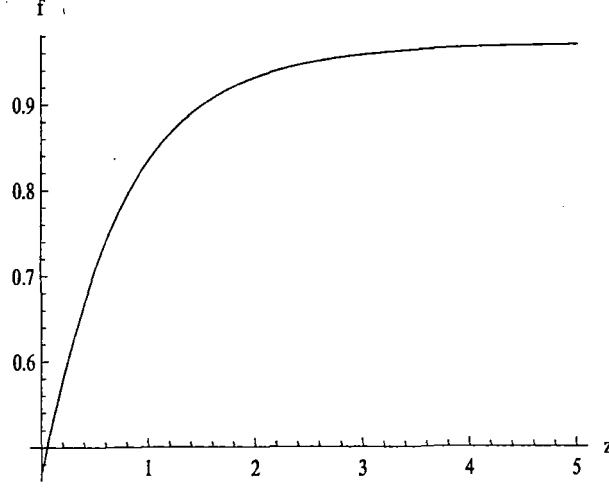


Figure 5.4: Evolution of growth function f with redshift at best-fit values: $A_s = 0.769$, $B = 0.008$, $\alpha = 0.002$

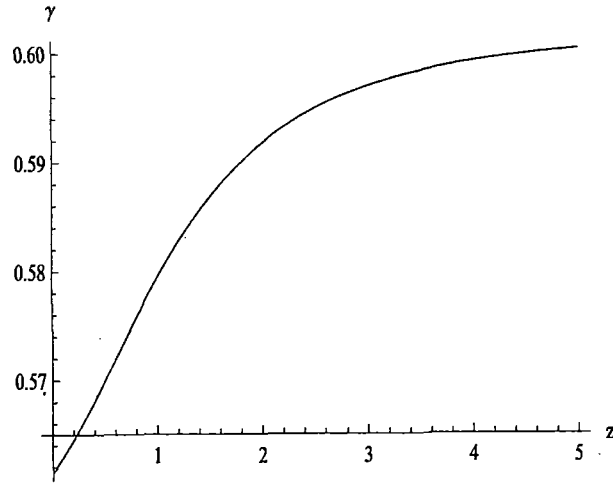


Figure 5.5: Evolution of growth index γ with redshift at best-fit values: $A_s = 0.769$, $B = 0.008$, $\alpha = 0.002$

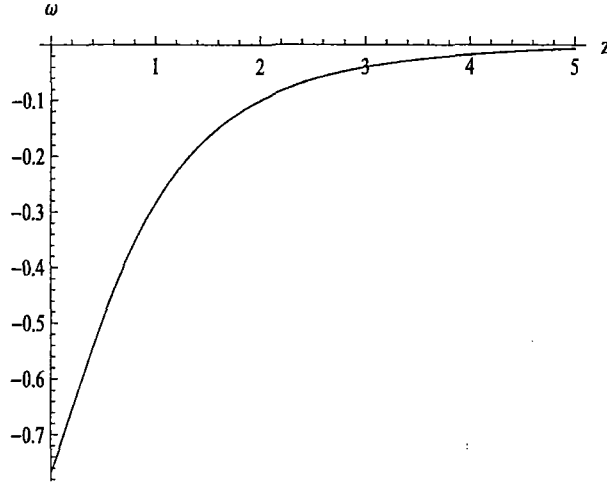


Figure 5.6: Evolution of the state parameter (ω) at best-fit values: $A_s= 0.769$, $B= 0.008$, $\alpha= 0.002$

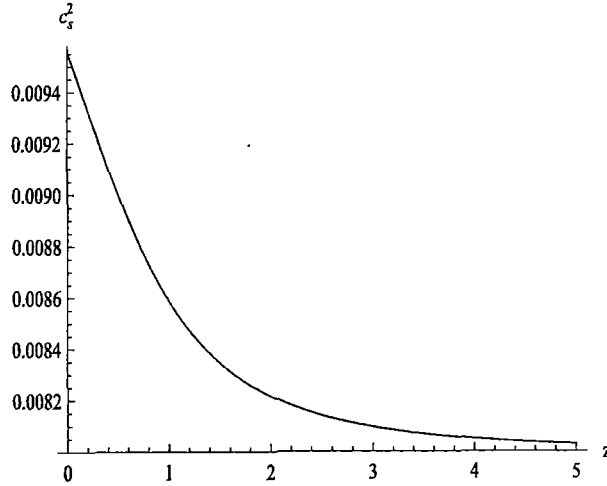


Figure 5.7: Square of sound speed variations with redshift at best-fit values: $A_s= 0.769$, $B= 0.008$, $\alpha= 0.002$

Data	A_s	B	α
<i>Growth</i>	0.810	-0.100	0.020
<i>Growth</i> + σ_8	0.816	-0.146	0.004
<i>Growth</i> + σ_8 + <i>OHD</i>	0.769	0.008	0.002

Table 5.3: Best-fit values of the EoS parameters

Data	CL	A_s	B
<i>Growth</i>	95.4%	(0.6638, 0.8932)	(-0.9758, 0.1892)
<i>Growth</i> + σ_8	95.4%	(0.6649, 0.896)	(-1.5000, 0.1765)
<i>Growth</i> + σ_8 + <i>OHD</i>	95.4%	(0.6711, 0.8346)	(-0.1412, 0.1502)

Table 5.4: Range of values of the EoS parameters for A_s & B

that c_s^2 varies between 0.0095 to 0.0080 in the above redshift range. A small positive value indicates the growth in the structures of the universe.

5.6 Discussion

Cosmological models with MCG as a candidate for dark energy is used here to estimate the range of values of the EoS parameters making use of recently observed data. The growth of perturbation for large scale structure formation in this model is studied using the theory. The observed data are employed here to study the growth of matter perturbation and to determine the range of values of growth index γ as considered in Ref. [132] with MCG similar to the method adopted in Ref. [143]. The model parameters are constrained using the latest observational data from redshift distortion of galaxy power spectra and the *r.m.s* mass fluctuation (σ_8) from Ly- α surveys. The growth data set given in Table-(5.1) including the Wiggle-Z survey

Data	CL	A_s	α
<i>Growth</i>	95.4%	(0.0497, 0.9935)	(-0.9469, 1.460)
<i>Growth</i> + σ_8	95.4%	(0.0458, 0.9975)	(-0.9469, 1.442)
<i>Growth</i> + σ_8 + <i>OHD</i>	95.4%	(0.5094, 0.9204)	(-0.4770, 0.6562)

Table 5.5: Range of values of the EoS parameters A_s & α

data [164] are employed here for the analysis. Table-(5.2) consists of 17 data points, which are employed to study growth rate in addition to σ_8 data from the power spectrum of Ly- α surveys. Stern data set [99] corresponding to $H(z)$ vs. z data (OHD) given in Table-(2.1) are also used.

The best-fit values of the parameters are obtained by minimizing the function $\chi^2_{tot}(A_s, B, \alpha)$ are $A_s = 0.769$, $B = 0.008$, $\alpha = 0.002$ (Table-(5.3)). The following ranges are obtained (i) $0.6711 < A_s < 0.8346$ and $-0.1412 < B < 0.1502$ at 95.4 percent confidence limit. However, in the 2σ level we found that A_s lies between 0.6711 and 0.8346, with B in between -0.1412 and 0.1502 . Thus B may be negative. The contours for A_s vs. B , A_s vs. α and B vs. α are drawn for growth data, growth+ σ_8 data and growth+ σ_8 + H vs. z data in figs. (5.1 a - 5.1 c), (5.2 a - 5.2 c) and (5.3 a - 5.3 c) respectively. The constraints imposed on EoS parameters are determined (Table-(5.4-5.6)).

The best-fit value of the growth parameter at present epoch ($z = 0$) is $f = 0.472$ with growth index $\gamma = 0.562$, state parameter $\omega = -0.767$ and $\Omega_{m0} = 0.262$, which are in good agreement with the Λ CDM model. It is also noted that the growth function f varies between 0.472 to 1.0 and the growth index γ varies between 0.562 to 0.60 for a variation of redshift from $z = 0$ to $z = 5$. In this case the state parameter ω lies between -0.767 to 0, square of the sound speed is $c_s^2 < 1$ always.

Data	CL	B	α
<i>Growth</i>	95.4%	(-0.9764, 0.1979)	(-0.2439, 0.3525)
<i>Growth</i> + σ_8	95.4%	(-1.186, 0.2754)	(-0.2436, 0.3423)
<i>Growth</i> + σ_8 + <i>OHD</i>	95.4%	(-0.1449, 0.1386)	(-0.1818, 0.2360)

Table 5.6: Range of values of the EoS parameters for B & α

Model	A_s	B	α	f	γ	Ω_{m0}	ω_0
<i>MCG</i>	0.769	0.008	0.002	0.472	0.562	0.262	-0.767
<i>GCG</i>	0.708	0	-0.140	0.477	0.564	0.269	-0.708
Λ CDM	0.761	0	0	0.479	0.562	0.269	-0.761

Table 5.7: Values of the EoS parameters obtained in different models

Here the growth and Hubble data are employed to test the suitability of MCG in FRW universe. The viability of the model is explored using the growth function f , growth index γ , state parameter ω and the square of sound speed c_s^2 with redshift z at the best-fit values of the EoS parameters. It is found that a satisfactory cosmological model emerges permitting present accelerating universe. The negative values of state parameter ($\omega \leq -\frac{1}{3}$) signifies the existence of such a phase of the universe. Thus it is noted that MCG is a good candidate for a universe which can reproduce the cosmic growth with inhomogeneity admitting a late time accelerating phase. It is evident

Model	Data	A_s	α	B	Ref.
<i>GCG</i>	<i>Supernovae</i>	0.6-0.85	-	0	[172]
<i>GCG</i>	<i>CMBR</i>	0.81-0.85	0.2-0.6	0	[173]
<i>GCG</i>	<i>WMAP</i>	0.78-0.87	-	0	[56]
<i>GCG</i>	<i>CMBR</i> + <i>BAO</i>	≈ 0.77	≤ 0.1	0	[174]
<i>GCG</i>	<i>Growth</i> + σ_8 + <i>OHD</i>	0.708	-0.140	0	this paper
<i>MCG</i>	<i>Growth</i> + σ_8 + <i>OHD</i>	0.769	0.002	0.008	this paper
Λ CDM	<i>Growth</i> + σ_8 + <i>OHD</i>	0.761	0	0	this paper

Table 5.8: Comparison of the values of EoS parameters for Λ CDM, GCG and MCG models

from Table-(5.7) that the observational constraints that are estimated in the MCG model are agreeing close to Λ CDM model compared to the GCG model. It may be mentioned here that the MCG model reduces to GCG model for $B = 0$ and Λ CDM model for $B = 0$ and $\alpha = 0$. In Table-(5.8) a comparison of values of EoS parameters corresponding to previously probed GCG model with that of Λ CDM, GCG and MCG models obtained by us are also shown.

Chapter 6

Cosmological models with Holographic Dark Energy

6.1 Introduction:

As discussed earlier, the discovery of Riess *et al.* in 1998 and Perlmutter *et al.* in 1999 changed the landscape scenario of the universe that we see today. In addition to other observations it predicts that the current universe is accelerating. The origin of the acceleration is considered to be due to a mysterious component of matter with a negative pressure called dark energy (DE). In the literature it is mainly focused on theory [175, 176, 177], probes of DE [178] and on cosmological constant [179, 180]. The preferred candidate for DE is a small cosmological constant (Λ). A Λ CDM model is then constructed as an alternative approach to the DE problem. Although Λ CDM fits most observational data well, it suffers from two main shortcomings: (i) the low value of vacuum energy (ii) the cosmic coincidence problem. In order to address the

above issues a constant Λ is replaced by a time varying Λ , resulting in a dynamical DE models. When cosmological observations are analyzed in Big Bang framework it predicts that 23% matter in the universe is due to dark matter (DM). DM and DE in some cases are considered independent but coupling between them may exist. DM and DE manifests through their gravitational action. From unified models in the cosmological substratum DM & DE may be considered as single entity. In the previous Chapters a MCG is considered which play a significant role in this direction in cosmological model building. Among the many different approaches to describe the dark cosmological sectors considerable attention is focused with holographic DE. According to Holographic principle, the number of degrees of freedom in a bounded system should be finite and related to the area of its boundary. Recently Holographic principle ([181]-[186]) is applied in cosmology ([187]-[198]) to track the dark energy content of the universe following the work of Cohen *et al.* [199]. Holographic principle is a speculative conjecture about quantum gravity theories proposed by G't Hooft. Fischler and Susskind [181, 182, 183] subsequently promoted the idea claiming that all the information contained in a spatial volume may be represented by a theory that lives on the boundary of that space. For a given finite region of space the volume may contain matter and energy within it. If this energy suppresses a critical density then the region collapses to a black hole. A black hole is known theoretically to have an entropy which is proportional to its surface area of its event horizon. A black hole event horizon encloses a volume, thus a more massive black hole have larger event horizon and encloses larger volumes. The most massive black hole that can fit in a given region is the one whose event horizon corresponds exactly to the boundary of

the given region under consideration. The maximal limit of entropy for an ordinary region of space is directly proportional to the surface area of the region and not to its volume. The basic idea of a holographic dark energy in cosmology is that the saturation of the entropy bound may be related to an unknown ultra-violet (UV) scale Λ to some known cosmological scale in order to enable it to find a viable formula for the dark energy which may be quantum gravity in origin and it is characterized by Λ . The choice of UV-Infra Red (IR) connection from the covariant entropy bound leads to a universe dominated by black hole states. Cohen *et al.* [199] proposed that any state in Hilbert space with an energy E corresponds to Schwarzschild radius $R_s \sim E$ which is less than the IR cut off value L (where L is a cosmological scale). It may now be possible to obtain a relation between the UV cut-off $\rho_\Lambda^{1/4}$ and the IR cut off which eventually leads to a constraint $\left(\frac{8\pi G}{c^2}\right) L^3 \left(\frac{\rho_\Lambda}{3}\right) \leq L$ [200, 201] where ρ_Λ is the energy density corresponding to dark energy characterized by Λ . The holographic dark energy density is

$$\rho_\Lambda = 3c^2 M_P^2 L^{-2}, \quad (6.1)$$

where $M_P^{-2} = 8\pi G$. The present acceleration may be described in the case when $\omega_\Lambda = \frac{p_\Lambda}{\rho_\Lambda} < -\frac{1}{3}$. If one considers $L \sim \frac{1}{H}$ it leads to $\omega_\Lambda = 0$. However it is known that holographic cosmological constant model based on Hubble scale as IR cut off does not permit an accelerating universe. The holographic dark energy model based on the particle horizon as the IR cut off is unable to achieve an accelerating universe noted in Ref. [187]. Subsequently an alternative model of dark energy using particle horizon in closed model is proposed [202]. Later, Li [188] obtained an accelerating universe considering event horizon as the cosmological scale. The model is consistent with the

cosmological observations. Thus a cosmological model consistent with observations may be admitted adopting the covariant entropy bound and choosing L as an event horizon.

6.2 Modified Chaplygin gas in FRW universe:

Using the metric (1.6) and the energy momentum tensor, the Einstein's field equation (1.5) can be written as

$$H^2 + \frac{k}{a^2} = \frac{1}{3M_P^2}\rho \quad (6.2)$$

where $M_P^{-2} = 8\pi G$. The energy conservation equation is given by eq. (1.12). Let us now define the following density parameters:

$$\Omega_\Lambda = \frac{\rho_\Lambda}{\rho_{cr}}, \quad \Omega_m = \frac{\rho_m}{\rho_{cr}}, \quad \Omega_k = \frac{k}{a^2 H^2} \quad (6.3)$$

where $\rho_{cr} = 3M_P^2 H^2$. Ω_Λ , Ω_m and Ω_k represents density parameter corresponding to Λ , matter and curvature respectively. We assume here that the origin of dark energy is due to a scalar field in order to obtain potential for the dark energy model. Using Barrow's scheme [203, 204], we obtain the following equations for homogeneous scalar field:

$$\rho_\phi = \frac{1}{2}\dot{\phi}^2 + V(\phi) = \left(\frac{A}{B+1} + \frac{C}{a^n} \right)^{\frac{1}{\alpha+1}}, \quad (6.4)$$

$$p_\phi = \frac{1}{2}\dot{\phi}^2 - V(\phi) = \frac{-\frac{A}{B+1} + B\frac{C}{a^n}}{\left(\frac{A}{B+1} + \frac{C}{a^n} \right)^{\frac{\alpha}{\alpha+1}}}, \quad (6.5)$$

where $n = 3(1+B)(1+\alpha)$ and C is the integration constant. The corresponding scalar field potential and its kinetic energy term are given by

$$V(\phi) = \frac{\frac{A}{B+1} + \frac{1-B}{2}\frac{C}{a^n}}{\left(\frac{A}{B+1} + \frac{C}{a^n} \right)^{\frac{\alpha}{\alpha+1}}}, \quad (6.6)$$

$$\dot{\phi}^2 = \frac{(B+1) \frac{C}{a^n}}{\left(\frac{A}{B+1} + \frac{C}{a^n}\right)^{\frac{\alpha}{\alpha+1}}}. \quad (6.7)$$

In a flat universe ($k = 0$), eq. (6.7) can be integrated which yields

$$\phi = \pm \frac{2}{\sqrt{n}} \sinh^{-1} \left[\sqrt{\frac{C(B+1)}{A}} a^{-\frac{n}{2}} \right] \quad (6.8)$$

and the potential is given by

$$V(\phi) = \frac{\frac{A}{1+B} + \frac{A(1-B)}{2(1+B)} \sinh^2 \left(\frac{\sqrt{3(1+B)(1+\alpha)}}{2} \phi \right)}{\left(\frac{A}{1+B}\right)^{\frac{\alpha}{\alpha+1}} \cosh^{\frac{2\alpha}{1+\alpha}} \left(\frac{\sqrt{3(1+B)(1+\alpha)}}{2} \phi \right)}. \quad (6.9)$$

It may be mentioned here that for a non flat universe it is not so simple to obtain ϕ in known form.

6.3 Holographic dark energy as MCG:

For a non-flat universe ($k \neq 0$), the holographic dark energy density given by eq. (6.1) becomes

$$\rho_\Lambda = 3c^2 M_P^2 L^{-2}, \quad (6.10)$$

where c is the speed of light and L is the cosmological length scale for tracking the field corresponding to holographic dark energy in the universe. The parameter L is

$$L = ar(t) \quad (6.11)$$

where $a(t)$ is the scale factor of the universe and $r(t)$ is relevant to the future event horizon of the universe. Using Robertson-Walker metric one gets ([189]-[197])

$$L = \frac{a(t) \sinh \left[\frac{\sqrt{|k|} R_h(t)}{a(t)} \right]}{\sqrt{|k|}}, \quad (6.12)$$

where R_h represents the event horizon which is given by

$$R_h = a(t) \int_t^\infty \frac{dt'}{a(t')} = a(t) \int_0^{r_1} \frac{dr}{\sqrt{1 - kr^2}}. \quad (6.13)$$

Here R_h is measured in r direction and L represents the radius of the event horizon measured on the sphere of the horizon. Using the definition of $\Omega_\Lambda = \frac{\rho_\Lambda}{\rho_{cr}}$ and $\rho_{cr} = 3M_P^2 H^2$, one can derive [198]

$$HL = \frac{c}{\sqrt{\Omega_\Lambda}}. \quad (6.14)$$

Using eqs. (6.12)-(6.13), we determine the rate of change of L which is

$$\dot{L} = \frac{c}{\sqrt{\Omega_\Lambda}} - \frac{1}{\sqrt{|k|}} \cos n \left(\frac{\sqrt{|k|} R_h}{a(t)} \right), \quad (6.15)$$

where

$$\frac{1}{\sqrt{|k|}} \cos n \left(\sqrt{|k|} x \right) = \cos(x) \quad [1, \cosh(x)] \text{ for } k = 1 \quad [0, -1]. \quad (6.16)$$

Using eqs. (6.10)-(6.15), it is possible to construct the required equation for the holographic energy density ρ_Λ , which is given by

$$\frac{d\rho_\Lambda}{dt} = -2H \left[1 - \frac{\sqrt{\Omega_\Lambda}}{c} \frac{1}{\sqrt{|k|}} \cos n \left(\frac{\sqrt{|k|} R_h}{a(t)} \right) \right] \rho_\Lambda. \quad (6.17)$$

The energy conservation equation is

$$\frac{d\rho_\Lambda}{dt} + 3H(1 + \omega_\Lambda)\rho_\Lambda = 0 \quad (6.18)$$

which is used to determine the equation of state parameter

$$\omega_\Lambda = - \left(\frac{1}{3} + \frac{2\sqrt{\Omega_\Lambda}}{3c} \frac{1}{\sqrt{|k|}} \cos n \left(\frac{\sqrt{|k|} R_h}{a(t)} \right) \right). \quad (6.19)$$

Now we assume that the holographic dark energy density may be replaced by a modified Chaplygin gas energy density. The corresponding energy density then obtained

from eq. (4.1). The equation of state parameter becomes

$$\omega = \frac{p}{\rho} = B - \frac{A}{\rho^{\alpha+1}}. \quad (6.20)$$

To determine dark energy fields we use eqs. (6.4) and (6.5) in eqs. (6.19)-(6.20), the following expressions for A and C are obtained:

$$A = (3c^2 M_P^2 L^{-2})^{\alpha+1} \left[B + \frac{1}{3} + \frac{2\sqrt{\Omega_\Lambda}}{3c} \frac{1}{\sqrt{|k|}} \cos n \left(\frac{\sqrt{|k|} R_h}{a(t)} \right) \right], \quad (6.21)$$

$$C = (3c^2 M_P^2 L^{-2})^{\alpha+1} a^n \left[1 - \frac{3B+1}{3(B+1)} - \frac{2\sqrt{\Omega_\Lambda}}{3(B+1)c} \frac{1}{\sqrt{|k|}} \cos n \left(\frac{\sqrt{|k|} R_h}{a(t)} \right) \right]. \quad (6.22)$$

The scalar field potential becomes

$$V(\phi) = 2c^2 M_P^2 L^{-2} \left[1 + \frac{\sqrt{\Omega_\Lambda}}{2c} \frac{1}{\sqrt{|k|}} \cos n \left(\frac{\sqrt{|k|} R_h}{a(t)} \right) \right], \quad (6.23)$$

and the corresponding kinetic energy of the field is given by

$$\dot{\phi}^2 = 2c^2 M_P^2 L^{-2} \left[1 - \frac{\sqrt{\Omega_\Lambda}}{c} \frac{1}{\sqrt{|k|}} \cos n \left(\frac{\sqrt{|k|} R_h}{a(t)} \right) \right]. \quad (6.24)$$

Considering $x (= \ln a)$, we transform the time derivative to the derivative with logarithm of the scale factor, which is the most useful function in this case. We get

$$\phi' = M_P \sqrt{2\Omega_\Lambda \left(1 - \frac{\sqrt{\Omega_\Lambda}}{c} \frac{1}{\sqrt{|k|}} \cos n \left(\frac{\sqrt{|k|} R_h}{a(t)} \right) \right)} \quad (6.25)$$

where $()'$ prime represents derivative with respect to x . Thus, the evolution of the scalar field is given by

$$\phi(a) - \phi(a_o) = \sqrt{2} M_P \int_o^{\ln a} \sqrt{\Omega_\Lambda \left(1 - \frac{\sqrt{\Omega_\Lambda}}{c} \frac{1}{\sqrt{|k|}} \cos n \left(\frac{\sqrt{|k|} R_h}{a(t)} \right) \right)} dx. \quad (6.26)$$

6.4 Squared speed of sound:

For a closed universe model ($k = 1$), the equation of state parameter for dark energy given in eq. (6.19) reduces to

$$\omega_\Lambda = -\frac{1}{3} \left(1 + \frac{2}{c} \sqrt{\Omega_\Lambda} \cos y \right) \quad (6.27)$$

where $y = \frac{R_H}{a(t)}$. The minimum value it can take is $\omega_{min} = -\frac{1}{3} (1 + 2\sqrt{\Omega_\Lambda})$ and one obtains a lower bound $\omega_{min} = -0.9154$ for $\Omega_\Lambda = 0.76$ with $c = 1$. Taking variation of the state parameter with respect to $x = \ln a$, we get [198]

$$\omega'_\Lambda = -\frac{\sqrt{\Omega_\Lambda}}{3c} \left[\frac{1 - \Omega_\Lambda}{1 - \gamma a} + \frac{2\sqrt{\Omega_\Lambda}}{c} (1 - \Omega_\Lambda \cos^2 y) \right], \quad (6.28)$$

where $\frac{\Omega_k}{\Omega_m} = \gamma a$. We now introduce the squared speed of holographic dark energy fluid as

$$v_\Lambda^2 = \frac{dp_\Lambda}{d\rho_\Lambda} = \frac{\dot{p}_\Lambda}{\dot{\rho}_\Lambda} = \frac{p'_\Lambda}{\rho'_\Lambda}, \quad (6.29)$$

where variation of eq. (6.20) w.r.t. x is given by

$$p'_\Lambda = \omega'_\Lambda \rho_\Lambda + \omega_\Lambda \rho'_\Lambda. \quad (6.30)$$

Using the eqs. (6.29) and (6.30) we get

$$v_\Lambda^2 = \omega'_\Lambda \frac{\rho_\Lambda}{\rho'_\Lambda} + \omega_\Lambda$$

which becomes

$$v_\Lambda^2 = -\frac{1}{3} - \frac{2}{3c} \sqrt{\Omega_\Lambda} \cos y + \frac{1}{6c} \sqrt{\Omega_\Lambda} \left[\frac{\frac{1-\Omega_\Lambda}{1-\gamma a} + \frac{2}{c} \sqrt{\Omega_\Lambda} (1 - \Omega_\Lambda \cos^2 y)}{1 - \frac{\Omega_\Lambda}{c} \cos y} \right]. \quad (6.31)$$

The variation of v_Λ^2 with Ω_Λ is shown in fig. (6.1) for different y values. It is found that for a given value of c , a , γ , the model admits a positive squared speed for

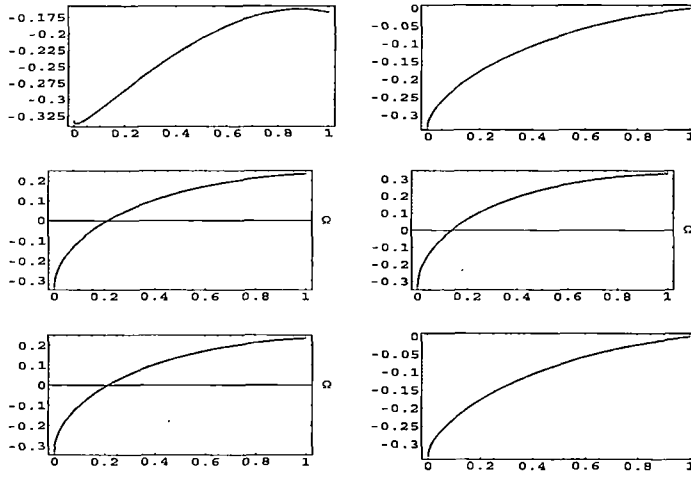


Figure 6.1: Variation of v_Λ^2 with Ω_Λ for different values of y at $c = 1$, $\gamma = \frac{1}{3}$ and $a = 1$, in the first array the figures are for $y = \frac{\pi}{3}$ and $y = \frac{\pi}{2}$, in the second array for $y = \frac{1.5\pi}{2}$, $y = \pi$ and in the third array for $y = \frac{2.5\pi}{2}$, $y = \frac{3\pi}{2}$.

$\Omega_\Lambda > 0$. However, Ω_Λ is bounded below otherwise instability develops. We note also that for $\frac{(2n+1)\pi}{2} < y < \frac{(2n+3)\pi}{2}$, (where n is an integer) no instability develops. We plot the case for $n = 0$ in fig. (6.1), it is evident that for $y \leq \frac{\pi}{2}$ and $y \geq \frac{3\pi}{2}$, the squared speed for holographic dark energy becomes negative which led to instability. But for the region $\frac{\pi}{2} < y < \frac{3\pi}{2}$ with $n = 0$ no such instability develops. It is also found that for $y = 0$ i.e., in flat case the holographic dark energy model is always unstable [205].

6.5 Discussions:

The holographic dark energy model in FRW universe is studied with a scalar field equivalent to MCG. For a large energy density $\rho \rightarrow \infty$ i.e., $a \rightarrow 0$ one obtains the following: (i) $V(\phi) \rightarrow \infty$ for $B \neq 1$, (ii) $V(\phi) \rightarrow 0$ for $B = 1$. However, for large size of the universe i.e., $a \rightarrow \infty$ leads to $\phi \rightarrow 0$, the potential asymptotically attains

a constant value $(\phi) \rightarrow \left(\frac{A}{B+1}\right)^{\frac{1}{1+\alpha}}$. We obtain the evolution of the holographic dark energy field and the corresponding potential in the framework of MCG in a non flat universe. For $B = 0$ and $\alpha = 1$, the EoS given by (1.3) reduces to the Chaplygin gas which was considered by Setare [206] to derive the fields of dark energy. It is also observed that inclusion of a barotropic fluid in addition to Chaplygin gas (which is modified CG) does not alter the form of potential and evolution of the holographic dark energy field but the parameter B in the equation of state varies as a^n where $n = 3(1+B)(1+\alpha)$. Thus the contribution of the holographic dark energy is more as ($B \neq 0$) compared to the case $B = 0$ in Ref. [206]. Thus it is noted that although the form of the potential does not change due to addition of a barotropic fluid, it changes the overall holographic dark energy density. It is found that the holographic dark energy is stable for a restricted domain of the values of Ω_Λ in a closed model of the universe.

1

^{1*} We use EoS for modified Chaplygin gas as $p = B\rho - \frac{A}{\rho^\alpha}$ which is different from that used in the published paper $p = A\rho - \frac{B}{\rho^\alpha}$ for a consistent representation

Chapter 7

Modified Chaplygin Gas in Horava-Lifshitz Gravity and Constraints on its B parameter

7.1 Introduction

Recently modification to the gravitational sector of the Einstein-Hilbert action is considered widely to accommodate the present accelerating phase. A polynomial Lagrangian in scalar curvature R with different powers are considered to address some of the recent issues in cosmology ([76]-[80]). However no significant cosmological model came up which describes the evolution of the universe consistently. Horava-Lifshitz gravity is considered as an alternative theory of gravity. It is known that the Big Bang singularity does not arise in the Horava-Lifshitz gravity due to higher order terms in the spatial curvatures R_{ij} . Horava-Lifshitz gravity is considered to

be a UV complete theory of gravity. HL gravity may reduce to classical general relativistic theory of gravity in the low energy limit. HL gravity is useful to construct cosmological model as it has a number of novel features in connection with evolution of the universe. A number of issues in the universe namely, gravitational wave production [207, 208, 209], perturbation spectrum [210, 211, 212], black-hole properties [213, 214, 215], dark energy phenomenology [216, 217], the problems of determining observational constraints in the theory [218], astrophysical phenomenology [219, 220, 221], thermodynamic properties [222, 223] are studied in the framework of HL gravity. Setting aside the foundational and conceptual issues of HL gravity, cosmological scenario with generalized Chaplygin gas (GCG) [224] is also studied in the literature. In the HL gravity, generally two conditions are assumed: (i) detailed balance with projectibility and (ii) projectibility in beyond detailed balance. Under the detailed balance condition in HL gravity, it is found that the Friedmann equation gets modified by extra $\frac{1}{a^4}$ term [81, 82, 83], where a is the scale factor. Here cosmological models with MCG in HL gravity are obtained and used to determine the constraints on model parameters from observations for both the closed and open universe. Thereafter the suitability of a cosmological model is examined using Union Compilation data [102].

7.2 Horava-Lifshitz cosmology

In Horava-Lifshitz (in short, HL) gravity [82, 83], it is convenient to use the Arnowitt-Deser-Misner decomposition of the metric which is given by eq. (1.22). The full action of HL gravity consists of kinetic and potential terms which is given

by eq. (1.23). In the next section we study cosmological model with detailed balance and projectibility.

7.2.1 Cosmological model:

Using symmetry property of the Lagrangian L_V , Horava noted that it reduces the number of invariants which one should actually consider in the action to begin with [72]. The symmetry is known as detailed balance and it requires that the Lagrangian L_V should be derivable from a super-potential W [83]. Under the detailed balance condition the full action of HL gravity is given by

$$I_g = \int dt d^3x \sqrt{g} N \left[\frac{2(K_{ij}K^{ij} - \lambda K^2)}{\kappa^2} + \frac{\kappa^2 C_{ij}C^{ij}}{2\omega^4} - \frac{\kappa^2 \mu \epsilon^{ijk} R_{il} \nabla_j R_k^l}{2\omega^2 \sqrt{g}} + \frac{\kappa^2 \mu^2 R_{ij}R^{ij}}{8} - \frac{k^2 \mu^2}{8(3\lambda - 1)} \left[\frac{(1 - 4\lambda)R^2}{4} + \Lambda R - 3\Lambda^2 \right] \right] \quad (7.1)$$

where

$$C^{ij} = \frac{\epsilon^{ijk} \nabla_k (R_i^j - \frac{R \delta_i^j}{4})}{\sqrt{g}} \quad (7.2)$$

is the *Cotton tensor* and the covariant derivatives are determined with respect to the spatial metric g_{ij} . ϵ^{ijk} is a totally antisymmetric unit tensor, λ is a dimensionless constant with κ , ω and μ .

In order to incorporate the matter components one needs to add a cosmological stress-energy tensor to the gravitational field equations, that recovers the usual general relativity formulation in the low-energy limit [216, 225, 226, 227]. The matter-tensor is a hydrodynamical approximation which contains the matter energy density ρ_m and the corresponding pressure p_m in Friedmann equation. Here ρ_m represents the

total matter energy density, that accounts for both the baryonic density ρ_b as well as that of the dark matter density ρ_{dm} , including the normal matter. Horava obtained the gravitational action assuming that the lapse function is just a function of time *i.e.*, $N = N(t)$. Here we use FRW metric with $N = 1$, $g_{ij} = a^2(t)\gamma_{ij}$, $N^i = 0$, $\gamma_{ij}dx^i dx^j = \frac{dr^2}{1-Kr^2} + r^2 d\Omega_2^2$, where $K = -1, 1, 0$, corresponds to open, closed and flat universe respectively. Varying N and g_{ij} , one obtains the following field equations:

$$H^2 = \frac{\kappa^2}{6(3\lambda - 1)}(\rho_m + \rho_r) + \frac{\kappa^2}{6(3\lambda - 1)} \left[\frac{3\kappa^2 \mu^2 K^2}{8(3\lambda - 1)a^4} + \frac{3\kappa^2 \mu^2 \Lambda^2}{8(3\lambda - 1)} \right] - \frac{\kappa^4 \mu^2 \Lambda K}{8(3\lambda - 1)^2 a^2}, \quad (7.3)$$

$$\dot{H} + \frac{3H^2}{2} = -\frac{\kappa^2}{4(3\lambda - 1)}(\rho_m \omega_m + \rho_r \omega_r) - \frac{\kappa^2}{4(3\lambda - 1)} \left[\frac{\kappa^2 \mu^2 K^2}{8(3\lambda - 1)a^4} - \frac{3\kappa^2 \mu^2 \Lambda^2}{8(3\lambda - 1)} \right] - \frac{\kappa^4 \mu^2 \Lambda K}{16(3\lambda - 1)^2 a^2}, \quad (7.4)$$

where $H = \frac{\dot{a}}{a}$, is the Hubble parameter. In the above, the term proportional to a^{-4} may be considered as the usual “dark radiation term”, characteristic of the HL cosmology [82, 83] and the constant term as the cosmological constant. The conservation equation for matter and radiation are

$$\dot{\rho}_m + 3H(\rho_m + p_m) = 0, \quad (7.5)$$

$$\dot{\rho}_r + 3H(\rho_r + p_r) = 0 \quad (7.6)$$

where

$$G_{cosmo} = \frac{\kappa^2}{16\pi(3\lambda - 1)}, \quad \frac{\kappa^4 \mu^2 \Lambda}{8(3\lambda - 1)^2} = 1, \quad G_{grav} = \frac{\kappa^2}{32\pi}. \quad (7.7)$$

7.3 Observational constraints on EoS parameters of MCG

Here MCG is considered to determine observational constraints on EoS parameters for a viable cosmology in the framework of Horava-Lifshitz gravity. Observational constraints on the EoS parameters are determined using the recent observational data namely, Observed Hubble data (OHD), BAO peak parameter and CMB shift parameter.

7.3.1 Constraints obtained from detailed balance

In this case, using eq. (7.7), the Friedmann equation can be re-written as:

$$H^2 = \frac{8\pi G}{3}(\rho_b + \rho_c + \rho_r) + \left[\frac{K^2}{2\Lambda a^4} + \frac{\Lambda}{2} \right] - \frac{K}{a^2}, \quad (7.8)$$

$$\dot{H} + \frac{3}{2}H^2 = -4\pi G(p_c + \frac{1}{3}\rho_r) - \left[\frac{K^2}{4\Lambda a^4} - \frac{3\Lambda}{4} \right] - \frac{K}{2a^2}. \quad (7.9)$$

We define the following dimensionless density parameters:

(i) for matter component

$$\Omega_i \equiv \frac{8\pi G}{3H^2}(\rho_i) \quad (7.10)$$

(ii) for curvature

$$\Omega_K \equiv -\frac{K}{H^2 a^2} \quad (7.11)$$

(iii) for cosmological constant

$$\Omega_0 \equiv \frac{\Lambda}{2H_0^2} \quad (7.12)$$

The dimensionless parameter for the expansion rate is defined as:

$$E(z) \equiv \frac{H(z)}{H_0}. \quad (7.13)$$

Using the above parameters the Friedmann equation can be re-written as:

$$E^2(z) = \Omega_{b0}(1+z)^3 + \Omega_{c0}F(z) + \Omega_{r0}(1+z)^4 + \Omega_{K0}(1+z)^2 + \left[\Omega_0 + \frac{\Omega_{K0}^2(1+z)^4}{4\Omega_0} \right] \quad (7.14)$$

where $F(z) = \left[A_s + \frac{1-A_s}{a^{3(1+B)(1+\alpha)}} \right]^{\frac{1}{1+\alpha}}$. At the present epoch $E(z=0) = 1$, which leads to

$$\Omega_{b0} + \Omega_{c0} + \Omega_{r0} + \Omega_{K0} + \Omega_0 + \frac{\Omega_{K0}^2}{4\Omega_0} = 1 \quad (7.15)$$

where Ω_{b0} , Ω_{c0} , Ω_{r0} , Ω_{K0} represent the present day baryon, MCG, radiation and curvature energy density respectively. Here Ω_0 is the energy density associated with the cosmological constant. The last term in eq. (7.15) corresponds to dark radiation, which is a characteristic feature of the Horava-Lifshitz theory of gravity. The dark radiation component may be important during nucleo-synthesis. Thus a suitable bound from Big Bang Nucleo-synthesis (BBN) may be incorporated in the EoS. Using the upper limit on the total amount of Horava-Lifshitz dark radiation that is permitted during BBN era is expressed by the parameter ΔN_ν which represents the effective neutrino species [228, 229]. The constraints on $\frac{\Omega_{K0}^2}{4\Omega_0}$ determined in Ref. [218] in the framework of HL gravity which is:

$$\frac{\Omega_{K0}^2}{4\Omega_0} = 0.135\Delta N_\nu\Omega_{r0}. \quad (7.16)$$

The BBN limit on ΔN_ν is $-1.7 \leq \Delta N_\nu \leq 2.0$, follows from Refs. [229, 230]. A negative value of ΔN_ν is usually associated with models involving decay of massive particles which is not considered here. Again $\Delta N_\nu = 0$ corresponds to the zero curvature scenario (a non-interesting case since Horava-Lifshitz cosmology with zero curvature becomes indistinguishable from Λ CDM). Therefore we consider values of

ΔN_ν which lies within the bound $0 \leq \Delta N_\nu \leq 2.0$.

To sum up, in HL gravity the following parameters, Ω_{b0} , Ω_{c0} , Ω_{r0} , Ω_{K0} , Ω_0 , ΔN_ν , H_0 , A_s , B , α are involved. We fix some of the parameters using 7 year WMAP data [93]. The fixed parameters are $\Omega_{m0}(\equiv \Omega_{b0} + \Omega_{c0})$, Ω_{b0} , H_0 , Ω_{r0} and the corresponding values of the parameters are chosen as follows: $\Omega_{m0} = 0.27$, $\Omega_{b0} = 0.04$, $H_0 = 71.4 \text{ Km/sec/Mpc}$, $\Omega_{r0} = 8.14 * 10^{-5}$. Therefore now six free parameters are left to be determined which are Ω_{K0} , Ω_0 , A_s , B , α , ΔN_ν . Using eq. (7.16) in eq. (7.15) one obtains

$$\begin{aligned} \Omega_0(K, \Delta N_\nu, A_s, \alpha) = 1 - \Omega_{m0} - (1 - 0.135\Delta N_\nu)\Omega_{r0} \\ - 0.73(K)\sqrt{\Delta N_\nu}\sqrt{\Omega_{r0} - \Omega_{m0}\Omega_{r0} - \Omega_{r0}^2} \end{aligned} \quad (7.17)$$

and

$$\Omega_{K0}(\Delta N_\nu, A_s, \alpha) = \sqrt{0.54\Delta N_\nu\Omega_{r0}\Omega_0(K, \Delta N_\nu, A_s, \alpha)}. \quad (7.18)$$

Now, there are four free parameters, namely, A_s , B , α , ΔN_ν in the above equations. To determine the EoS parameters of the MCG, three values of α namely, $\alpha=0.999$, 0.500 , 0.001 are considered in closed universe and open universe respectively. In this case each of these values of α determined the best-fit values of the rest three parameters (*i.e.*, A_s , B , ΔN_ν). Then at the best-fit values of ΔN_ν we plot contours for the parameters A_s , B at different confidence limits for a given α . From the contours of A_s , B drawn at different values of α and best-fit ΔN_ν we determine the permissible range of values of the B parameter for the MCG in HL gravity in the framework of open or closed universe.

7.4 Numerical analysis

In this section we use three sets of observational data to determine EoS parameters of the MCG, namely, Stern data set for $(H - z)$ data (OHD), BAO peak parameter and CMB shift parameter by numerical analysis. *Chi-square* minimization technique is used to determine the limiting values of the EoS parameters in the next section.

7.4.1 $(H - z)$ data (OHD) as a tool for constraining

The best-fitted parameters of the model considered here are obtained minimizing the *Chi-square* function which is defined as

$$\chi_{OHD}^2(H_0, A_s, B, \alpha, \Delta N_\nu, z) = \sum \frac{(H(H_0, A_s, B, \alpha, \Delta N_\nu, z) - H_{obs}(z))^2}{\sigma_z^2} \quad (7.19)$$

where $H_{obs}(z)$ is the observed Hubble parameter at redshift z and σ_z is the associated error with that particular observation. Hubble parameter is given by

$$H(z) = H_0 E(z) \quad (7.20)$$

where

$$E(z) = \left(\Omega_{b0}(1+z)^3 + \Omega_{c0}F(z) + \Omega_{r0}(1+z)^4 + \Omega_{K0}(1+z)^2 + \left[\Omega_0 + \frac{\Omega_{K0}^2(1+z)^4}{4\Omega_0} \right]^{1/2} \right) \quad (7.21)$$

with $F(z) = \left[A_s + \frac{1-A_s}{a^{3(1+B)(1+\alpha)}} \right]^{\frac{1}{1+\alpha}}$. Here $(H(z) - z)$ data (OHD) is taken from Stern data analysis [99] from Table-(2.1).

Model	B	A_s	ΔN_ν
$\alpha = 0.999$	0.0037	0.0628	0.2330
$\alpha = 0.500$	0.0166	0.1105	0.0999
$\alpha = 0.001$	0.0062	0.0521	0.8071

Table 7.1: Best-fit values of MCG for $K = 1$

7.4.2 BAO peak parameter as a tool for constraining

Using the definition of a model independent BAO peak parameter defined for low redshift (z_1) measurements given in eq. (1.30) we analyze the model. The *Chi-square* function χ^2_{BAO} defined in eq. (1.31) is used.

7.4.3 CMB shift parameter as a tool for constraining

The CMB shift parameter defined in eq. (1.34) is used here. The *Chi-square* function χ^2_{CMB} defined in eq. (1.35) is employed here for the analysis.

7.4.4 Joint analysis with OHD + BAO + CMB data

Total *Chi-square* function for the joint analysis:

$$\chi^2_{tot} = \chi^2_{OHD} + \chi^2_{BAO} + \chi^2_{CMB}. \quad (7.22)$$

The statistical analysis with χ^2_{tot} gives the bounds on the model parameters specially on B . The best-fit values of the closed universe and the corresponding range of values of the EoS parameters are shown in Table-(7.1) and in Table-(7.3) respectively. The contours between A_s , B for closed universe are shown in fig. (7.1) and that for open universe in fig. (7.2). The figures are drawn for three values of α at the best-fit value of ΔN_ν . From fig. (7.1 a) which is plotted for $\alpha = 0.999$ for closed

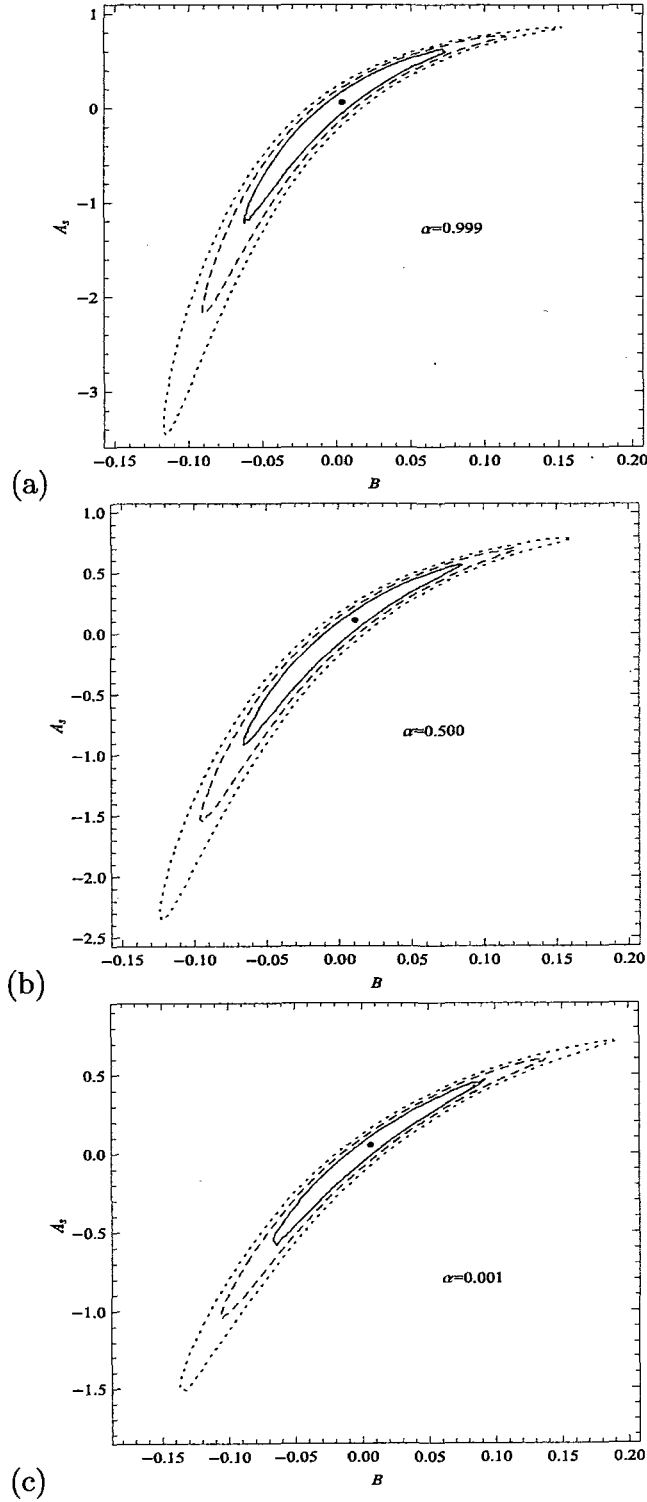


Figure 7.1: $A_s - B$ contours for (a) $\alpha = 0.999$, (b) $\alpha = 0.500$ and (c) $\alpha = 0.001$ for closed universe using ($OHD + SDSS (BAO) + CMB$ shift) data at 68.3% (Solid), 95.4% (Dashed) and 99.7% (Dotted) confidence level.

Model	A_s	ΔN_ν
$\alpha = 0.999$	0.0138	0.0662
$\alpha = 0.500$	0.0108	0.0808
$\alpha = 0.001$	0.0073	0.0761

Table 7.2: Best-fit values of GCG ($B = 0$) for $K = 1$

Data	CL	B	A_s
$\alpha = 0.999$	68.3%	(-0.0630, 0.0773)	(-1.206, 0.6321)
	95.4%	(-0.0900, 0.1146)	(-2.175, 0.7623)
	99.7%	(-0.1144, 0.1531)	(-3.478, 0.8347)
$\alpha = 0.500$	68.3%	(-0.0654, 0.0785)	(-0.9372, 0.5396)
	95.4%	(-0.0951, 0.1158)	(-1.544, 0.6846)
	99.7%	(-0.1234, 0.1673)	(-2.374, 0.7901)
$\alpha = 0.001$	68.3%	(-0.0724, 0.0898)	(-0.6392, 0.4532)
	95.4%	(-0.1081, 0.1334)	(-1.043, 0.5838)
	99.7%	(-0.1358, 0.1901)	(-1.53, 0.7025)

Table 7.3: Range of values of the EoS parameters for $K = 1$ in MCG

universe we get at 68.3% confidence limit the acceptable range for B lies between $(-0.0630, 0.0773)$ and for A_s it is $(-1.206, 0.6321)$. For 95.4% confidence limit, the bound on B widens and it takes up values between $(-0.0900, 0.1146)$ and A_s takes $(-2.175, 0.7623)$. At 99.7%, it is $(-0.1144, 0.1531)$ for B and $(-3.478, 0.8347)$ for A_s . The best-fit value for the effective neutrino parameter $\Delta N_\nu = 0.2330$. From fig. (7.1 b) which is plotted for $\alpha = 0.5000$ for closed universe we get at 68.3% confidence limit the acceptable range for B lies in $(-0.0654, 0.0785)$, for A_s $(-0.9372, 0.5396)$. At 95.4% confidence limit B lies in $(-0.0951, 0.1158)$ and A_s in $(-1.544, 0.6846)$. At 99.7%, it is $(-0.1234, 0.1673)$ for B and $(-2.374, 0.7901)$ for A_s . The best-fit value for the effective neutrino parameter $\Delta N_\nu = 0.0999$. From fig. (7.1 c) which is plotted for $\alpha = 0.001$ for closed universe at 68.3% confidence limit the acceptable limit for

Model	B	A_s	ΔN_ν
$\alpha = 0.999$	0.0075	0.1079	0.1001
$\alpha = 0.500$	0.0105	0.1106	0.1000
$\alpha = 0.001$	0.0165	0.1143	0.1000

Table 7.4: Best-fit values of MCG for $K = -1$

Model	A_s	ΔN_ν
$\alpha = 0.999$	0.0168	0.0859
$\alpha = 0.500$	0.0131	0.1000
$\alpha = 0.001$	0.0090	0.0999

Table 7.5: Best-fit values of GCG ($B = 0$) for $K = -1$

B is obtained as $(-0.0724, 0.0898)$, the limit for A_s is $(-0.6392, 0.4532)$. At 95.4% confidence limit B lies in $(-0.1081, 0.1334)$ and A_s in $(-1.043, 0.5838)$. At 99.7%, B lies in $(-0.1358, 0.1901)$ and A_s lies in $(-1.53, 0.7025)$. The best-fit value for the effective neutrino parameter $\Delta N_\nu = 0.8071$.

So combining all the figures for closed universe we get at 68.3% confidence limit the acceptable range for B which lies between $(-0.0724, 0.0898)$ and the parameter A_s lies in the range $(-1.206, 0.6321)$. At 95.4% confidence limit B lies in $(-0.1081, 0.1334)$ and A_s in the range $(-2.175, 0.7623)$. At 99.7% confidence limit, B lies in the range $(-0.1358, 0.1901)$ with A_s in the range $(-3.478, 0.8347)$.

Best-fit values of the open universe and the corresponding range of values of the EoS parameters are shown in Table-(7.4) and in Table-(7.6) respectively. Fig. (7.2 a) is plotted for $\alpha = 0.999$ in the case of open universe, at 68.3% confidence limit, the acceptable range for B lies in $(-0.0604, 0.0773)$ and A_s lies in $(-1.191, 0.6321)$. For 95.4% confidence limit B lies in $(-0.0887, 0.1133)$ and A_s lies in $(-2.175, 0.7623)$. At 99.7%, B lies in $(-0.1157, 0.1519)$ and A_s lies in $(-3.449, 0.8492)$. The best-fit

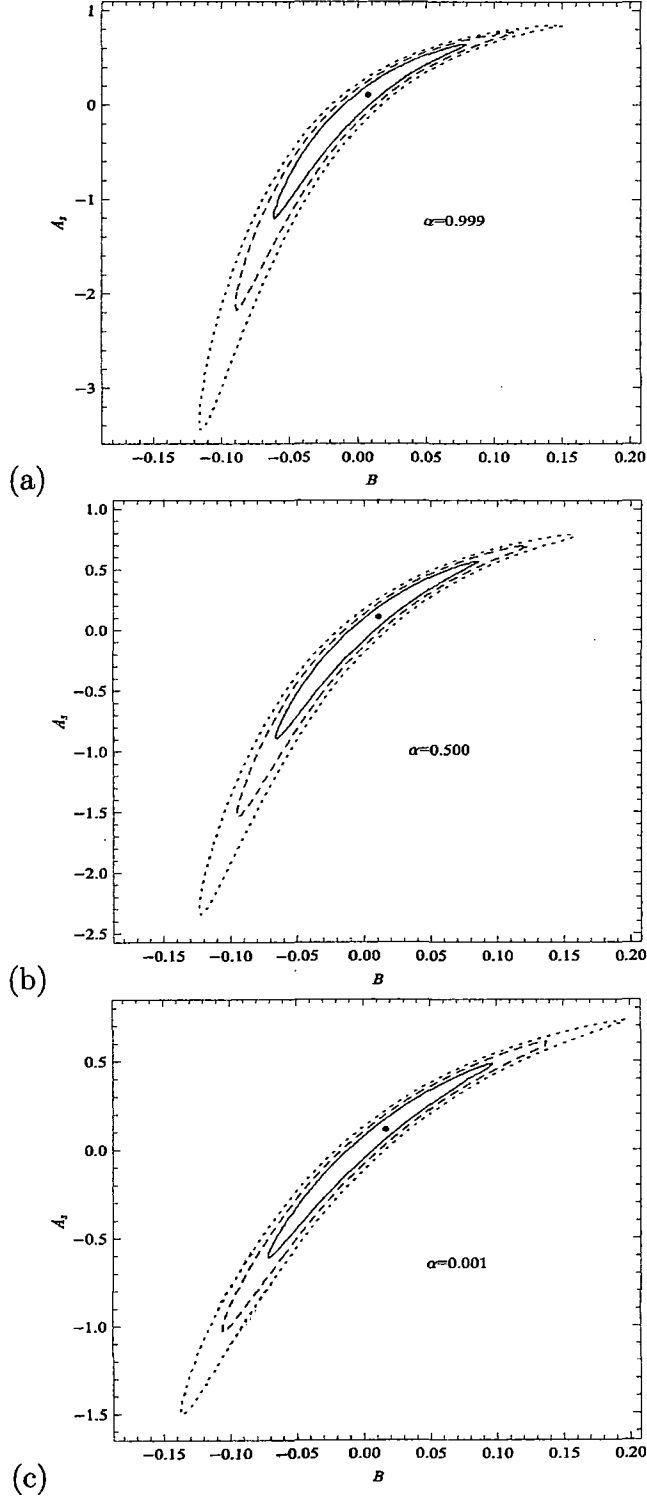


Figure 7.2: $A_s - B$ contours for (a) $\alpha = 0.999$, (b) $\alpha = 0.500$ and (c) $\alpha = 0.001$ for open universe using ($OHD + SDSS$ (BAO) + CMB shift) data at 68.3% (Solid), 95.4% (Dashed) and 99.7% (Dotted) confidence level.

<i>Data</i>	<i>CL</i>	<i>B</i>	<i>A_s</i>
$\alpha = 0.999$	68.3%	(-0.0604, 0.0773)	(-1.191, 0.6321)
	95.4%	(-0.0887, 0.1133)	(-2.175, 0.7623)
	99.7%	(-0.1157, 0.1519)	(-3.449, 0.8492)
$\alpha = 0.500$	68.3%	(-0.0643, 0.0773)	(-0.8977, 0.5264)
	95.4%	(-0.0951, 0.1223)	(-1.531, 0.6846)
	99.7%	(-0.1234, 0.1673)	(-2.348, 0.8033)
$\alpha = 0.001$	68.3%	(-0.0712, 0.0918)	(-0.6336, 0.4598)
	95.4%	(-0.1072, 0.1430)	(-1.049, 0.6114)
	99.7%	(-0.1387, 0.1942)	(-1.535, 0.7231)

Table 7.6: Range of values of the EoS parameters for $K = -1$ in MCG

value for the effective neutrino parameter $\Delta N_\nu = 0.1001$. Fig. (7.2 b) is plotted for $\alpha = 0.5000$ in the case of open universe, in this case 68.3% confidence limit the acceptable range for B becomes $(-0.0643, 0.0773)$ and A_s becomes $(-0.8977, 0.5264)$. At 95.4% confidence limit B lies in $(-0.0951, 0.1223)$ and A_s lies in $(-1.531, 0.6846)$. At 99.7%, B lies in $(-0.1234, 0.1673)$ and A_s lies in $(-2.348, 0.8033)$. The best-fit value for the effective neutrino parameter $\Delta N_\nu = 0.1000$. Fig. (7.2 c) is plotted for $\alpha = 0.001$ in the case of open universe, we get at 68.3% confidence limit the acceptable range for B which lies in $(-0.0712, 0.0918)$, that of A_s lies in $(-0.6336, 0.4598)$. At 95.4% confidence limit B lies in $(-0.1072, 0.1430)$ and A_s lies in $(-1.049, 0.6114)$. At 99.7%, B lies in $(-0.1387, 0.1942)$ and A_s lies in $(-1.535, 0.7231)$. The best-fit value for the effective neutrino parameter $\Delta N_\nu = 0.1000$.

Now for all the figures together for open universe one obtains at 68.3% confidence limit the range for B which lies in the range $(-0.0712, 0.0918)$ and A_s lies in the range $(-1.191, 0.6321)$. At 95.4% confidence limit B lies in the range $(-0.1072, 0.1430)$ and A_s lies in the range $(-2.175, 0.7623)$. At 99.7% confidence limit B lies in the range $(-0.1387, 0.1942)$ and A_s lies in the range $(-3.449, 0.8492)$.

Comparing closed and open universe together it is found that for a closed universe at 68.3% confidence limit B lies in $(-0.0724, 0.0898)$ compared to $(-0.0712, 0.0918)$ for an open universe. At 95.4% confidence limit B lies in the range $(-0.1081, 0.1334)$ compared to that of $(-0.1072, 0.1430)$ in the case of open universe. For closed universe B , satisfies the limit $-0.1358 < B < 0.1901$ and that for open universe it becomes $-0.1387 < B < 0.1942$ in 99.7% confidence level.

7.5 Test of MCG in HL gravity

In this section we discuss some of the implications of the present scenario of the universe. The evolution of the equation of state parameter of the total cosmic fluid of the universe is defined as $w(z) = \frac{p_{tot}}{\rho_{tot}}$, with the total pressure and energy density given by

$$p_{tot} = p_c + \frac{1}{3}\rho_r + \frac{2}{\kappa^2} \left[\frac{K^2}{\Lambda a^4} - 3\Lambda \right], \quad (7.23)$$

$$\rho_{tot} = \rho_c + \rho_b + \rho_r + \frac{2}{\kappa^2} \left[\frac{3K^2}{\Lambda a^4} + 3\Lambda \right]. \quad (7.24)$$

In the above the scale factor of the universe is replaced by redshift parameter, consequently the density parameter and the Hubble parameter are accordingly written. The variation of state parameter $w(z)$ with the redshift parameter z for both open and closed universe are plotted in fig. (7.3). It is evident from the curves that the model accommodates most of the evolutionary phases of the universe. At high redshift (early times) the state parameter is close to $\frac{1}{3}$, indicating radiation dominance in that epoch which is permitted both in closed and open universe. In the intermediate redshift dust dominates through MCG for quite a long period of time. It is noted that

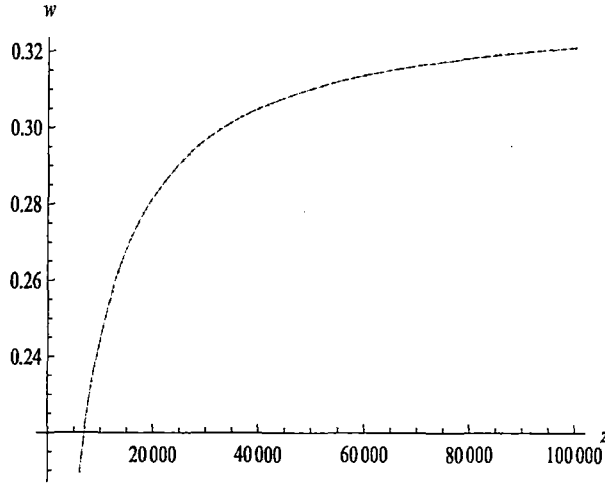


Figure 7.3: Variation of equation of state parameter for closed (Dotted line) and open (Solid line) universe

the state parameter becomes negative at small redshift, *i.e.*, in very recent past. In the case of closed or open universe the present value of the EoS parameter is negative (-0.7) which permits an accelerating universe.

In order to test the validity of the model best-fit values of the parameters of the MCG is used to find supernovae magnitudes (μ) at different redshift (z) and plotted μ *vs.* z curves for a closed universe. We compared these with original curves of Union Compilation data [102] and observed an excellent agreement. Similar agreement is observed in the case of an open universe.

7.6 Discussion

Cosmological models with MCG in the framework of HL gravity is studied to determine observational constraints on EoS parameters using $(H(z) - z)$ (OHD),

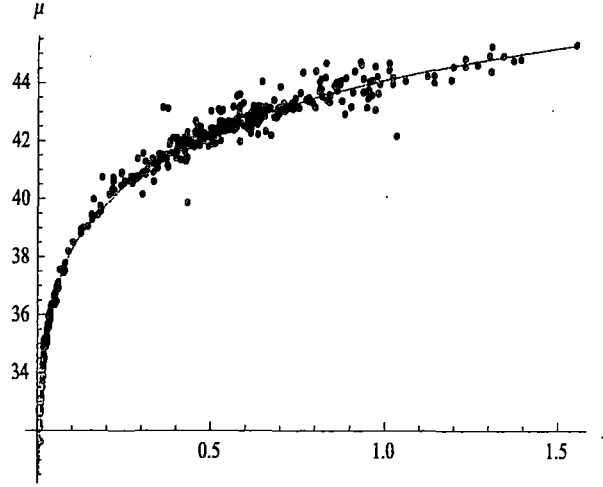


Figure 7.4: The comparison of the Union compilation data with the best-fit values in closed universe.

BAO peak parameter, CMB shift parameter. The analysis is done for the open and closed universe at 68.3%, 95.4%, 99.7% confidence limits. Comparing closed and open universe models we see that in a closed universe at 68.3% confidence limit B lies between $(-0.0724, 0.0898)$ compared to $(-0.0712, 0.0918)$ for an open universe model. At 95.4% confidence limit B lies between $(-0.1081, 0.1334)$ compared to that one obtains for an open universe $(-0.1072, 0.1430)$. For closed universe the limit is $(-0.1358, 0.1901)$ (Table-7.3) and for open universe it is $(-0.1387, 0.1942)$ (Table-7.6) with 99.7% confidence level. Comparing closed and open universe we see that in a closed universe the range of B is lesser compared to that in an open universe in the case of 68.3%, 95.4%, 99.7% confidence levels respectively. The range of B is quite small and may be negative as well. The negative value of B suggests that MCG corresponds to exotic matter. In the literature [231] the acceptable value of B was predicted to be very small, which is once again gets support from our analysis.

The plot of $w(z)$ vs. z at high redshift (early times) in fig. (7.3) shows that $w(z)$

attains $\frac{1}{3}$ in the case of closed and open universe respectively. This corresponds to radiation dominated era. In the intermediate redshift it behaves as dust for an extended period of time. EoS parameter picks up a negative value at small redshift, i.e., at very recent past. From the plot it is also ensured that in the case of closed or open universe the effective state parameter attains a negative value (-0.7) which favours an accelerating universe in accordance with observations. The best-fit values for both MCG and GCG EoS parameters in closed and open universe are determined. From the table for the best-fit values of the parameters it is quite obvious that the values of the parameters A_s , ΔN_ν pick up smaller values in GCG model than MCG model in both closed and open universe. In this model the parameter B plays a deterministic role of the evolution of the universe. The effective neutrino parameter is determined in MCG model as well as in GCG ($B = 0$) model. The effective neutrino parameter is found smaller in GCG model which is physically unrealistic. In addition the parameter A_s which is related to the speed of sound is also found small. On the other hand, both the neutrino parameter and A_s values obtained in the framework of MCG model in closed and open universe are physically relevant. Cosmological models with MCG are found to accommodate positive values for B when fitted with observational data. Thus it appears from the analysis that MCG is better than GCG in HL gravity because $B > 0$ is realistic. In MCG, the best-fit value for neutrino parameter may be less than one. The deviation of the value of the parameter from standard value is due to thermal history of the universe at the epoch such as the low reheating temperature [232]. The low value of the parameter signifies that the radiation-matter equality attains at earlier epoch which on the other hand leads to

an increase of matter energy density.

Using the best-fit values in closed universe model μ vs. redshift curve is plotted in fig. (7.4) and that compared with Union Compilation data. Similar curves may be drawn in open universe case also. It is found that both the plots agree quite satisfactorily. Thus it is evident that MCG is observationally acceptable matter constituents in Horava-Lifshitz gravity. The present analysis clearly shows the edge of MCG over GCG in the context of HL gravity. Earlier in the Einstein frame, MCG is employed to obtain viable cosmological models [233, 234], in this case MCG is employed in the HL gravity and determined various physical parameters of the universe which are supported from observations.

Chapter 8

Observational Constraints on MCG in Horava-Lifshitz Gravity with Dark Radiation

8.1 Introduction

In the previous Chapter cosmological models in HL gravity is studied in the presence of detailed balance condition and projectibility. Sotiriou, Visser and Weinfurtner (SVW) [225, 226] proposed another form of HL gravity with projectibility assuming beyond detailed balance condition which will be considered here. In a spatially curved Friedmann-Robertson-Walker universe, the SVW generalization yields an extra $\frac{1}{a^6}$ - term in the field equation compared to detailed balance scenario. Under this condition the field equations are modified in which a term similar to radiation known as dark radiation is found to exist. The EoS parameters of MCG in beyond detailed balance

scenario in presence of dark radiation is constrained here using observational data.

8.2 HL cosmology with beyond detailed balance condition and projectibility

As the scope of information with detailed balance condition is not enough for understanding observed universe in HL gravity [82, 83], in this section we investigate cosmologies in the HL gravity relaxing the detailed balance condition. Considering modified Chaplygin gas (MCG), baryon, radiation and dark radiation without detailed balance in the framework of HL gravity cosmological models are obtained. The motivation of considering such model is to explore the effects of the dark radiation on the parameters of the MCG model employing observational data. The Friedmann equations in this case can be written as [225, 226, 227, 235, 236, 237]:

$$H^2 = \frac{2\sigma_0}{(3\lambda - 1)}(\rho_m + \rho_r) + \frac{2}{(3\lambda - 1)} \left[\frac{\sigma_1}{6} + \frac{\sigma_3 K^2}{6a^4} + \frac{\sigma_4 K}{6a^6} \right] + \frac{\sigma_2 K}{3(3\lambda - 1)a^2}, \quad (8.1)$$

$$\dot{H} + \frac{3}{2}H^2 = \frac{3\sigma_0}{(3\lambda - 1)}(\rho_m \omega_m + \rho_r \omega_r) - \frac{3}{(3\lambda - 1)} \left[-\frac{\sigma_1}{6} + \frac{\sigma_3 K^2}{18a^4} + \frac{\sigma_4 K}{6a^6} \right] + \frac{\sigma_2 K}{6(3\lambda - 1)a^2}, \quad (8.2)$$

where $\sigma_0 = \kappa^2/12$, we define some useful dimensionless parameters, given below

$$G_{cosmo} = \frac{6\sigma_0}{8\pi(3\lambda - 1)}, \sigma_2 = -3(3\lambda - 1), G_{grav} = \frac{6\sigma_0}{16\pi}, \quad (8.3)$$

where $\sigma_2 < 0$ and $\sigma_4 > 0$. In the case of the beyond detailed balance condition and in the IR limit ($\lambda = 1$), the two parameters G_{cosmo} and G_{grav} become equal.

8.3 Observational constraints on EoS parameters

The EoS parameters of MCG given by eq. (1.3) are to be determined here for viable cosmologies in the framework of HL gravity using the recent observational data namely, Observed Hubble data (OHD), BAO peak parameter and CMB shift parameter.

8.3.1 Constraints obtained from beyond detailed balance

In beyond detailed balance scenario for $\lambda = 1$, the field eqs. (8.1) and (8.2) become

$$H^2 = \frac{8\pi G}{3}(\rho_b + \rho_c + \rho_r) + \left[\frac{\sigma_1}{6} + \frac{\sigma_3 K^2}{6a^4} + \frac{\sigma_4 K}{6a^6} \right] - \frac{K}{a^2} \quad (8.4)$$

$$\dot{H} + \frac{3}{2}H^2 = -4\pi G(p_c + \frac{1}{3}\rho_r) - \frac{3}{2} \left[-\frac{\sigma_1}{6} + \frac{\sigma_3 K^2}{18a^4} + \frac{\sigma_4 K}{6a^6} \right] - \frac{K}{2a^2}. \quad (8.5)$$

Finally, a dimensionless Hubble parameter ($E(z)$) can be obtained as

$$E^2(z) = \Omega_{b0}(1+z)^3 + \Omega_{c0}F(z) + \Omega_{r0}(1+z)^4 + \Omega_{K0}(1+z)^2 + [\Omega_1 + \Omega_3(1+z)^4 + \Omega_4(1+z)^6] \quad (8.6)$$

where $F(z) = \left[A_s + \frac{1-A_s}{a^{3(1+B)(1+\alpha)}} \right]^{\frac{1}{1+\alpha}}$. The dimensionless parameters, namely, $\Omega_1, \Omega_3, \Omega_4$ are related to the model parameters $\sigma_1, \sigma_3, \sigma_4$ as follows:

$$\Omega_1 = \frac{\sigma_1}{6H_0^2}, \quad \Omega_3 = \frac{\sigma_3 H_0^2 \Omega_{K0}^2}{6}, \quad \Omega_4 = -\frac{\sigma_4 \Omega_{K0}}{6}. \quad (8.7)$$

At the present epoch $E(z=0) = 1$, it leads to

$$\Omega_{b0} + \Omega_{c0} + \Omega_{r0} + \Omega_{K0} + \Omega_1 + \Omega_3 + \Omega_4 = 1. \quad (8.8)$$

In the above equations Ω_4 is required to be a positive quantity in order that the Hubble parameter and the gravitational perturbations [225, 226, 235] are positive definite at all values of redshifts. Ω_3 is also assumed to be positive definite. Following the procedure adopted in Ref. [218] for ΔN_ν , we consider the upper limit of dark radiation in the standard model from the Big Bang Nucleo-synthesis (BBN). Consequently, at the time of BBN ($z = z_{BBN}$) [228, 229, 230, 238] we get :

$$\Omega_3 + \Omega_4(1 + z_{BBN}^2)^2 = \Omega_{3max} = 0.135\Delta N_\nu\Omega_{r0}, \quad (8.9)$$

where the Ω_3 represents the usual dark radiation and Ω_4 represents a kinetic-like component (a quintessence field dominated by kinetic energy) [239, 240]. The above equation will be used to replace Ω_4 in terms of other parameters in the analysis. For simplicity we define

$$\beta = \frac{\Omega_3}{\Omega_{3max}} \quad (8.10)$$

where Ω_{3max} is the upper limit on Ω_3 . Consequently Ω_3 can be expressed in terms of the other parameters. Following the detailed balance scenario we consider ΔN_ν , so that it satisfies the bound $0 < \Delta N_\nu \leq 2.0$, taking into account the importance of curvature in dark energy models and treating Ω_{K0} as a free parameter as was taken in Ref. ([241, 242]). The Hubble parameter contains thirteen free parameters, namely, Ω_{b0} , Ω_{c0} , Ω_{r0} , Ω_{K0} , Ω_1 , Ω_3 , Ω_4 , ΔN_ν , H_0 , A_s , B , α , β . To analyze numerically some of them are fixed using the best-fit values from WMAP 7 data [93]. The parameters are $\Omega_{m0}(\equiv \Omega_{b0} + \Omega_{c0})$, Ω_{b0} , H_0 , Ω_{r0} and the corresponding values of the parameters are chosen as follows: $\Omega_{m0} = 0.27$, $\Omega_{b0} = 0.04$, $H_0 = 71.4 Km/sec/Mpc$, $\Omega_{r0} = 8.14 \times 10^{-5}$. Using the constraint eqs. (8.7) - (8.10) one can replace Ω_1 , Ω_3 , Ω_4 in terms of the other six free parameters for the numerical analysis. Thus six free

parameters are left to be determined which are Ω_{K0} , A_s , B , α , β , ΔN_ν .

To determine the constraints on the parameters of the MCG in beyond detailed balance scenario, we consider three values of α satisfying $0 \leq \alpha \leq 1$ ($\alpha=0.999, 0.500, 0.001$) and determine the best-fit values for the rest five parameters (*i.e.*, A_s , B , β , Ω_{K0} , ΔN_ν). Thereafter, at the best-fit value of ΔN_ν , β , Ω_{K0} for three values of α we plot 2d contours for the pair of parameters (A_s , B) at different confidence levels. The contours of A_s , B drawn at different values of α , determines the permissible range of values of the B parameter for the MCG in HL gravity in the framework of beyond detailed balance scenario. The effect of dark radiation (*i.e.*, effective neutrino parameter) on the constraints on the parameters of the MCG, is studied here considering two extreme values of α ($\alpha=0.999, 0.001$) in the limit $0 \leq \alpha \leq 1$ for the two extreme values of ΔN_ν (0.01, 2.0). In this case each of these values of α , ΔN_ν determines the best-fit values of the rest four parameters (*i.e.*, A_s , B , β , Ω_{K0}). Thereafter, at the extreme values of ΔN_ν for two extreme values of α we plot 2d contours for the parameters A_s , B for the best-fitted values of β , Ω_{K0} at different confidence levels. From the contours of A_s , B drawn at different values of α and ΔN_ν we determine the permissible range of values of the B parameter for the MCG in HL gravity in the framework of beyond detailed balance scenario. We note that the range of values of B is narrower due to the effect of effective neutrino parameter on B .

8.4 Numerical analysis

In this section, we determine constraints on the parameters of the MCG in beyond detailed balance scenario employing observed data namely, Stern data set for $(H(z) -$

z) data (OHD), BAO peak parameter and CMB shift parameter. We adopt numerical technique to determine the constraints with the help of a *Chi-square* function. The limiting values for the EoS parameters are determined by minimization the *Chi-square* function thereafter.

8.4.1 (H- z) data (OHD) as a tool for constraining

The *Chi-square* function is defined as

$$\chi_{OHD}^2(H_0, \Omega_{K0}, A_s, B, \alpha, \beta, \Delta N_\nu, z) = \sum \frac{(H(H_0, \Omega_{K0}, A_s, B, \alpha, \beta, \Delta N_\nu, z) - H_{obs}(z))^2}{\sigma_z^2} \quad (8.11)$$

where $H_{obs}(z)$ is the observed Hubble parameter at redshift z and σ_z is the associated error with that particular observation. Hubble parameter is given by

$$H(z) = H_0 E(z) \quad (8.12)$$

where

$$\begin{aligned} E^2(z) = & \Omega_{b0}(1+z)^3 + \Omega_{c0}F(z) + \Omega_{r0}(1+z)^4 + \Omega_{K0}(1+z)^2 \\ & + [\Omega_1 + \Omega_3(1+z)^4 + \Omega_4(1+z)^6] \end{aligned} \quad (8.13)$$

with $F(z) = \left[A_s + \frac{1-A_s}{a^3(1+B)(1+\alpha)} \right]^{\frac{1}{1+\alpha}}$. Here $(H(z) - z)$ data (OHD) is taken from Stern data analysis [99] which is shown in Table-(2.1).

8.4.2 BAO peak parameter as a tool for constraining

The *Chi-square* function χ_{BAO}^2 given by eq. (1.31) with \mathcal{A} (0.469 ± 0.017) from the SDSS (Sloan Digital Sky Survey) data for LRG (Luminous Red Galaxies) survey [88] is used here for numerical analysis.

Data	CL	B
$\alpha = 0.999$	68.3%	(-0.0550, 0.0381)
	95.4%	(-0.0799, 0.0735)
	99.7%	(-0.1035, 0.1128)
$\alpha = 0.500$	68.3%	(-0.0574, 0.0442)
	95.4%	(-0.0835, 0.0829)
	99.7%	(-0.1060, 0.1305)
$\alpha = 0.001$	68.3%	(-0.0926, 0.0707)
	95.4%	(-0.1326, 0.1493)
	99.7%	(-0.1727, 0.2247)

Table 8.1: Range of values of the EoS parameters in beyond detailed balance scenario

8.4.3 CMB shift parameter as a tool for constraining

The definition of CMB shift parameter given by eq. (1.34) with the WMAP 7 data giving $R = 1.726 \pm 0.018$ at $z = 1091.3$ [93] is also used to define a *Chi-square* function χ_{CMB}^2 .

8.4.4 Joint analysis with OHD + BAO+ CMB data

The total *Chi-square* function for the joint analysis is given by:

$$\chi_{tot}^2 = \chi_{OHD}^2 + \chi_{BAO}^2 + \chi_{CMB}^2. \quad (8.14)$$

The statistical analysis with χ_{tot}^2 gives the bounds on the model parameter specially on B . Range of values of the EoS parameters in beyond detailed balance scenario are shown in Table-(8.1). Fig. (8.1 a) is plotted for $\alpha = 0.999$ with best-fitted values of β , ΔN_ν and Ω_{K0} . The parameter B lies in $(-0.0550, 0.0381)$, $(-0.0799, 0.0735)$, $(-0.1035, 0.1128)$ at 68.3%, 95.4%, 99.7% confidence levels respectively. Fig. (8.1 b) is plotted for $\alpha = 0.500$ for best-fitted values of β , ΔN_ν and Ω_{K0} . The parameter B in this case satisfies the following limits: $(-0.0574, 0.0442)$,

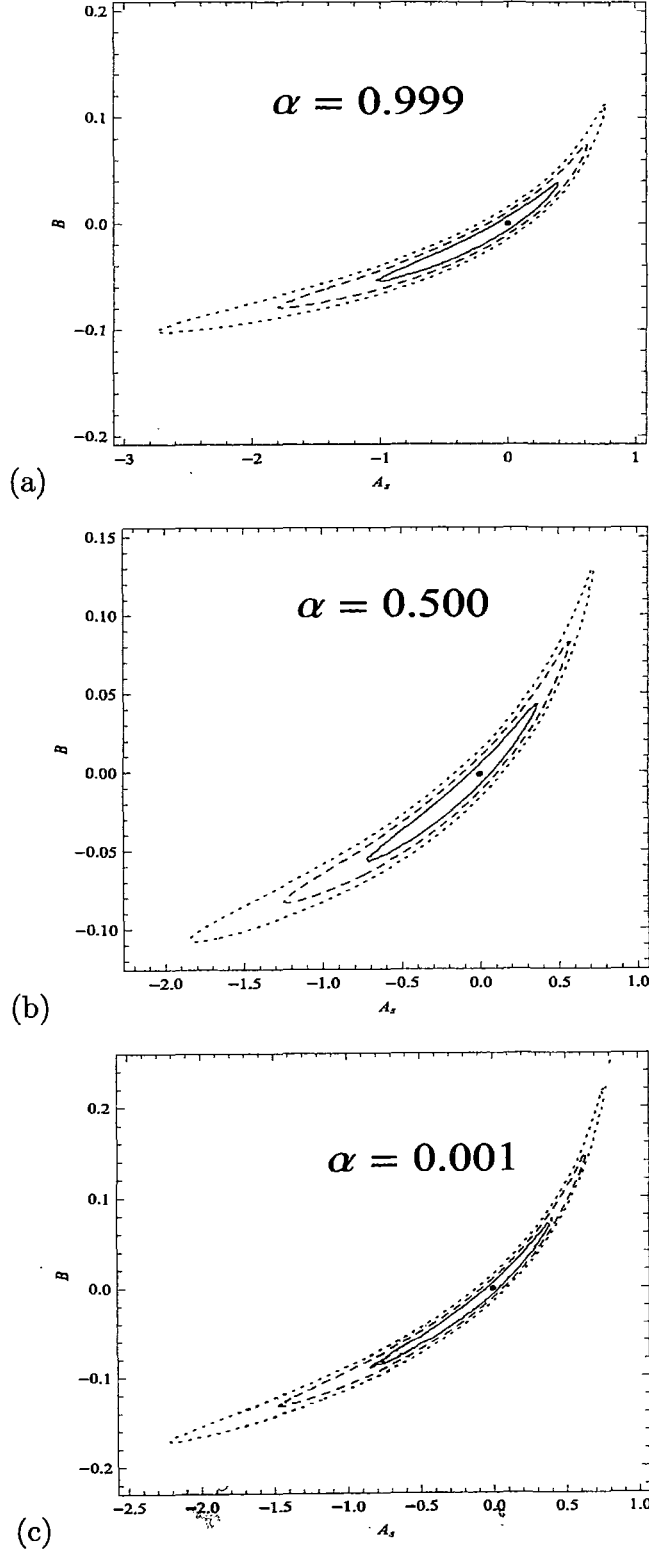


Figure 8.1: $A_s - B$ contours for (a) $\alpha = 0.999$, (b) $\alpha = 0.500$ and (c) $\alpha = 0.001$ in beyond detailed balance scenario using ($OHD + SDSS (BAO) + CMB$ shift) data at 68.3% (Solid), 95.4% (Dashed) and 99.7% (Dotted) confidence level.

<i>Data</i>	<i>CL</i>	<i>B</i>
$\alpha = 0.999, \Delta N_\nu = 0.01$	68.3%	(-0.0534, 0.0335)
	95.4%	(-0.0794, 0.0745)
	99.7%	(-0.1013, 0.1224)
$\alpha = 0.999, \Delta N_\nu = 2.0$	68.3%	(-0.0546, 0.0362)
	95.4%	(-0.0798, 0.0766)
	99.7%	(-0.1032, 0.1162)

Table 8.2: Acceptable range of B parameter in beyond detailed balance scenario for $\alpha = 0.999$

(-0.0835, 0.0829), (-0.1060, 0.1305) at 68.3%, 95.4%, 99.7% confidence levels respectively. Fig. (8.1 c) is plotted for $\alpha = 0.001$ for best-fitted value of β , ΔN_ν and Ω_{K0} . We note that the parameter B satisfies the following limiting values (-0.0926, 0.0707), (-0.1326, 0.1493), (-0.1727, 0.2247) at 68.3%, 95.4%, 99.7% confidence levels respectively. It is evident that the allowed range of values of the parameter B is wider compared to that of the detailed balance scenario [243]. The range of B parameter in beyond detailed balance scenario for one extreme alpha ($\alpha = 0.999$) is shown in Table-(8.2). Fig. (8.2 a) is plotted for $\alpha = 0.999$ and $\Delta N_\nu=0.01$ with best-fitted value of β and Ω_{K0} . It is evident that B can take both positive and negative values in the ranges: (-0.0534, 0.0335), (-0.0794, 0.0745), (-0.1013, 0.1224) at 68.3%, 95.4%, 99.7% confidence levels respectively. Fig. (8.2 b) is plotted for $\alpha = 0.999$ and $\Delta N_\nu=2.0$, it is evident that the value of B lies in the range (-0.0546, 0.0362), (-0.0798, 0.0766), (-0.1032, 0.1162) at 68.3%, 95.4%, 99.7% confidence levels respectively. The figs. (8.2 a - 8.2 b) show that the range of permissible values of B decreases with an increase in the effective neutrino parameter. The range of B parameter in beyond detailed balance scenario for smaller alpha ($\alpha = 0.001$) are shown in Table-(8.3) at different confidence limit. Fig. (8.3

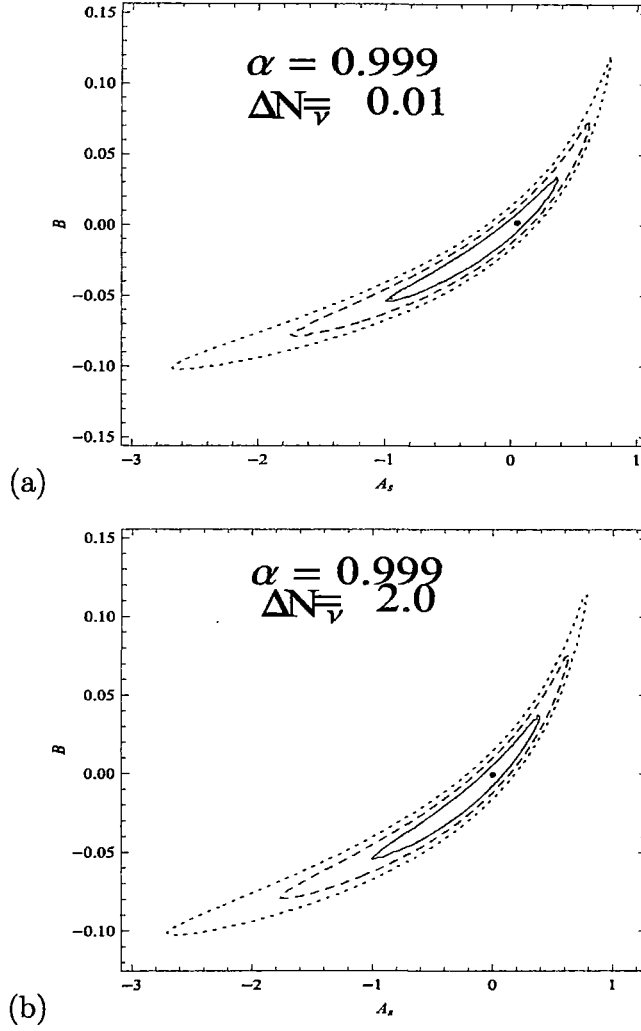


Figure 8.2: Constraints in beyond detailed balance for $\alpha = 0.999$ using (*OHD* + *SDSS* (*BAO*) + *CMB* shift) data at 68.3% (Solid), 95.4% (Dashed) and 99.7% (Dotted) confidence level.

<i>Data</i>	<i>CL</i>	<i>B</i>
$\alpha = 0.001, \Delta N_\nu = 0.01$	68.3%	(-0.0668, 0.0407)
	95.4%	(-0.0943, 0.0892)
	99.7%	(-0.1206, 0.1416)
$\alpha = 0.001, \Delta N_\nu = 2.0$	68.3%	(-0.0635, 0.0484)
	95.4%	(-0.0924, 0.0924)
	99.7%	(-0.1194, 0.1414)

Table 8.3: Acceptable range of *B* parameter in beyond detailed balance scenario for $\alpha = 0.001$

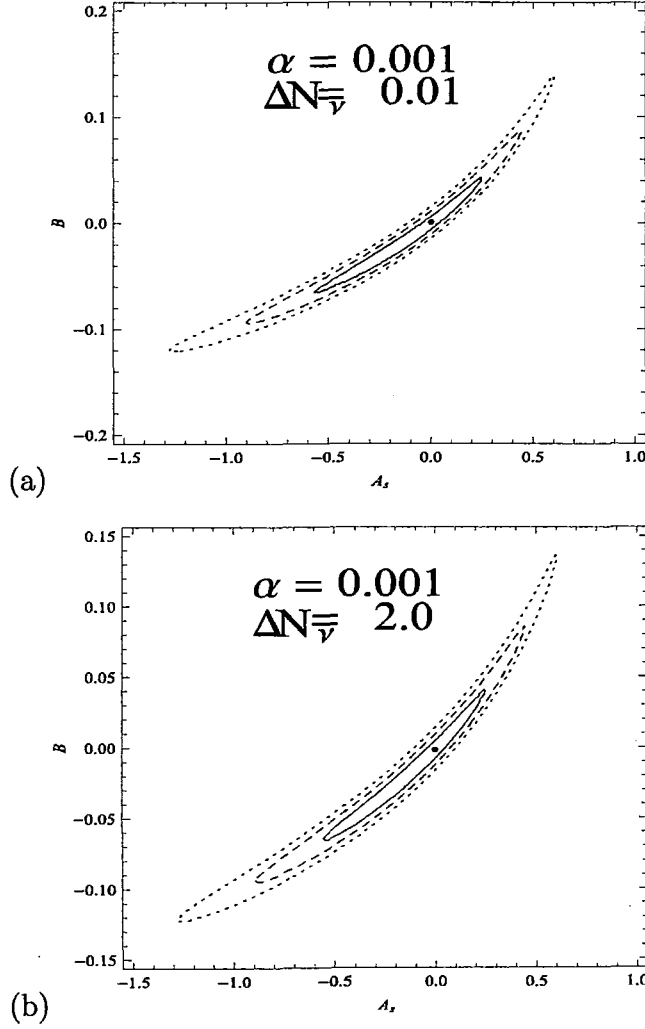


Figure 8.3: Constraints in beyond detailed balance for $\alpha = 0.001$ using (*OHD* + *SDSS* (*BAO*) + *CMB* shift) data at 68.3% (Solid), 95.4% (Dashed) and 99.7% (Dotted) confidence level.

a) is plotted for $\alpha = 0.001$ and $\Delta N_\nu = 0.01$ for best-fitted value of β and Ω_{K0} , it is evident that the permissible values of B now lies in the range $(-0.0668, 0.0407)$, $(-0.0943, 0.0892)$, $(-0.1206, 0.1416)$ at 68.3%, 95.4%, 99.7% confidence levels respectively. Fig. (8.3 b) is plotted for $\alpha = 0.001$ and $\Delta N_\nu = 2.0$, it is evident that the values of B lies in the range $(-0.0635, 0.0484)$, $(-0.0924, 0.0924)$, $(-0.1194, 0.1414)$ at 68.3%, 95.4%, 99.7% confidence levels respectively. The contours drawn in figs. (8.3 a) and (8.3 b) show that the range of permissible values of B now decreases with an increase in the effective neutrino parameter. It is noted that the allowed range of values of the parameter B , decreases appreciably here compared to that permitted from figs. (8.1 a - 8.1 c). This signifies the fact that as the contribution of dark radiation increases (through effective neutrino parameter) the range of admissible values of B decreases in the case of beyond detailed balance scenario.

8.5 Viability of MCG in HL gravity

In the case of beyond detailed balance scenario the total pressure and the energy density is given respectively as

$$p_{tot} = p_c + \frac{1}{3}\rho_r + \left[-\frac{\sigma_1}{6\sigma_0} + \frac{\sigma_3 K^2}{18\sigma_0 a^4} + \frac{\sigma_4 K}{6\sigma_0 a^6} \right], \quad (8.15)$$

$$\rho_{tot} = \rho_c + \rho_b + \rho_r + \left[\frac{\sigma_1}{6\sigma_0} + \frac{\sigma_3 K^2}{6\sigma_0 a^4} + \frac{\sigma_4 K}{6\sigma_0 a^6} \right]. \quad (8.16)$$

In the above equations the scale factor is replaced by redshift parameter and consequently the density parameter and the Hubble parameter can be expressed in terms of redshift parameter. The EoS parameter in terms of the redshift parameter z is

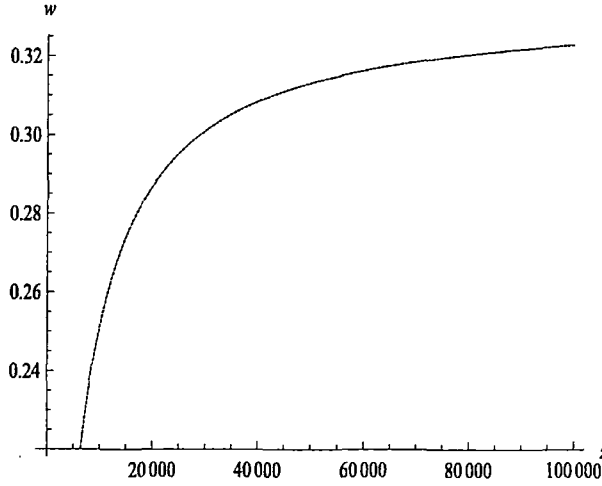


Figure 8.4: Equation of state parameter in beyond detailed balance scenario

given by

$$w(z) = \frac{p_{tot}}{\rho_{tot}}. \quad (8.17)$$

From the plot of $w(z)$ with z , for beyond detailed balance scenario we note that at high redshift (*i.e.*, early times) it attains a fixed value $\frac{1}{3}$ since radiation dominates in that epoch. In the intermediate redshift it behaves as dust for quite a long time. It is observed that the equation of state parameter picks up negative values at small redshift, *i.e.*, in the recent past. The present value of the equation of state parameter attains a negative value (-0.7) in the case of closed or open universe. In order to test the validity of cosmological models, the best-fit values of the parameters of MCG are employed for drawing curve for supernovae magnitudes (μ) at different redshift (z). We also plot μ *vs.* z curve to compare with observation. The plot of Union2 data [244] from the observations is in excellent agreement with the model.

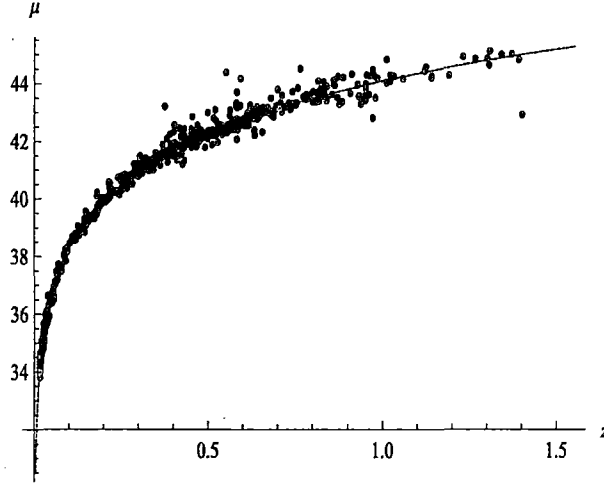


Figure 8.5: The comparison of the Union2 data with the best-fit values in beyond detailed balance

8.6 Discussion

Cosmological models with MCG in HL gravity scenario are studied considering beyond detailed balance conditions both in the presence and in the absence of dark radiation. Constraints on EoS parameters are determined using observational data namely, $(H(z) - z)$ (OHD), BAO peak parameter, CMB shift parameter data. For the MCG, the parameter B corresponds to the matter part. The allowed range of values of B for viable cosmologies are determined.

In the beyond detailed balance scenario there are six free parameters, namely Ω_{K0} , A_s , B , α , β , ΔN_ν . It is found that the entire range of effective neutrino parameter is consistent with observations from our numerical analysis. The contours drawn in figs. (8.1 a - 8.1 c) for beyond detailed balance condition with whole range of α for best-fitted values of other parameters (β , ΔN_ν and Ω_{K0}) projects the admissible values of B that lies in the range $(-0.0926, 0.0707)$, $(-0.1326, 0.1493)$, $(-0.1727, 0.2247)$

(Table-8.1) at 68.3%, 95.4%, 99.7% confidence levels respectively. The range of B obtained for beyond detailed balance scenario are found larger than that of detailed balance scenario and without dark radiation [243]. It is evident from figs. (8.2 a - 8.2 b) that the permitted range of values of B decreases with an increase of the effective neutrino parameter for $\alpha = 0.999$. It is also evident from fig. (8.3) for $\alpha = 0.001$ with different (ΔN_ν) that the range of values of B decreases with an increase of the effective neutrino parameter. It is noted that the range of values of B decreases appreciably here compared to that obtained from figs. (8.1 a - 8.1 c). This signifies that as the contribution of dark radiation increases (through effective neutrino parameter) the contribution in the permissible range of values of B decreases in beyond detailed balance scenario. In figure (8.4) we plot the variation of the equation of state parameter $w(z)$ with the redshift parameter z for beyond detailed balance scenario. The curve shows the evolutionary phases of the universe satisfactorily. It is evident that at high redshift (early times) the equation of state parameter attains $\frac{1}{3}$, indicating radiation domination phase in that epoch. However, in the intermediate redshift we note that dust dominates and MCG dominates in recent times for quite a long period. Using the best-fit values in beyond detailed balance scenario we plot μ vs. redshift curve in fig. (8.5) and the figure is then compared with the Union Compilation data [244]. It is evident from the figure that cosmologies in HL gravity with MCG fits well with the experimental result.

Chapter 9

Concluding remark and Future plan of work

General theory of Relativity (in short, GTR) is the basis for understanding the dynamics of the universe. However, it has been realized today that the GTR is not enough for understanding the universe as a whole. Therefore in theoretical cosmology the evolution and composition of the universe are studied as a system by constructing cosmological models in the framework of GTR, or in a modified theory of GTR confronting them with experiments and observations. Cosmology at the present time deals to a large extent with statistical predictions and measurements of its different parameters. In recent years, advances in experiments and computational techniques along with several astronomical and cosmological missions have made it possible to consider cosmology as an experimental science. It is predicted from cosmological observations that the universe might have originated from Big Bang in the past. Some of the relics of the Big Bang namely, CMBR, abundances of Helium etc., are the

evidences in favour of Big Bang model. Although the standard Big Bang model is successful in many aspects yet it fails to predict the observed universe both in the early and in the late era. If the early universe be probed in Big Bang model some of the conceptual issues in cosmology namely, horizon problem, flatness problem and singularity problem emerged which do not have solution in the perfect fluid assumptions. In order to address those issues, the concept of inflation was introduced in cosmology in 1981 by Guth [3]. A handful of inflationary models have been proposed in the literature in the last 30 years to realize early inflation ([3]-[48]). Inflationary scenario is attractive as it solves some of the outstanding problems of cosmology and particle physics satisfactorily. It also opens up new avenues in the interface of particle physics and cosmology. In modern cosmology [245, 246, 247] inflation is therefore considered as one of the essential ingredient to build a viable cosmological model. It may be pointed out here that inflation can be realized if matter is described in terms of quantum fields. The homogeneous scalar field of standard model in GTR gives rise to an inflationary phase when the potential energy of the field dominates over the kinetic energy. Although there is a progress in realizing early universe, it remains to be understood when and how the universe entered into the phase. Thus, early inflation in cosmology is still an open area of research.

In recent times cosmological observations, such as high redshift surveys of SNe Ia [49, 50, 51, 104], CMBR ([105]-[109]), WMAP ([110]-[114]) discovered another interesting phenomena that the present universe is passing through a phase of accelerated expansion. This is a new area in theoretical physics. It is known that the standard model of particle physics with GTR cannot provide a satisfactory explanation of this

new predictions. Thus, a new form of energy is needed to realize the late acceleration in cosmology which is termed as dark energy, it is different from that of dark matter. It has now become a challenge in theoretical physics to address the recent observational issues. However, in the literature following proposals: (i) a modification of the matter sector, (ii) a modification of the gravitational sector of the Einstein-Hilbert action or both may be considered. Modification of the matter sector of the Einstein gravity with exotic matter having negative pressure namely, phantoms [118, 119, 120], tachyons [121, 122, 123], quintessence [124, 125, 126], K-essence [127, 128, 129], Chaplygin gas etc. are considered widely.

A number of modified gravity with a polynomial in Lagrangian with scalar curvature R have also been considered in the literature ([76]-[80]). Another modified gravity proposed by Horava and Lifshitz known as HL gravity is also considered in recent times because of its successes ([207]-[217]) in condensed matter physics. Emergent universe model [68] obtained in GTR with a non-linear EoS provided an interesting area of cosmology to explore. EU model permits a universe with a composition of three different types of fluids which can be realized by a non-linear EoS. Emergent universe scenario is ever existing without an initial singularity and which accommodates a late accelerating phase satisfactorily. If this is tuned efficiently it can produce the late accelerating phase as well. The EoS for EU model contains two free parameters which are constrained using the observed data in Ref. [248, 249]. The constituents of this universe may vary as the value of the parameter B varied. For a given value of B parameter, it can accommodate dark energy as one of its constituents. The dark energy with negative pressure responsible for the present acceleration, is found

to exist in the EoS required for EU model in all cases.

In Chapter 2, a general model of EU scenario of Mukherjee *et al.* is considered. The EoS parameters are constrained employing the $(H(z) - z)$ data (OHD) [99], BAO peak parameter and CMB shift parameters using *Chi-square* minimization technique. The best-fit values of the model along with the range for the EoS parameters are estimated. Variation of deceleration parameter, density parameter are also studied here. The viability of the model is tested by plotting μ - z curves.

In Chapter 3, best-fit values of one of the EoS parameters and an integration constant of the models are determined for $B = -\frac{1}{3}, 0, \frac{1}{3}, 1$. Thereafter, the range of values of the corresponding parameters at different confidence levels are determined using χ^2 minimization technique. Viability of the models is further tested by comparing μ - z plot of the model and that of union compilation supernovae data.

In Chapter 4, MCG is chosen as a candidate of dark energy in standard gravity model. In this scenario EoS parameters are constrained with the age constancy of the universe and $(H(z) - z)$ data ([130]). Best-fit values and range of values are thereby determined by numerical analysis. Viability of the model is tested through the distance modulus μ vs. z plot.

In Chapter 5, MCG is chosen as a candidate of dark energy which is used to analyze in the context of the structure formation of the universe. Growth data set which is related to the structure formation through initial density perturbation of the universe is used here to explore dynamical aspects of the universe. Also *r.m.s* mass fluctuation σ_8 data obtained from various source such as Lyman- α data is used here along with $(H(z) - z)$ (Stern) data (OHD) [99]. Thereafter, MCG model parameters obtained

from the observational data analysis are then compared with that of GCG and Λ CDM model parameters.

In Chapter 6, holographic dark energy (in short, HDE) model of the universe is considered with a scalar field equivalent to MCG. Holographic dark energy field and its potential are determined for a non flat universe. Inclusion of a barotropic fluid (which is MCG) does not alter the form of potential and evolution of the holographic dark energy field. Holographic dark energy contributes more for ($B \neq 0$) compared to the case $B = 0$. It is found that the holographic dark energy is stable for a restricted domain of the values of Ω_Λ in a closed model of the universe.

In Chapter 7, HL gravity model in the detailed balance scenario is considered. In this framework MCG is used to obtain late time accelerating scenario and determine the EoS parameters for a viable cosmology. Best-fit values for EoS parameters of GCG are determined and have been compared with that of MCG.

In Chapter 8, HL gravity model in the beyond detailed balance scenario is considered. Here the effect of the dark radiation on the matter parameters have been considered in details. The best-fit values of the parameters along with their range of values have been calculated and compared with that of detailed balance scenario.

In the above analysis it is found that the EoS parameters of the different models considered here permit late accelerating phase satisfactorily. In the general EU model EoS parameters A, B and the other parameter K are found very small, whereas, for the particular EU models with $B = 0, \frac{1}{3}, 1$ the parameters A, K may pick up considerably higher values. In both the types, the model parameters allow accelerating universe, at late time.

The EoS parameters for MCG are determined in GTR considering $(H - z)$ data [130] and dimensionless age parameter for CDM and UDME model which are presented in Chapter 4. In Chapter 5, $(H - z)$ data (OHD) [99], growth data and *r.m.s* mass fluctuation data for the numerical analysis are used. It is noted that the parameters determined in Chapter 4 are higher than that obtained in Chapter 5, where growth data are considered. In alternative gravity for example HL gravity with detailed balance scenario the best-fit values and the range of values for MCG in closed and in open universe are evaluated and it is found that the values of A_s, B are much much less than that obtained from GTR framework. In the case of beyond detailed balance scenario the range of A_s, B values are almost same as that obtained with detailed balance condition. It is also noted that in HL gravity values of A_s, B are smaller compared to that of GTR.

9.1 Future plan of work:

The numerical analysis adopted here in EU scenario involves kinematics only and it is also interesting to analyze cosmological model to determine the model constraints using the dynamical aspects like structure formation etc. A more stringent constraint on the EU model may be obtained for a viable candidate in cosmology. The recent Planck data [250] may be useful to probe the cosmologies in addition to WMAP 7 data.

HL gravity with MCG is considered to study the evolution of the universe and in the process it determines various physical parameters of the universe which are supported by observations. However, the present analysis does not enlighten the conceptual

issues in HL gravity. A number of issues *e.g.*, why the value of neutrino parameter is small in HL gravity with MCG remains to be explored. In GTR, MCG is analyzed using the *OHD*, BAO data, CMB data, growth data and *r.m.s* mass fluctuation data. The Planck data along with the predictions will be useful to figure out the suitability of cosmological models in future. The analysis adopted here may be extended for this purpose as future activity.

Bibliography

- [1] Penzias A A and Wilson R W, 1965, *Astrophys. J. Lett.* **142**, 419
- [2] Dicke R H, Peebles P J E, Roll P J and Wilkinson D T, 1965, *Astrophys. J. Lett.* **142**, 414
- [3] Guth A H, 1981, *Phys. Rev. D* **23**, 347
- [4] Linde A D, 1982, *Phys. Lett. B* **108**, 389
- [5] Linde A D, 1982, *Phys. Lett. B* **114**, 431
- [6] Albrecht A and Steinhardt P, 1982, *Phys. Rev. Lett.* **48**, 1220
- [7] Linde A D, 1983, *Phys. Lett. B* **129**, 177
- [8] Paul B C, Datta D P and Mukherjee S, 1986, *Mod. Phys. Letts. A* **1**, 149
- [9] Starobinsky A A, 1979, *J. Theor. Exper. Phys. Lett.* **30**, 682
- [10] Starobinsky A A, 1980, *Phys. Lett. B* **91**, 99
- [11] Guth A H and Weinberg E J, 1983, *Nucl. Phys. B* **212**, 321
- [12] Linde A D, 1984, *Rep. Prog. Phys.* **47**, 925

- [13] Abbott L F and Wise M B, 1984, *Nucl. Phys. B* **244**, 541
- [14] Lucchin F and Matarrese S, 1985, *Phys. Rev. D* **32**, 1316
- [15] Barrow J D, 1987, *Phys. Lett. B* **187**, 12
- [16] Yokoyama J and Maeda K, 1988, *Phys. Lett. B* **207**, 31
- [17] Liddle A R, 1989, *Phys. Lett. B* **220**, 502
- [18] La D and Steinhardt P J, 1989, *Phys. Rev. Lett.* **62**, 376
- [19] La D and Steinhardt P J, 1989, *Phys. Lett. B* **220**, 375
- [20] Copeland E J, Liddle A R, Lyth D H, Stewart E D and Wands D, 1994, *Phys. Rev. D* **49**, 6410
- [21] Yamaguchi M, 2001, *Phys. Rev. D* **64**, 063502, arXiv: hep-ph/0103045v2
- [22] Linde A D, 1991, *Phys. Lett. B* **259**, 38
- [23] Linde A D, 1994, *Phys. Rev. D* **49**, 748
- [24] Lyth D and Riotto A, 1999, *Phys. Rep.* **314**, 1
- [25] Halyo E, 1996, *Phys. Lett. B* **387**, 43
- [26] Binetruy P and Dvali G, 1996, *Phys. Lett. B* **388**, 241
- [27] Horava P and Witten E, 1996, *Nucl. Phys. B* **460**, 506
- [28] Horava P and Witten E, 1996, *Nucl. Phys. B* **475**, 94
- [29] Lukas A, Ovrut B A, Stelle K S and Waldram D, 1999, *Phys. Rev. D* **59**, 086001

-
- [30] Lukas A, Ovrut B A and Waldram D, 1999, *Phys. Rev. D* **60**, 086001
- [31] Randall L and Sundrum R, 1999, *Phys. Rev. Lett.* **83**, 3370
- [32] Randall L and Sundrum R, 1999, *Phys. Rev. Lett.* **83**, 4690
- [33] Liddle A R, Mazumdar A and Schunck F E, 1998, *Phys. Rev. D* **58**, 061301, arXiv: astro-ph/9804177
- [34] Jokinen A and Mazumdar A, 2004, *Phys. Lett. B* **597**, 222, arXiv: hep-th/0406074
- [35] Randall L, Soljagic M and Guth A H, 1996, *Nucl. Phys. B* **472**, 377, arXiv: hep-ph/9512439
- [36] Armendariz-Picon C, Damour T and Mukhanov V, 1999, *Phys. Lett. B* **458**, 209, arXiv: hep-th/9904075
- [37] Dasgupta K, Herdeiro C, Hirano S and Kallosh R, 2002, *Phys. Rev. D* **65**, 126002, arXiv: hep-th/0203019
- [38] Koyama F, Tachikawa Y and Watari T, 2004, *Phys. Rev. D* **69**, 106001, arXiv: hep-th/0311191
- [39] Hsu J P and Kallosh R, 2004, *J. High Energy Phys.* **0404**, 042, arXiv: hep-th/0402047
- [40] Dasgupta K, Hsu J P, Kallosh R, Linde A and Zagermann M, 2004, *J. High Energy Phys.* **0408**, 030, arXiv: hep-th/0405247

- [41] Chen P, Dasgupta K, Narayan K, Shmakova M and Zagermann M, 2005, *J. High Energy Phys.* **0509**, 009, arXiv: hep-th/0501185
- [42] Gibbons G, 2002, *Phys. Lett. B* **537**, 1
- [43] Blanco-Pillado J J, Burgess C P, Cline J M, Escoda C, Gomez-Reino M, Kallosh R, Linde A and Quevedo F, 2004, *J. High Energy Phys.* **0411**, 063, arXiv: hep-th/0406230
- [44] Greene B R and Weltman A, 2006, *J. High Energy Phys.* **0603**, 035, arXiv: hep-th/0512135
- [45] Boubekur L and Lyth D H, 2005, *J. Cosmol. Astropart. Phys.* **0507**, 010
- [46] Kohri K, Lin C M and Lyth D H, 2007, *J. Cosmol. Astropart. Phys.* **0712**, 004, arXiv: 0707.3826
- [47] Lidsey J E and Huston I, 2007, *J. Cosmol. Astropart. Phys.* **0707**, 002, arXiv: hep-th/0705.0240 v2
- [48] Kinney W H and Tzirakis K, 2008, *Phys. Rev. D* **77**, 103517, arXiv: astro-ph/0712.2043v2
- [49] Perlmutter S *et al.*, 1998, *Nature* **391**, 51
- [50] Perlmutter S *et al.*, 1999, *Astrophys. J.* **517**, 565
- [51] Riess A G *et al.*, 1998, *Astron. J.* **116**, 1009
- [52] Riess A G *et al.*, 2004, *Astrophys. J.* **607**, 665

-
- [53] Chaplygin S, 1904, *Sci. Mem. Moscow Univ. Math. Phys.* **21**, 1
- [54] Kamenshchik A, Moschella U and Pasquier V, 2001, *Phys. Lett. B* **511**, 265
- [55] Zhu Z H, 2004, *Astron. Astrophys.* **423**, 421
- [56] Bento M C, Bertolami O and Sen A A, 2003, *Phys. Lett. B* **575**, 172
- [57] Bilic N, Tupper G B and Viollier R D, 2001, *Phys. Lett. B* **535**, 17
- [58] Bento M C, Bertolami O and Sen A A, 2002, *Phys. Rev. D* **66**, 043507
- [59] Fabris J C, de Oliveira P L C and Velten H E S, 2011, *Eur. Phys. J. C* **71**, 1773
- [60] Sandvik H, Tegmark M, Zaldarriaga M and Waga I, 2004, *Phys. Rev. D* **69**, 123524
- [61] Amendola L, Finelli F, Burigana C and Caruran D, 2003, *J. Cosmol. Astropart. Phys.* **0307**, 005
- [62] Xu Lixin, Wang Yuting and Noh Hyerim, 2012, *Eur. Phys. J. C* **72**, 1931
- [63] Debnath U, Banerjee A and Chakraborty S, 2004, *Class. Quant. Grav.* **21**, 5609
- [64] Wu Y, Li S, Lu J and Yang X, 2007, *Mod. Phys. Lett. A* **22**, 783
- [65] Bedran M L, Soares V and Araujo M E, 2008, *Phys. Lett. B* **659**, 462
- [66] Costa S, Ujevic M and dos Santos A F, 2008, *Gen. Rel. Grav.* **40**, 1683
- [67] Debnath U and Chakraborty S, 2008, *Int. J. Theor. Phys.* **47**, 2663
- [68] Mukherjee S *et al.*, 2006, *Class. Quant. Grav.* **23**, 6927

-
- [69] Ellis G F R and Maartens R, 2004, *Class. Quant. Grav.* **21**, 223
- [70] Harrison E R, 1967, *Mon. Not. Roy. Astron. Soc.* **69**, 137
- [71] Horava P, 2009, *J. High Energy Phys.* **0903**, 020
- [72] Horava P, 2009, *Phys. Rev. D* **79**, 084008
- [73] Deser S and Waldron A, 2013, *Phys. Rev. Lett.* **110**, 111101
- [74] Hinterbichler Kurt, 2012, *Reviews of Mod. Phys.* **84**, 671
- [75] Berezhiani L, Chkareuli G, de Rham C, Gabadadze G and Tolley A J, 2012, *Phys. Rev. D* **85**, 044024
- [76] Bertolami O, Boehmer C G, Harko T and Lobo F S N, 2007, *Phys. Rev. D* **75**, 104016
- [77] Paul B C, Debnath P S and Ghose S, 2009, *Phys. Rev. D* **79**, 083534
- [78] Koyama K, Taruya A and Hiramatsu T, 2009, *Phys. Rev. D* **79**, 123512
- [79] Domazet S, Radovanovic V, Simonovic M and Stefancic H, 2013, *Int. J. Mod. Phys. D* **22**, 1350006
- [80] Baker T, Ferreira P G and Skordis C, 2013, *Phys. Rev. D* **87**, 024015
- [81] Lu H, Mei J and Pope C N, 2009, *Phys. Rev. Lett.* **103**, 091301
- [82] Calcagni G, 2009, *J. High Energy Phys.* **0909**, 112
- [83] Kiritsis E and Kofinas G, 2009, *Nucl. Phys. B* **821**, 467

-
- [84] Banerjee A, Bandyopadhyay T and Chakraborty S, 2008, *Gen. Rel. Grav.* **40**, 1603
- [85] Beesham A, Chervon S V and Maharaj S D, 2009, *Class. Quant. Grav.* **26**, 075017
- [86] Paul B C and Ghose S, 2010, *Gen. Rel. Grav.* **42**, 795
- [87] Fabris J C, Goncalves S V B , Casarejos F and da Rocha J F V, 2007, *Phys. Lett. A* **367**, 423
- [88] Eisenstein D J *et al.*, 2005, *Astrophys. J.* **633**, 560
- [89] Bond J R, Efstathiou G and Tegmark M, 1997, *Mon. Not. Roy. Astron. Soc.* **291**, L33
- [90] Melchiorri A, Mersini L, Odman C J and Trodden M, 2003, *Phys. Rev. D* **68**, 043509
- [91] Odman C J, Melchiorri A, Hobson M P and Lasenby A N, 2003, *Phys. Rev. D* **67**, 083511
- [92] Efstathiou G and Bond J R, 1999, *Mon. Not. Roy. Astron. Soc.* **304**, 75
- [93] Komatsu E *et al.*, 2011, *Astrophys. J. Suppl.* **192**, 18
- [94] Viel M, Haehnelt M G and Spingel V, 2004, *Mon. Not. Roy. Astron. Soc.* **354**, 684
- [95] Viel M and Haehnelt M G, 2006, *Mon. Not. Roy. Astron. Soc.* **365**, 231

-
- [96] Marinoni C *et al.*, 2005, *A & A* **442**, 801
- [97] Dev A *et al.*, 2003, *Phys.Rev. D* **67**, 023515
- [98] del Campo S, Herrera R and Labrana P, 2007, *J. Cosmol. Astropart. Phys.* **0730**, 0711
- [99] Stern D *et al.*, 2010, *J. Cosmol. Astropart. Phys.* **1002**, 008
- [100] Freedman W *et al.*, 2001, *Astrophys. J.* **553**, 47
- [101] Wang Y and Mukherjee P, 2007, *Phys. Rev. D* **76**, 103533
- [102] Kowalaski M *et al.*, 2008, *Astrophys. J.* **686**, 749
- [103] Vishwakarma R G and Narlikar J V, 2010, *Res. Astron. Astrophys.* **10**, 1195
- [104] Tonry J L *et al.*, 2003, *Astrophys. J.* **594**, 1, arXiv: astro-ph/0305008
- [105] Melchiorri A *et al.*, 2000, *Astrophys. J.* **536**, L63
- [106] Lange A E *et al.*, 2001, *Phys. Rev. D* **63**, 042001
- [107] Jaffe A H *et al.*, 2001, *Phys. Rev. Lett.* **86**, 3475
- [108] Netterfield C B *et al.*, 2002, *Astrophys. J.* **571**, 604
- [109] Halverson N W *et al.*, 2002, *Astrophys. J.* **568**, 38
- [110] Bridle S *et al.*, 2003, *Science* **299**, 1532
- [111] Bennett C L *et al.*, 2003, *Astrophys. J. Suppl.* **148**, 1, arXiv: astro-ph/0302207
- [112] Hinshaw G *et al.*, 2003, *Astrophys. J. Suppl.* **148**, 135, arXiv: astro-ph/0302217

- [113] Kogut A *et al.*, 2003, *Astrophys. J. Suppl.* **148**, 161, arXiv: astro-ph/0302213
- [114] Spergel D N *et al.*, 2003, *Astrophys. J. Suppl.* **148**, 175, arXiv: astro-ph/0302209
- [115] Dodelson S, Kaplinghat M and Stewart E, 2000, *Phys. Rev. Lett.* **85**, 5276
- [116] Sadjadi H M and Alimohammadi M, 2006, *Phys. Rev. D* **74**, 103007
- [117] del Campo S, Harrera R and Pavon D, 2008, *Phys. Rev. D* **78**, 021302
- [118] Faraoni V, 2005, *Class. Quant. Grav.* **22**, 3235
- [119] Coley A A, Hervik S and Lim W C, 2006, *Phys. Lett. B* **638**, 310
- [120] Andrianov A A, Cannata F and Kamenshchik A Y, 2006, *J. Phys. A* **39**, 9975
- [121] Gorini V, Kamenshchik A Y, Moschella U and Pasquier V, 2004, *Phys. Rev. D* **69**, 123512
- [122] Canfora F, 2006, *Phys. Lett. B* **625**, 277
- [123] Calcagni G and Liddle A R, 2006, *Phys. Rev. D* **74**, 043528
- [124] Bludman S A and Roos M, 2002, *Phys. Rev. D* **65**, 043503
- [125] Barriero T, Bento M C, Santos N M C and Sen A A, 2003, *Phys. Rev. D* **68**, 043515
- [126] Colombo L P L and Gervasi M, 2006, *J. Cosmol. Astropart. Phys.* **0610**, 001
- [127] Malquarti M, Copeland E J and Liddle A R, 2003, *Phys. Rev. D* **68**, 023512

- [128] Chimento L P and Lazkoz R, 2005, *Phys. Rev. D* **71**, 023505
- [129] Sen A A, 2006, *J. Cosmol. Astropart. Phys.* **0603**, 010
- [130] Wu P *et al.*, 2007, *Phys. Lett. B* **664**, 16
- [131] Peebles P J E, 1980, ed. *Large-Scale Structures of the Universe*, (Princeton U. Press)
- [132] Wang L and Steinhardt P J, 1998, *Astrophys. J.* **508**, 483
- [133] Linder E V, 2005, *Phys. Rev. D* **72**, 043529
- [134] Laszlo I and Bean R, 2008, *Phys. Rev. D* **77**, 024048
- [135] Jain B and Zhang P, 2008, *Phys. Rev. D* **78**, 063503
- [136] Hu W and Sawicki I, 2007, *Phys. Rev. D* **76**, 104043
- [137] Lue A, Scoccimarro R and Starkman G D, 2004, *Phys. Rev. D* **69**, 124015
- [138] Acquaviva V, Hajian A, Spergel D N and Das S, 2008, *Phys. Rev. D* **78**, 043514
- [139] Koyama K and Maartens R, 2006, *J. Cosmol. Astropart. Phys.* **0601**, 016
- [140] Koivisto T and Mota D F, 2006, *Phys. Rev. D* **73**, 083502
- [141] Daniel S, Caldwell R, Cooray A and Melchiorri A, 2008, *Phys. Rev. D* **77**, 103513
- [142] Ishak M, Upadhye A and Spergel D N, 2006, *Phys. Rev. D* **74**, 043513
- [143] Gupta G, Sen S and Sen A A, 2012, *J. Cosmol. Astropart. Phys.* **1204**, 028

-
- [144] Velten H and Schwarz B J, 2011, *J. Cosmol. Astropart. Phys.* **1109**, 016
- [145] Hawkins E *et al.*, 2003, *Mon. Not. Roy. Astron. Soc.* **346**, 78
- [146] Kaiser N, 1998, *Astrophys. J.* **498**, 26
- [147] Mantz A, Allen S W, Ebeling H and Rapetti D, 2008, *Mon. Not. Roy. Astron. Soc.* **387**, 1179
- [148] Rees M J and Sciama D W, 1968, *Nature* **217**, 511
- [149] Amendola L, Kunz M and Sapone D, 2008, *J. Cosmol. Astropart. Phys.* **0804**, 013
- [150] Hoekstra H *et al.*, 2006, *Astrophys. J.* **647**, 116
- [151] Crittenden R G and Turok N, 1996, *Phys. Rev. Lett.* **76**, 575
- [152] Pogosian L, Corasaniti P S, Stephan-Otto C, Crittenden R and Nichol R, 2005, *Phys. Rev. D* **72**, 103519
- [153] Padmanabhan T, *Theoretical Astrophysics Vol. III* (CUP 2002)
- [154] Liddle A R and Lyth D H, *Cosmological Inflation and Large Scale Structures* (CUP 1999)
- [155] Zhengxiang Li, Puxun W and Hongwei Y, 2012, *Astrophys. J.* **744**, 176
- [156] Linder E V and Cahn R N, 2007, *Astropart. Phys.* **28**, 481
- [157] Fry J N, 1985, *Phys. Lett. B* **158**, 211

- [158] Nesseris S and Perivolaropoulos L, 2008, *Phys. Rev. D* **77**, 023504
- [159] D Polarski and R Gannouji, 2008, *Phys. Lett. B* **660**, 439
- [160] Gannouji R and Polarski D, 2008, *J. Cosmol. Astropart. Phys.* **0805**, 018
- [161] Ishak M and Dossett J, 2009, *Phys. Rev. D* **80**, 043004
- [162] Dossett J, Ishak M, Moldenhauer J, Gong Y and Wang A, 2010, *J. Cosmol. Astropart. Phys.* **1004**, 022
- [163] Verde L *et al.*, 2002, *Mon. Not. Roy. Astron. Soc.* **335**, 432
- [164] Blake C *et al.*, 2011, *Mon. Not. Roy. Astron. Soc.* **415**, 2876
- [165] Reyes R *et al.*, 2010, *Nature* **464**, 256
- [166] Tegmark M *et al.*, 2006, *Phys. Rev. D* **74**, 123507
- [167] Ross N P *et al.*, 2006, *Mon. Not. Roy. Astron. Soc.* **381**, 573
- [168] Guzzo L *et al.*, 2008, *Nature* **451**, 541
- [169] da Angela J *et al.*, 2008, *Mon. Not. Roy. Astron. Soc.* **383**, 565
- [170] McDonald P *et al.*, 2005, [*SDSS Collaboration*] *Astrophys. J.* **635**, 761
- [171] Di Porto C and Amendola L, 2008, *Phys. Rev. D* **77**, 083508
- [172] Makler M, de Oliveira S D and Waga I, 2003, *Phys. Lett. B* **555**, 1
- [173] Bento M C, Bertolami O and Sen A A, 2003, *Phys. Rev. D* **67**, 063003
- [174] Barriero T, Bertolami O and Torres P, 2008, *Phys. Rev. D* **78**, 043530

-
- [175] Copeland E J, Sami M and Tsujikawa S, 2006, *Int. J. Mod. Phys. D* **15**, 1753, arXiv: hep-th/0603057
- [176] Tsujikawa S, 2010, *Dark energy: Investigation and modeling*, arXiv: 1004.1493
- [177] Tsujikawa S, 2011, *Lect. Notes Phys.* **800 (2010)** 99, arXiv: 1101.0191
- [178] Frieman J, Turner M and Huterer D, 2008, *Ann. Rev. Astron. Astrophys.* **46**, 385, arXiv: 0803.0982
- [179] Carrol S M, 2001, *Living Rev. Rel.* **4**, 1
- [180] Martin J, 2012, *Comptes Rendus Phys.* **13**, 566, arXiv: 1205.3365
- [181] Fischler W and Susskind L, 1998, *Holography and Cosmology*, arXiv: hep-th/9806039
- [182] Susskind L, 1999, *Holography in the flat space limit*, arXiv: hep-th/9901079
- [183] Bigatti D and Susskind L, 2000, *TASI Lectures on the Holographic Principle*, arXiv: hep-th/0002044.
- [184] Bousso R, 1999, *J. High Energy Phys.* **9907**, 004
- [185] Bousso R, 1999, *J. High Energy Phys.* **9906**, 028
- [186] Bousso R, 2000, *Class. Quant. Grav.* **17**, 997
- [187] Hsu S D H, 2004, *Phys. Lett. B* **594**, 13
- [188] Li M, 2004, *Phys. Lett. B* **603**, 1

-
- [189] Zhang J, Zhang X and Liu H, 2007, *Phys. Lett. B* **651**, 84, arXiv: 0706.1185
- [190] Zhang X, 2007, *Phys. Lett. B* **648**, 1
- [191] Chen B, Li M and Wang Y, 2007, *Nucl. Phys. B* **774**, 256
- [192] Setare M R and Shafei S, 2006, *J. Cosmol. Astropart. Phys.* **0609**, 011
- [193] Beltran Almeida J P and Pereirs J G, 2006, *Phys. Lett. B* **636**, 75, arXiv: gr-qc/0602103
- [194] Zhang X, 2006, *Phys. Rev. D* **74**, 103505, arXiv: astro-ph/0609699
- [195] Nojiri S and Odintsov S D, 2006, *Gen. Rel. Grav.* **38**, 1285, arXiv: hep-th/0506212
- [196] Gong Y and Zhang Y Z, 2005, *Class. Quant. Grav.* **22**, 4895, arXiv: hep-th/0505175
- [197] Zhang X and Wu F Q, 2005, *Phys. Rev. D* **72**, 043524
- [198] Huang Q G and Li M, 2004, *J. Cosmol. Astropart. Phys.* **0408**, 13, arXiv: astro-ph/0404229
- [199] Cohen A G, Kaplan D B and Nelson A E, 1999, *Phys. Rev. Lett.* **82**, 4971
- [200] Horava P and Minic D, 2000, *Phys. Rev. Lett.* **85**, 1610
- [201] Thomas S, 2002, *Phys. Rev. Lett.* **89**, 081301
- [202] Simpson F, 2007, *J. Cosmol. Astropart. Phys.* **0703**, 016, arXiv: astro-ph/0609755

-
- [203] Barrow J D, 1988, *Nucl. Phys. B* **310**, 743
- [204] Barrow J D, 1990, *Phys. Lett. B* **235**, 40
- [205] Myung Y S, 2007, *Phys. Lett. B* **652**, 223, arXiv: gr-qc/0706.375
- [206] Setare M R, 2007, *Phys. Lett. B* **648**, 329
- [207] Mukohyama S, Nakayama K, Takahashi F and Yokoyama S, 2009, *Phys. Lett. B* **679**, 06
- [208] Myung Y S, 2010, *Phys. Lett. B* **684**, 1
- [209] Park M I, 2011, *Class. Quant. Grav.* **28**, 15004
- [210] Cai Y F and Zhang X, 2009, *Phys. Rev. D* **80**, 043520
- [211] Gao X, Wang Y, Brandenberger R and Riotto A, 2010, *Phys. Rev. D* **81**, 083508
- [212] Wang A and Maartens R, 2010, *Phys. Rev. D* **81**, 024009
- [213] Cai R G, Cao L M and Ohta N, 2009, *Phys. Rev. D* **80**, 024003
- [214] Danielsson U H and Thorlacius L, 2009, *J. High Energy Phys.* **0903**, 070
- [215] Kehagias A and Sfetsos K, 2009, *Phys. Lett. B* **678**, 123
- [216] Chaichian M, Nojiri S, Odintsov S D, Oksanen M and Tureanu A, 2010, *Class. Quant. Grav.* **27**, 185021
- [217] Park M I, 2010, *J. Cosmol. Astropart. Phys.* **1001**, 001
- [218] Dutta S and Saridakis E N, 2010, *J. Cosmol. Astropart. Phys.* **1001**, 013

-
- [219] Harko T, Kovacs T and Lobo F S N, 2011, *Proc. Royal Soc. A* **467**, 1390
- [220] Iorio L and Ruggiero M L, 2010, *Int. J. Mod. Phys. A* **25**, 5399
- [221] Kim S S, Kim T and Kim Y, 2009, *Phys. Rev. D* **80**, 124002
- [222] Cai R G, Cao L M and Ohta N, 2009, *Phys. Lett. B* **679**, 504
- [223] Wang A and Wu Y, 2009, *J. Cosmol. Astropart. Phys.* **0907**, 012
- [224] Ali A, Dutta S, Saridakis E N and Sen A, 2012, *Gen. Rel. and Grav.* **44**, 657
- [225] Sotiriou T, Visser M and Weinfurtner S, 2009, *Phys. Rev. Lett.* **102**, 251601
- [226] Sotiriou T, Visser M and Weinfurtner S, 2009, *J. High Energy Phys.* **0910**, 033
- [227] Carloni S, Elizalde E and Silva P J, 2010, *Class. Quant. Grav.* **27**, 045004,
arXiv: hep-th/0909.2219
- [228] Hagiwara K *et al.*, 2002, *Phys. Rev. D* **66**, 010001
- [229] Olive K A, Steigman G and Walker T P, 2000, *Phys. Rept.* **333**, 389
- [230] Steigman G, 2006, *Int. J. Mod. Phys. E* **15**, 01
- [231] Fabris J C, Velten H E S, Ogouyandjou C and Tossa J, 2011, *Phys. Lett. B* **694**, 289
- [232] Ichikawa K, Seekiguchi T and Takahashi T, 2008, *Phys. Rev. D* **78**, 083526
- [233] Thakur P, Ghose S and Paul B C, 2009, *Mon. Not. Roy. Astron. Soc.* **397**, 1935

- [234] Jianbo L, Lixin X, Jiechao L, Baorong C, Yuanxing G and Hongya L, 2008, *Phys. Lett. B* **662**, 87
- [235] Bogdanos C and Saridakis E N, 2010, *Class. Quant. Grav.* **27**, 075005
- [236] Charmousis C, Niz G, Padilla A and Saffin P M, 2009, *J. High Energy Phys.* **0908**, 070, arXiv: hep-th/0905.2579
- [237] Leon G and Saridakis E N, 2009, *J. Cosmol. Astropart. Phys.* **0911**, 006, arXiv: hep-th/ 0909.3571
- [238] Malaney R A and Mathews G J, 1993, *Phys. Rept.* **229**, 145
- [239] Joyce M, 1997, *Phys. Rev. D* **55**, 1875
- [240] Joyce M and Prokopec T, 1998, *Phys. Rev. D* **57**, 6022
- [241] Clarkson C, Cortes M and Bassett B A, 2007, *J. Cosmol. Astropart. Phys.* **0708**, 011
- [242] Virey J M, Talon-Esmieu D, Ealet A, Taxil P and Tilquin A, 2008, *J. Cosmol. Astropart. Phys.* **0812**, 008
- [243] Paul B C, Thakur P and Saha A, 2012, *Phys. Rev. D* **85**, 024039
- [244] Wang Shuang, Li Xiang-Dong and Li M, 2011, *Phys. Rev. D* **83**, 023010
- [245] Dodelson S, *Modern Cosmology* (ACADEMIC PRESS)
- [246] Liddle A, *An Introductio to Modern Cosmology, Second Edition* (WILEY)

-
- [247] Hawley J F and Holcomb K A, *Foundation to Modern Cosmology, Second Edition* (Oxford University Press)
- [248] Paul B C, Thakur P and Ghose S, 2010, *Mon. Not. Roy. Astron. Soc.* **407**, 415
- [249] Ghose S, Paul B C and Thakur P, 2012, *Mon. Not. Roy. Astron. Soc.* **421**, 20
- [250] Marra V, Amendola L, S awicki I and Valkenburg W, 2013, *Phy. Rev. Lett.* **110**, 241305